# Beamforming for Wireless Powered Communication Networks

Amanthi Ratnayake Thudugalage
ORCID ID: 0000-0001-9318-642X

Submitted in partial fulfilment of the requirements of the degree of
Doctor of Philosophy

November, 2018

*Department of Electrical and Electronic Engineering*

Melbourne School of Engineering
University of Melbourne

## Abstract

Wireless energy harvesting is one of the promising alternative methods to power next generation wireless networks such as wireless sensor networks and wireless communication networks. In Wireless Energy Transfer, in order to improve the energy harvesting capability, energy beamforming has recently drawn significant research attention, where we can direct the majority of transmit signal energy to a particular set of receivers.

In this thesis, we consider energy harvesting in wireless networks and investigate optimum energy harvesting schemes with different objectives. This thesis is divided into two parts. In the first part, we focus on transmit energy beamforming for multi-user networks. We first obtain the optimum beamforming scheme in order to maximize the total energy harvested by all users. Next, we identify that total energy maximization can lead to big differences in the energy harvested by the users. Therefore, in the proceeding chapters we investigate different beamforming schemes to increase the fairness among the users. Furthermore, we extend our analysis to obtain transmit beamforming schemes to achieve throughput fairness among users. In the second part of this thesis, we focus on wireless energy transfer in point-to-point networks. In particular, we look at opportunistic energy transfer schemes to transfer energy from a power transmitter to a receiver when the receiver is imposed with a strict time deadline. We first formulate the problem for a general model to handle multi-antenna networks with different models for channel fading with the assumption that the energy consumed for channel estimation is negligible.We look at different special cases of the problem and compare the proposed solution to a non-causal solution as an upper bound. Then we reformulate the problem to consider the channel estimation energy and obtain the optimum opportunistic energy transfer scheme.

# Declaration

This is to certify that

1. the thesis comprises only my original work towards the Ph.D.,
2. due acknowledgement has been made in the text to all material used,
3. the thesis is less than 100,000 words in length, excluding tables, maps, bibliography and appendices.

---

Amanthi Thudugalage, November, 2018

# Preface

This thesis describes the body of work that I performed during my Ph.D. candidature. As a Ph.D. student transferred from Monash University, this includes my work at the Department of Electrical and Computer Systems Engineering, Monash University, Clayton from September, 2014 to February, 2016, followed by the rest of my candidature at the Department of Electrical and Electronic Engineering, The University of Melbourne since February, 2016. I would like to acknowledge the funding support from the studentships awarded to me from both universities during my tenure, and the Australian Research Council (ARC) through the Discovery Project DP140101050. Furthermore, I would like to acknowledge the travel grant awarded by AusCTW2018 organizing committee to attend the workshop in Newcastle, Australia.

The original contributions of this Thesis are presented in Chapters 2 to 7. I performed the majority of the work including problem formulation and analysis, verification of results through simulations and manuscript composition. Prof. Jamie Evans and Dr. Saman Atapattu supervised all of my work and provided me with feedback and corrections for the manuscripts.

The works in Chapter 2 and Chapter 4 are adopted from two of my manuscripts published in Australian Communication Theory Workshop (AusCTW) 2016 and IEEE International Conference in Communication (ICC) 2016, respectively. The work in Chapter 5 is submitted for publication and is under review. The work described in Chapters 6 and 7 are being prepared for submission as two publications. All papers produced from this thesis are co-authored by Dr. Saman Atapattu and Prof. Jamie Evans.

# Acknowledgements

I am extremely fortunate to have been surrounded by many incredible individuals over the course of my Ph.D. First and foremost, I would like to express my utmost gratitude to my principle supervisor, Professor Jamie Evans. I am grateful to him for his exemplary guidance, constant encouragement and patience throughout the past four years. I have been extremely lucky to have him as my supervisor.

I would also like to express my deepest gratitude to my co-supervisor, Dr. Saman Atapattu. The number of times I've come to him with queries is countless. I am thankful to him for taking his valuable time to support me.

In addition, special thanks to my Ph.D. advisory panel members at the University of Melbourne, Professor Girish Nair and Professor Stan Skafidas, and my first year advisory panel members at Monash University, Professor Lindsay Kleeman, Professor Jean Armstrong and Dr. David Boland. Furthermore, I would like to thank Dr. Iman Shames for his exceptional teaching during the Introduction to Optimization course.

During my internship at Telstra Corporation, I had the opportunity to work with many remarkable individuals. I wouldn't have completed my internship with such success without the guidance of Dr. Max Downey. I would also like to express my heartfelt gratitude to Dr. Milosh Ivanovich, Dr. Taka Sakurai, Dr. Paul Fitzpatrick and David Aders for their wholehearted support. This internship was an entirely pleasant experience because of the kind words from Dr. Enn Vinnal, John Campbell, Terry Black and many others. Furthermore, I deeply appreciate Rachel Geddes, Margo Brown and Sophie Kennedy from APRintern for assistance throughout the internship.

I would like to thank all my friends who have helped me in the past, and deserve my gratitude: Yeqing Hu, Yunus Sarikaya, Anand Sivamalai, Rajitha Senanayake, Yuanyuan He, Hazer Inaltekin, Zhe Wang, Trang Cao, Maneendra Pilanawithana, Samiru Hewa Halpage and Keith James. Also, I am deeply thankful to Daniel Kostoski for his support during the past few months, for listening, encouraging, and making me smile.

My heart felt gratitude goes to my family, Anjalie Thudugalage, Nuwan Ratnayake, Lakmini Ratnayake, Anton Dinesh and Ilana Kosakiewicz. Without their support I would not have completed my Ph.D.

Last but not least, I would like to express my greatest gratitude to my loving parents, Rohini Kodithuwakku and T.C.K. Ratnayake, for the unconditional love, patience, sacrifice and endless support. This thesis is dedicated to you.

*To Amma & Thaththa*

# Contents

# List of Figures

# List of Tables

# Notations

Unless state otherwise, boldface lower-case and upper-case letters denote vectors and matrices, respectively.

| | |
|---|---|
| $\mathbb{R}$ | real numbers |
| $\mathbb{C}$ | complex numbers |
| $\mathbf{X}^T$ | transpose of matrix $\mathbf{X}$ |
| $\mathbf{X}^\dagger$ | complex conjugate of matrix $\mathbf{X}$ |
| $\mathbf{X}^{-1}$ | inverse of matrix $\mathbf{X}$ |
| $[\mathbf{X}]_{i,j}$ | the $(i,j)$th element of matrix $\mathbf{X}$ |
| $\mathbf{I}_K$ | identity matrix of size $K \times K$ |
| $\Re(\mathbf{X})$ | matrix with real components of $\mathbf{X}$ |
| $\Im(\mathbf{X})$ | matrix with imaginary components of $\mathbf{X}$ |
| $\mathrm{Tr}(\mathbf{X})$ | trace of matrix $\mathbf{X}$ |
| $\mathrm{Rank}(\mathbf{X})$ | rank of matrix $\mathbf{X}$ |
| $\lambda_1(\mathbf{X})$ | principle eigenvalue of matrix $\mathbf{X}$ |
| $\mathbf{v}_1(\mathbf{X})$ | principle eigenvector of matrix $\mathbf{X}$ |
| $\|\mathbf{x}\|$ | the Euclidean norm of vector $\mathbf{x}$ |
| $\mathcal{CN}(0,1)$ | circular symmetric complex Gaussian random variable with zero mean and unit variance |
| $\mathbb{E}[X]$ | the expectation of random variable $X$ |
| $\mathbb{P}[X]$ | probability of event $X$ |
| $\|z\|$ | the absolute value of z |

# List of Abbreviations

| | |
|---|---|
| **BAN** | Body Area Network |
| **BS** | Base Station |
| **CDF** | Cumulative Distribution Function |
| **CE** | Channel Estimation |
| **CSI** | Channel State Information |
| **DC** | Direct Current |
| **DL** | Downlink |
| **EH** | Energy Harvesting |
| **ER** | Energy Receiver |
| **GUE** | Gaussian Unitary Ensemble |
| **H-AP** | Hybrid Access Point |
| **IPM** | Interior Point Method |
| **IR** | Information Receiver |
| **KKT** | Karush-Kuhn-Tucker |
| **LICQ** | Linear Independence Constraint Qualifications |
| **LOS** | Line of Sight |
| **LTE-A** | Long Term Evolution- Advanced |
| **MIMO** | Multiple-Input Multiple-Output |
| **MSE** | Minimum Mean Square Error |
| **MRC** | Maximum Ratio Combining |
| **MU-MISO** | Multi-User Multiple-Input Single-Output |

| | |
|---|---|
| **NLOS** | Non-Line of Sight |
| **PB** | Power Beacon |
| **QCQP** | Quadratically constrained quadratic program |
| **RF** | Radio Frequency |
| **SDP** | Semi-Definite Programming |
| **SDR** | Semi-Definite Relaxation |
| **SISO** | Single-Input Single-Output |
| **SNR** | Signal-to-Noise Ratio |
| **SWIPT** | Simultaneous Information and Power Transfer |
| **TDMA** | Time Division Multiple Access |
| **UL** | Uplink |
| **WET** | Wireless Energy Transfer |
| **WPCN** | Wireless Powered Communication Networks |
| **WSN** | Wireless Sensor Network |
| **ZF** | Zero Forcing |

# Chapter 1

# Introduction and Background

## 1.1 Motivation of the Thesis

Wireless communications have advanced tremendously in the past decades to become an essential and inseparable part of our daily lives. The current fourth-generation (4G) networks, also known as long term evolution-advanced (LTE-A) networks, support virtually all forms of modern communications including voice, email, video, and data for other applications without requiring the devices and users to be tethered to wired lines. Technologies for 5G and future generations of connectivity will provide higher bandwidth and lower latency than current-generation 4G technology. Most importantly, these technologies are expected to enable fundamentally new applications that will transform the way humanity lives, works, and engages with its environment [1]. Given the growth trends of smart wireless phones and devices that can support advanced data intensive applications such as video conferencing, we can anticipate major challenges to arise in wireless communications such as increasing demand for data rates, spectrum crunch, high energy consumption and environment impact [2]–[4]. As more and more essential medical, educational, safety and governmental services move online and ubiquitous wireless access becomes the norm, the need for resolving these challenges becomes increasingly pressing [5].

Currently, wireless networks contribute to around $2-2.5\%$ of global green-house gas

emissions, with the expected wireless traffic growth making the situation much worse. This becomes one of the major challenges in meeting the green environment where more efficient and environment friendly communications are achieved via wireless infrastructure implemented with low-carbon systems and possible ways of using and managing energy harvested from renewable sources such as solar and ambient radio signals. Energy efficiency of wireless networks refers to both user and network energy savings. To prolong the users battery lifetime as well as to achieve green communications, an appealing solution is to harvest energy from environmental energy sources such as solar and wind. Powering communication nodes by wind or solar allows telecommunication networks to expand beyond the limits of the general power grid, but leads to many challenges due to constant unavailability, limited space, implementation overhead, and requirement of large scale infrastructure. Motivated by these challenges, recent research specifically focuses on *wireless energy harvesting (or wireless energy transfer)* that enables a more convenient wireless environment. However, one of the major drawbacks of wireless energy transfer (WET) is the poor efficiency due to the path loss with the transmission distance. This effect is much worse when we use omni-directional transmit antennas. Using advanced energy beamforming techniques in multi-anntenna systems can improve the energy transfer efficiency significantly. By carefully shaping the transmit waveform at each antenna, energy beamforming can control the collective behaviour of the radiated waveforms causing them to coherently combine at a specific receiver. This means that, compared to single antenna omni-directional transmission, using multi-antenna transmission with beamforming, energy transfer efficiency can be further improved without additional bandwidth or increased transmit power. Motivated by this phenomenon, This research focuses on beamforming techniques for wireless powered communication networks. Specifically, we study different energy beamforming schemes in order to achieve a given objective in the network performance and investigate on different beamforming schemes to improve the harvested energy at the receiving end.

## 1.2 Outline of the Thesis

The focus of this thesis is to investigate different beamforming schemes and energy transfer policies for efficient wireless energy transfer. We focus on theoretical analysis as well as the design of practical algorithms. This thesis is presented in two parts. Figure 1.1 gives an overview of the thesis and the relationships between the chapters. We present a chapter-by-chapter summary of the thesis below.

- In Chapter 2, we develop an analytical framework to design a beamforming vector which maximizes the total energy harvested by all users in the network. Then, the effect of the network size is discussed in terms of number of transmitting antennas/users. Further, a comparison between the proposed total energy maximization scheme and equally weighted scheme is given.

- The total energy maximization scheme discussed in Chapter 2 may introduce severe unfairness among the energy levels harvested by each user. In some cases, the user may not achieve an adequate level of energy in order to perform a given task. In such cases, these users must not be considered in the optimization problem. Hence, in Chapter 3 we reformulate the problem such that only active users (users who are able to achieve their minimum energy requirements) will be considered for total energy maximization. We show that the optimization problem is non-convex and obtain approximate solutions using a gradient projection based algorithm. We further show that when all the users are in reasonable radio conditions and able to achieve their minimum requirements, the optimization problem can be reformulated into a sub-problem such that the minimum energy constraints of all users are achieved. We show that this optimization problem is non-convex and we obtain the approximate solution using an interior-point method based algorithm. We compare the performance of the proposed interior-point-based algorithm for the sub-problem against the results obtained by using the CVX optimization toolbox for the semidefinite-relaxed problem. As a performance benchmark for the

general problem, we solve the sub-problem using CVX toolbox for all the subset of users and then obtain the maximum total energy harvested.

- In multi-user networks, different nodes harvest different energy levels depending on their locations. Thus, in order to introduce more fairness, the max-min criterion is used in Chapter 4. In particular, we maximize the minimum energy level among all users. This may guarantee that all other users harvest energy more than the minimum level. We identify that this problem is NP-hard in general and we use semidefinite relaxation techniques to solve the optimization problem approximately. Further, we investigate the use of multiple beamforming vectors instead of a single beamforming vector with the max-min criterion. Then, we compare this scheme with the single beamforming scheme, total energy maximization, equally weighted).

- Chapters 2- 4 are merely for energy harvesting. In Chapter 5, we consider data transmission as well. In particular, we have two phases: i) energy harvesting: all the users harvest a certain amount of energy at downlink; and ii) data transmission: all users transmit data using the harvested energy. We consider a time division multiple access (TDMA) based system with maximum ratio combining (MRC). We formulate an optimization problem in order to maximize the minimum throughput among all users. We compare the amount of data transmitted by each user with this scheme and the equally weighted scheme.

- In Chapter 6 we consider a point-to-point network with multi-antenna system. In particular, we consider the problem in which the energy transmitter is required to transmit energy towards the energy harvesting user such that the user is able to harvest energy before a given deadline. By considering perfect yet causal channel state information, we obtain the optimum energy transfer policy. Specifically, we jointly optimize for the level of energy transmitted at each frame and the optimum beamforming vector to be used. As a benchmark we compare the proposed policy

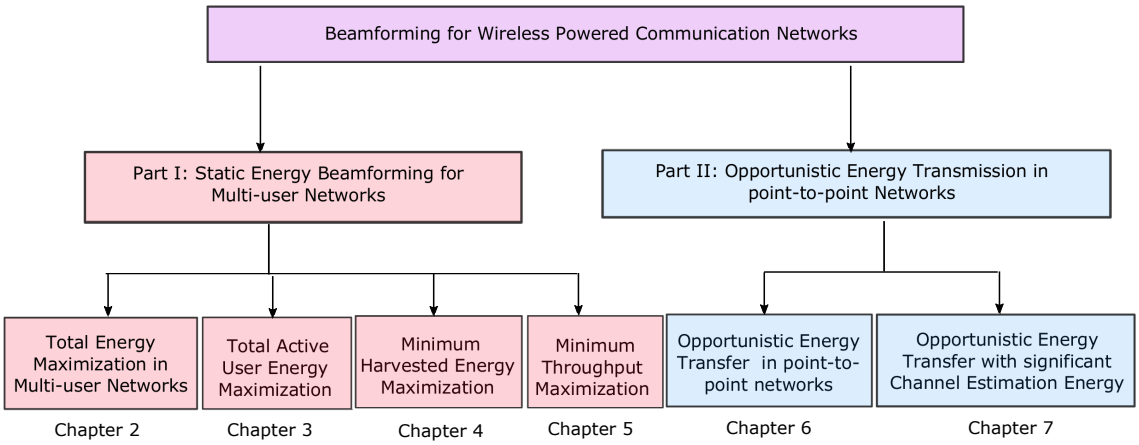

Figure 1.1: Overview of the Thesis.

against the genie-aided method under different multi-antenna models and channel fading. For the SISO Rayleigh case, we provide asymptotic analysis for both the proposed energy transfer policy and the genie aided method.

- In Chapter 7, we extend the problem in Chapter 6 in order to consider the scenario where the energy associated with channel estimation is not negligible. In this case, we obtain the optimum energy transfer policy and show that it reduces to an all-or-nothing threshold policy. We verify the analytical results by using Monte-Carlo simulations.

## 1.3 Background

This chapter provides a broad background on wireless energy transfer in communication networks. More specific literature reviews can be found in the introduction sections in each chapter.

### 1.3.1 Wireless Energy Transfer

Wireless energy transfer is the transmission of electrical power from a power source to a consuming device over wireless medium (without using solid wires or conductors). This concept was originally conceived by Nikola Tesla in the $1890$s with successful demonstration of lighting electric lamps wirelessly. While wireless energy transfer can avoid the costly process of planning and installing power cables in buildings and infrastructure, it may have low energy transfer efficiency (i.e., a small fraction of the emitted energy can be harvested at the receiver), which is one of main challenges in implementation [6]. Path loss has a significant impact on wireless energy transfer. However, this can be mitigated by using free-space beaming and large aperture antennas. For example, in $1969$, a microwave beam was developed to power a hover platform which was in the form of a helicopter [7]. This small helicopter which was capable of hovering at $50$ feet height, harvested energy from an RF source with a $270$ W DC power supply operating at $2.45$ GHz [7]. Due to high power consumption of early electronic devices, wireless energy transfer had not received much attention. The recent upsurge of research interest is motivated by the widespread use of low-power devices and the tremendous success of wireless sensor networks (WSNs) [6], [8].

### 1.3.2 Wireless Sensor Networks (WSNs)

Wireless sensor networks are composed of a large number of devices, called sensor nodes, which are able to sense, process, and transmit information about the environment in which they are deployed. These devices are usually distributed in a geographical area to collect information for users interested in monitoring and controlling a given phenomenon [9]. Some possible applications of WSNs are:

- In health monitoring, it is anticipated that people will soon be able to carry a personal body area network (BAN) with them that will provide users with information and various reporting capabilities for medical, lifestyle, assisted living, sports or entertainment purposes [10].

- Precision agriculture: where sensor nodes are deployed outdoors to monitor soil conditions like temperature, moisture, and mineral content. In high value agricultural sectors, the information collected from the sensors can be used to manage the cultivation process to control pests and achieve high quality crops [10].

- Smart Buildings have the potential to become positive energy office buildings that generate more energy than they consume. This can be achieved by drastically decreasing the current power demand. One element in such a program is to turn on heating and lighting only in those areas where they are needed. At present, $42\%$ of the energy consumed is used for heating, ventilation, and air conditioning (HVAC), and $23\%$ is used for lighting. This situation calls for a large deployment of sensors able to detect the presence or absence of human beings [10].

Moreover, WSNs can be used in environmental monitoring, habitat monitoring, seismic detection, acoustic detection, industrial process monitoring, military surveillance, terror threat detection, protection of critical infrastructure, intrusion detection, monitoring of large crowds, and guidance in case of unexpected events [11].

### 1.3.3 Energy Harvesting in WSNs

WSNs research has predominantly assumed that sensor nodes are powered by a portable and limited energy source such as batteries. Once the power supply of sensor is exhausted, it can no longer fulfill its role unless the source of energy is replenished. This can become an expensive and tedious task, or impractical for most scenarios [12]–[14]. Battery-powered WSNs also pose an environmental risk. This has led to the development of innovative new solutions based on wireless energy harvesting techniques [15].

For example, WSNs can be powered using ambient RF energy available through public telecommunication services (e.g., GSM and WLAN frequencies). However, ambient RF signals have very low power density, e.g. for distances of $25 - 100$ m from a GSM base station, we may receive $0.1 - 1.0$ mW/m$^2$ power density levels [10].

Alternatively, sensor nodes can be charged using a dedicated RF source, limiting the transmission power levels according to international regulations. Such a commercial system, produced by *Powercast*, is currently in the market [16]. In ideal conditions i.e., no reflections and aligned polarization, this system can harvest $15$ mW at distance $30$ cm when the transmitted power is $2 - 3$ W at frequency $906$ MHz.

### 1.3.4 RF Energy Harvesting in Wireless Communication Networks

There has been a recent growing interest in studying wireless powered communication networks (WPCNs), where energy harvested from ambient RF signals is used to power wireless terminals in the network [17]. Thus, individual base stations (BSs) in macro cells or small cells are now capable of becoming energy providers. Such a network architecture is proposed in [18] in which stations called power beacons (PBs) are deployed in an existing cellular network to recharge mobile nodes. Since RF signals carry both energy and information at the same time, a joint investigation of simultaneous wireless information and power transfer (SWIPT) has recently drawn significant attention [17]. Efficient SWIPT requires some fundamental changes in the design of wireless communication networks. For example, the conventional criteria for evaluating the performance of a wireless system are the information transfer rates and the reception reliability. However, with SWIPT, we have to consider the trade-off between the achievable information rates and the amount of harvested energy [6].

# Part I

# Static Energy Beamforming for Multi-user Networks

# Chapter 2

# Total Energy Maximization in Multi-user Networks

*In this chapter, we consider a multi-user multiple input single output (MU-MISO) energy harvesting network with total energy maximization under a transmit power constraint. Since the harvested energy depends on the network size, i.e., number of transmit antennas and number of users, we discuss their effects on maximum total harvested energy. Further, by using results on the convergence of the maximum eigenvalue of certain large random matrices, we study the total harvested energy for large networks. Moreover, we study the distribution of the maximum total harvested energy from large networks and show that with appropriate scaling, this distribution approaches the Tracy-Widom distribution of Type 2. We then give examples for two network structures: i) where users are located as clusters; and ii) where users are distributed uniformly around the power transmitter. We verify the analysis using numerical and simulation results.*

## 2.1 Introduction

Wireless energy transfer (WET) is the transmission of electrical power from a power source to a consuming device over a wireless medium. Although near-field WET techniques such as inductive coupling and magnetic resonance coupling have already found their way to the market, they are not suitable for remote charging [19]. Thus, far-field WET has caught wireless researchers' attention recently as this technique may be a promising alternative to prolong the constrained lifetime of wireless networks, e.g., wireless sensor networks. These networks are highly energy constrained, and often the lifetime of wireless sensor networks is limited by the battery life. Therefore, energy efficient communication techniques such as multiple-input multiple-output (MIMO) and relaying have been introduced to extend the lifetime of wireless sensor networks [20]. However, these techniques may not help to avoid battery replacement or recharging. Further, depending on applications, battery replacement and recharging may be a tedious, time consuming, expensive or even an impossible task [12], [21]. Therefore, researchers have focused on WET in order to replenish the energy sources of wireless networks [22]–[24]. However, one of the major challenges in WET is the poor efficiency due to the path loss with the transmission distance. This effect is much worse when we use omni-directional transmit antennas. Thus, energy beamforming has been proposed as one of the promising techniques [22].

Energy beamforming can be applied in energy harvesting to improve received energy levels by shaping the transmit signals at each antenna such that they constructively combine at the receiver. Thus, compared with omni-directional transmission, beamforming can improve energy transfer efficiency without additional bandwidth or increased transmit power [19]. Therefore, energy beamforming has drawn significant attention in the research community recently.

Different energy beamforming schemes have been explored focusing only on energy transfer, and both information and energy transfer in [24]–[28]. In [22], a multiple-input multiple-output (MIMO) wireless network is considered with an energy harvesting re-

ceiver (EH) and an information receiver (IR), when RF signals are transmitted from a common transmitter. As a special case, for perfect channel state information (CSI), the beamforming vector at the transmitter is determined to maximize the energy harvested at EH when there is no IR. In [23], this result is extended for a multi-user scenario in order to maximize the total harvested energy from the entire network by using multiple beamforming vectors. In [24], a multi-user MIMO network is also considered for weighted sum of energy maximization by introducing a single bit feedback scheme which reduces energy for channel estimation.

All these works provide optimization techniques for energy maximization for fixed network sizes. However, it is interesting to explore how network size, i.e., number of transmit antennas and number of energy harvesting users, affect the harvested energy. Further, it is worth noting that sum-energy maximization requires eigen-analysis. To the best of our knowledge, none has yet provided a rigorous analytical framework to analyse the behaviour of total harvested energy in large networks. To fill this research gap, this chapter makes the following contributions:

- We analyse the behaviour of maximum total harvested energy when the number of transmit antennas increases while the number of users remains constant, and vice-versa.

- We analyse the limit of the total harvested energy for large networks in which both number of transmit antennas and users increase.

- We analyse the probability distribution of the maximum total harvested energy from a large network.

We note that with more technology companies promising to provide systems solutions for wireless charging, such analysis may be useful in gaining insights to the solution being provided by these companies. For example, the WattUp® transmitter, which is a dedicated power transmitter, provided by Energous Solutions may be used

for charging remote controls, smoke detectors, toys or other gadgets in a small in-house environment. Some interesting demonstrations of such setup has been presented [29]. If such a solution is to be deployed in a commercial environment, the distribution of maximum total harvested energy may help to provide performance guarantees to the customer. In this case, when such dedicated power transmitters are deployed to transfer energy for multiple devices, the probability of total harvested energy being less than a desirable threshold can be used as a confidence measure to the provided service.

The rest of this chapter is organized as follows. Section 2.2 describes the system model. Section 2.3 formulates the total energy maximization problem, and presents the effect of network size. Section 2.4 derives the probability distribution for maximum total energy. Section 2.5 studies the asymptotic behaviour of maximum total harvested energy for a large network. Section 2.6 presents numerical and simulation results followed by concluding remarks in Section 2.7.

## 2.2 System Model

We consider multi-user multi-input single-output (MU-MISO) wireless communication network as shown in Figure 2.1. This enables downlink WET. The network consists of a power transmitter with $M$ co-located antennas denoted $\text{Tx}_1, \cdots, \text{Tx}_M$ and $K$ single-antenna users denoted $\text{Rx}_1, \cdots, \text{Rx}_K$. The frequency-flat quasi-static channel between $\text{Rx}_i$ and $\text{Tx}_j$ is $h_{ij}$. We assume that the transmitter has perfect channel state information (CSI). As all antennas are co-located at the power transmitter, the distance between $\text{Rx}_i$ and $\text{Tx}_j$ is $d_i$. Further, $w_j$ denotes the weighting factor of $\text{Tx}_j$. The additive noise at $\text{Rx}_i$ denoted by $n_i$ is a complex Gaussian random variable with zero-mean and unit-variance, i.e. $n_i \sim \mathcal{CN}(0, 1)$. Thus, the received signal at $\text{Rx}_i$ can be given as

$$y_i = \rho_i \sum_{j=1}^{M} h_{ij} w_j + n_i \tag{2.1}$$

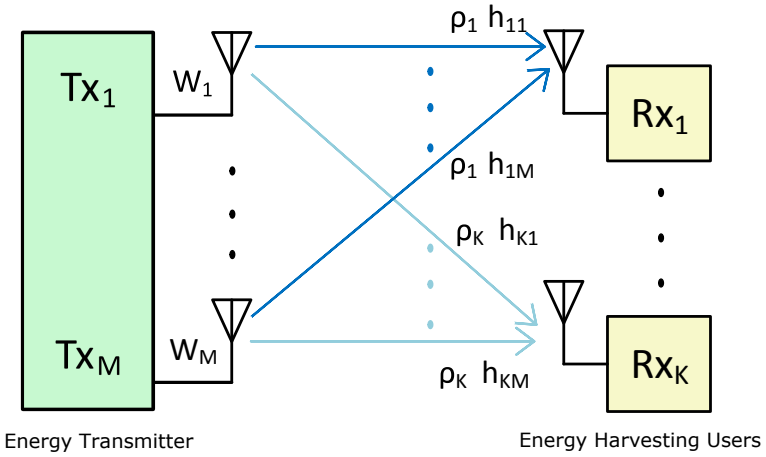

Figure 2.1: MU-MISO communication network with WET.

where $\rho_i$ is the path loss factor $\rho_i = 1/\sqrt{d_i^\alpha}$ and $\alpha$ is the path loss exponent. Then, the received signal vector $\mathbf{y}$ is given by

$$\mathbf{y} = \mathbf{DHw} + \mathbf{n} \tag{2.2}$$

where $\mathbf{y} = [y_1, \cdots, y_K]^T$, $\mathbf{D} = \text{diag}(\rho_1, \cdots, \rho_K)$, $\mathbf{H} \in \mathbb{C}^{K \times M}$ is the channel matrix with $h_{ij}$ at $(i, j)$ position, $\mathbf{w} = [w_1, \cdots, w_M]^T$ is the weight vector or the beamforming vector, and $\mathbf{n} = [n_1, \cdots, n_K]^T$ is the noise vector. The noise vector $\mathbf{n}$ at the receivers is independent from the beanforming vector $\mathbf{w}$. Therefore, we cannot control $\mathbf{n}$ by changing $\mathbf{w}$. In other words, we cannot change the noise power at the receivers by adjusting the beamforming vector. Due to the additive nature of the noise, we simply ignore the energy associated with noise as it does not affect the optimal beamformer.

Furthermore, considering the entire system, the total harvested energy by all $K$ users at a unit time can be given as

$$P_T = \|\mathbf{y}\|^{\mathbf{2}} = \mathbf{w}^\dagger \mathbf{H}^\dagger \mathbf{D}^{\mathbf{2}} \mathbf{H} \mathbf{w}, \tag{2.3}$$

where $^\dagger$ denotes the conjugate transpose. We assume that $\|\mathbf{w}\|^2 \leq 1$. Thus, weights of the transmit antennas are designed in order to preserve this power budget of the

transmitter.

## 2.3 Transmit Beamforming for Total Harvested Energy Maximization

Based on the analytical model in Section 2.2, we maximize the total harvested energy $P_T$ of the network by using energy beamforming at the transmitter [22]. Since the transmit power is limited by the power budget, the optimization problem can be given as

$$\begin{aligned} \max_{\mathbf{w}\in\,\mathbb{C}^M} \quad & P_T = \mathbf{w}^\dagger \mathbf{H}^\dagger \mathbf{D}^\mathbf{2} \mathbf{H} \mathbf{w} \\ \text{subject to} \quad & \|\mathbf{w}\|^\mathbf{2} \leq 1. \end{aligned} \tag{2.4}$$

It is important to note that $\mathbf{H}^\dagger\mathbf{D}^\mathbf{2}\mathbf{H}$ is a Hermitian matrix. This problem can be solved using the Courant-Fischer theorem [30]. A similar problem is also considered in [22], [23]. Let the eigenvalues and corresponding eigen-vectors of the Hermitian matrix $\mathbf{H}^\dagger\mathbf{D}^\mathbf{2}\mathbf{H}$ be $\lambda_1 \geq \cdots \geq \lambda_M$ and $\mathbf{v}_1, \cdots, \mathbf{v}_M$, respectively. At the optimum solution, the maximum total harvested energy is given by the maximum eigenvalue $\lambda_1$, and the optimum beamforming vector is the corresponding eigen-vector (or the principal eigen-vector) $\mathbf{v}_1$. In other words, if we design the beamforming vector as the principal eigen-vector of $\mathbf{H}^\dagger\mathbf{D}^\mathbf{2}\mathbf{H}$, we can harvest the maximum $P_T$ which is the largest eigenvalue of $\mathbf{H}^\dagger\mathbf{D}^\mathbf{2}\mathbf{H}$. Further, the optimum solution depends on several parameters such as the number of transmit antennas $M$ and the number of users $K$. Thus, we discuss how these parameters affect the harvested energy.

### 2.3.1 Effect of Number of Transmit Antennas $M$

In this section, we assume that all channels are independent and identically distributed (i.i.d.) complex Gaussian random variables with zero-mean and unit-variance, i.e. $h_{ij} \sim \mathcal{CN}(0,1)$. We consider the effect of the number of transmit antennas $M$ on the total harvested energy $P_T$ by fixing the number of users $K$ and their path loss factors $\rho_i$. When there are $M$ transmit antennas with $K$ users, denoted as $M \times K$ system, the total

harvested energy, denoted as $P_{T_{(M,K)}}$, can be calculated with the aid of (2.3) as

$$\begin{aligned} P_{T_{(M,K)}} &= \mathbb{E}\left[\left|\sum_{i=1}^{K}\rho_i\sum_{j=1}^{M}h_{ij}w_j\right|^2\right] \\ &= \sum_{i=1}^{K}{\rho_i}^2\sum_{j=1}^{M}\mathbb{E}\left[\,|h_{ij}w_j|^2\right], \end{aligned} \tag{2.5}$$

where $\mathbb{E}[\cdot]$ is the expectation operation, and the second equality comes because $h_{ij}$s are independent. As discussed at the beginning of this section, maximum $P_T$ is achieved by the utilization of the principal eigenvector, $\mathbf{v_1} = [v_{11}, \cdots, v_{M1}]^T$ as the beamforming vector. Thus, the maximum harvested energy of $M \times K$ system $P^{max}_{T_{(M,K)}}$ can be given as

$$P^{max}_{T_{(M,K)}} = \sum_{i=1}^{K}{\rho_i}^2\sum_{j=1}^{M}\mathbb{E}[\,|h_{ij}v_{j1}|^2]. \tag{2.6}$$

If we consider a $(M+1) \times K$ system, then the corresponding beamforming vector is $\mathbf{r} = [r_1, \cdots, r_{M+1}]^T$. Following similar analysis as above, the harvested energy of $(M+1) \times K$ system can be given as

$$\begin{aligned} P_{T_{(M+1,K)}} &= \sum_{i=1}^{K}{\rho_i}^2\sum_{j=1}^{M+1}\mathbb{E}[\,|h_{ij}r_j|^2] \\ &= \sum_{i=1}^{K}{\rho_i}^2\sum_{j=1}^{M}\mathbb{E}[\,|h_{ij}r_j|^2] \\ &\quad + \sum_{i=1}^{K}{\rho_i}^2\mathbb{E}[\,|h_{i(M+1)}r_{M+1}|^2]. \end{aligned} \tag{2.7}$$

When we compare two systems, $M \times K$ and $(M+1) \times K$, they have two different beamforming vectors $\mathbf{v}_1$ and $\mathbf{r}$. Although, the beamforming vector $\mathbf{r}$ has an additional element, both vectors should satisfy the transmit power constraint, i.e., $\|\mathbf{v}_1\|^2 = \|\mathbf{r}\|^2 = 1$. We consider a case where the additional element $r_{M+1}$ of $\mathbf{r}$ is zero, i.e., the addi-

tional transmit antenna does not transmit RF signal. Then, the rest of the elements of $\mathbf{r}$ are chosen to be identical to $\mathbf{v}_1$, i.e. $r_i = v_{i1}$ for $1 \leq i \leq M$. Then, we have $P^{max}_{T_{(M,K)}} = P_{T_{(M+1,K)}}$. Since the maximum total harvested energy with the principle eigen-vector is larger than total harvested energy of any other beamforming vector, we have $P_{T_{(M+1,K)}} \leq P^{max}_{T_{(M+1,K)}}$. Therefore, we can claim that

$$P^{max}_{T_{(M,K)}} \leq P^{max}_{T_{(M+1,K)}}. \tag{2.8}$$

This means that the total harvested energy increases with the number of transmit antennas $M$. This scenario can also be interpreted as follows: when the number of transmit antennas $M$ is large, there is a high degree of freedom to change the beamforming vector smoothly. Thus, the antenna array can be finely tuned to maximize the total harvested energy.

### 2.3.2 Effect of the Number of Energy Harvesting Users $K$

In this section, we consider the effect of the number of users $K$ on the total harvested energy $P_T$ by fixing the number of transmit antennas $M$. For a $M \times K$ system, the total harvested energy is given in (2.6). If we consider a $M \times (K+1)$ system in which $K$ users, say $\text{Rx}_1, \cdots, \text{Rx}_K$, have similar path loss factors as in (2.6), and the additional user, say $\text{Rx}_{K+1}$, has path loss factor $\rho_{(K+1)}$. However, we use the same beamforming vector which is designed for the $M \times K$ system at the transmitter, i.e., we introduce an additional user to the $M \times K$ system without changing the beamforming vector. Then, the total harvested energy is given as

$$\begin{aligned} P_{T_{(M,K+1)}} &= \sum_{i=1}^{K+1} {\rho_i}^2 \sum_{j=1}^{M} \mathbb{E}[\, |h_{ij} v_{j1}|^2] \\ &= P^{max}_{T_{(M,K)}} + {\rho_{(K+1)}}^2 \sum_{j=1}^{M} \mathbb{E}[\, |h_{(K+1)j} v_{j1}|^2]. \end{aligned} \tag{2.9}$$

Since, the harvested energy by $(K+1)$th user, ${\rho_{(K+1)}}^2 \sum_{j=1}^{M} \mathbb{E}[\ |h_{(K+1)j} v_{j1}|^2]$, is non-negative, from (2.9), we have $P^{max}_{T_{(M,K)}} \leq P_{T_{(M,K+1)}}$. Further, as the total harvested energy using principal eigen-vector always gives the maximum energy, we have $P_{T_{(M,K+1)}} \leq P^{max}_{T_{(M,K+1)}}$. Therefore, we can claim that

$$P^{max}_{T_{(M,K)}} \leq P^{max}_{T_{(M,K+1)}}. \tag{2.10}$$

This means that the total harvested energy increases with the number of energy harvesting users $K$.

## 2.4 Distributions of the Maximum Total Harvested Energy

The solution for (2.4) is obtained using eigenanalysis of a Hermitian matrix $\mathbf{H}^{\dagger}\mathbf{D^2H}$. Thus, if the maximum total harvested energy is $P_T^{max}$, the distribution of $P_T^{max}$ may be obtained by using random matrix theory. Since the elements of the matrix $\mathbf{DH}$ are independent complex Gaussian random variables, $P_T^{max}$ satisfies [31], [32]

$$\left( \frac{P_T^{max} - M\mu_r}{M^{1/3}\sigma} \right) \Rightarrow \text{TW}_2 \tag{2.11}$$

where $\text{TW}_2$ denotes the Tracy-Widom distribution of Type 2 for Gaussian unitary ensembles (GUE) [33]. This is also known as the Tracy-Widom distribution with a Dyson index of 2. Further, $\mu_r$ and $\sigma$ can be obtained from

$$\mu_r = \frac{1}{c}\left[1 + \frac{1}{d_M}\int \frac{c\lambda}{1-c\lambda} dH_M(\lambda)\right] \tag{2.12}$$

and

$$\sigma^3 = \frac{1}{c^3}\left[1 + \frac{1}{d_M}\int \left(\frac{c\lambda}{1-c\lambda}\right)^3 dH_M(\lambda)\right], \tag{2.13}$$

with $d_M \in (0, \infty)$ and $d_M = M/K$ as $M \to \infty$. Further, $H_M(\lambda)$ is the empirical spectral distribution of $\mathbf{D}^2$, and $c := c(\mathbf{D}^2, M, K)$ is the unique solution of

$$\int \left( \frac{c\lambda}{1 - c\lambda} \right)^2 dH_M(\lambda) = d_M \tag{2.14}$$

in $[0, 1/\lambda_1(\mathbf{D}^2))$.

This result holds when the highest distance between the transmitter and receivers is finite and the shortest distance is nonzero, i.e., $\limsup \lambda_1(\mathbf{D}^2) < \infty$ and $\liminf \lambda_K(\mathbf{D}^2) > 0$.

Further, the cumulative distribution function (CDF) of $\text{TW}_2$, $F_2(x) = \mathbb{P}(X \leq x)$, can be given as [34], [35]

$$F_2(x) := \exp\left[ -\frac{1}{2} \int_x^\infty (s - x) u(s)^2 ds \right] \tag{2.15}$$

where $\mathbb{P}(.)$ stands for the probability function, $u(x)$ is the solution of the Painleve II equation $\frac{d^2u}{dx^2} = 2u^3 + xu$ with the boundary condition $u(x) \sim -\text{Ai}(x)$ as $x \to \infty$. Here, $\text{Ai}(x)$ is the Airy function given by

$$\text{Ai}(x) \sim \frac{\mathrm{e}^{-(2/3)x^(3/2)}}{s\sqrt{2\pi}x^{1/4}}. \tag{2.16}$$

It is worth noting that $F_2(x)$ is known and tabulated, e.g., [36].

By using the results in [33], this analysis can also be extended to any channel model which satisfies $\mathbb{E}[h_{ij}] = 0$, $\mathbb{E}[|h_{ij}|^2] = \frac{1}{M}$ and $\mathbb{E}[h_{ij}^2] = 0$, where $h_{i,j}$s are independent random variables. Therefore, this is a more general result. Since the Tracy-Widom distribution has rarely been applied in wireless communication literature, this is also a novel result which may be used to analyse the performance of multi-user wireless networks. Next, we consider how this result can be applied for practical networks.

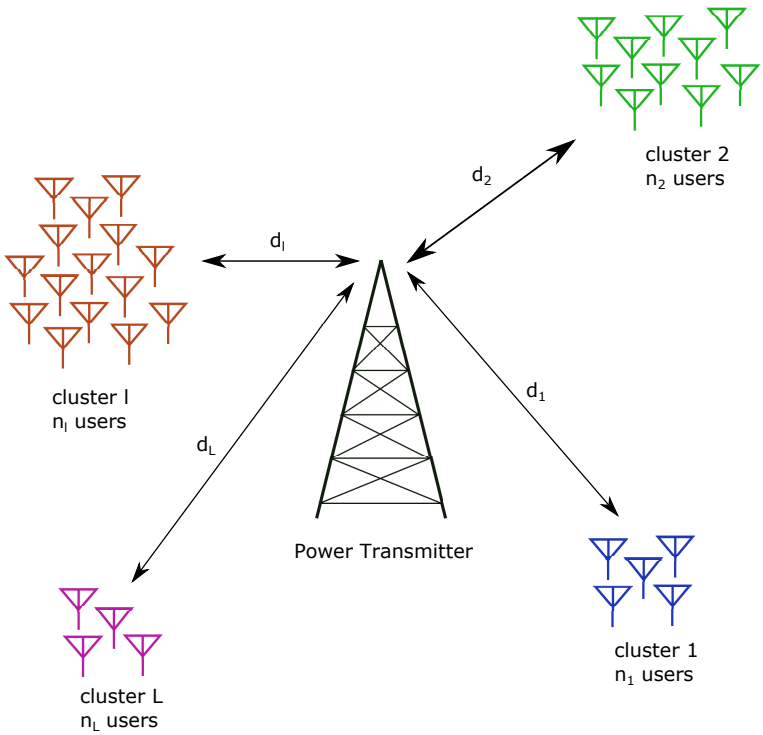


Figure 2.2: MU-MISO energy harvesting network with users clustered at different locations.

### 2.4.1 Examples

In this section, we consider two practical networks with a large number of users and transmitting antennas. Then, we study the probability distribution of the total harvested energy when the transmitter uses the optimum beamforming vector which is discussed in Section 2.3.

#### 2.4.1.1 Users Located as Clusters Around the Power Transmitter

As shown in Figure 2.2, we consider a network where a large number of $K$ users are located in a finite number of $L$ clusters around the power transmitter. There are $n_l$ users in the $l$th cluster $(l = 1, \cdots, L)$. We assume the distance between the power transmitter and users in the same cluster is equal. Then, the path-loss matrix $\mathbf{D^2}$ has a finite number of distinct values $\rho_l^2; l \in [1, L]$. Hence, the continuous equations given in section 2.4 can be transformed into discrete equations. This means that the integration can be replaced

by a summation. Therefore, the maximum total harvested energy satisfies

$$\left(\frac{P_T^{max} - M\mu_s}{M^{1/3}\sigma_s}\right) \Rightarrow \text{TW}_2 \tag{2.17}$$

with

$$\mu_s = \frac{1}{c}\left[1 + \frac{1}{M}\sum_{l=1}^{L} n_l\left(\frac{c\rho_l^2}{1 - c\rho_l^2}\right)\right] \tag{2.18}$$

and

$$\sigma_s^3 = \frac{1}{c^3}\left[1 + \frac{1}{M}\sum_{l=1}^{L} n_l\left(\frac{c\rho_l^2}{1 - c\rho_l^2}\right)^3\right], \tag{2.19}$$

where $c \in [0, 1/\max(\rho_l^2)]$ is the unique solution of

$$\sum_{l=1}^{L} n_l\left(\frac{c\rho_l^2}{1 - c\rho_l^2}\right)^2 = M.$$

Hence, the probability of the maximum total harvested energy can be given as

$$P_r = F_2\left(\frac{P_T^{max} - M\mu_s}{M^{1/3}\sigma_s}\right). \tag{2.20}$$

#### 2.4.1.2 Users Uniformly Distributed Around the Power Transmitter

As shown in Figure 2.3, we consider a network where a large number of $K$ users are uniformly distributed around the power transmitter between radii $R_0$ and $R$. The $i$th user is located at distance $d_i \in [R_0, R]$. The distribution of $d_i$, $f_{d_i}(d_i)$, can be given as

$$f_{d_i}(r) = \begin{cases} \frac{2r}{R^2 - R_0^2}, & \text{if } R_0 \leq r \leq R. \\ 0, & \text{otherwise.} \end{cases} \tag{2.21}$$

When we use $\varrho = A_0\big(r/d_0\big)^{-\alpha}$ transformation, where $A_0$ is the reference path-loss at a reference distance of $d_0$, the distribution function of elements of the path-loss matrix

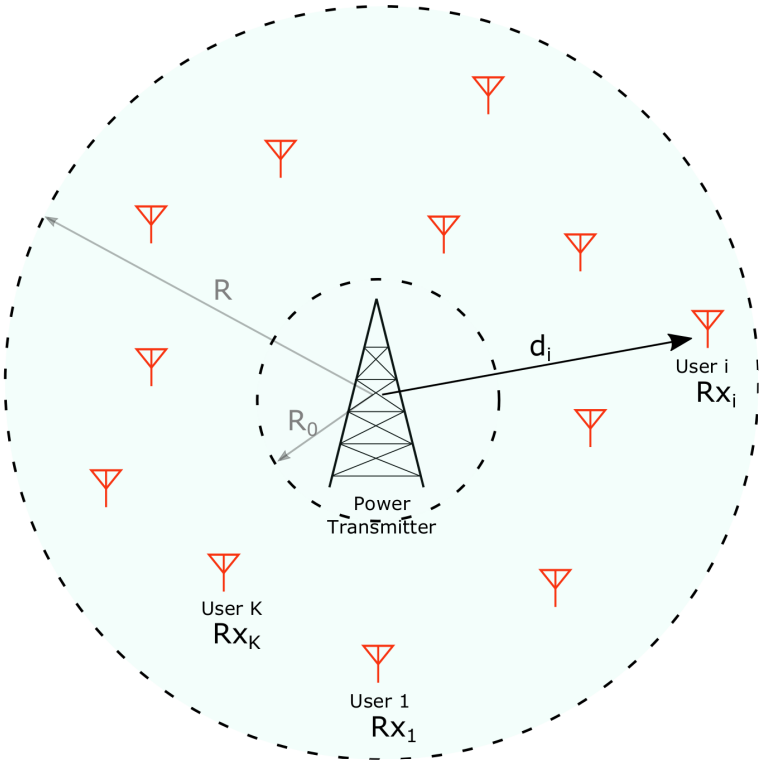


Figure 2.3: MU-MISO energy harvesting network with uniformly distributed users.

$\mathbf{D^2}$ can be obtained as

$$g_P(\varrho) = \frac{2d_0}{\alpha A_0^{-4/\alpha}(R^2 - R_0^2)} \varrho^{\frac{-(2+\alpha)}{\alpha}}. \tag{2.22}$$

Hence, the spectral distribution of the path-loss matrix $\mathbf{D^2}$ is given by,

$$G_P(\varrho) = \frac{d_0^2}{A_0^{-4/\alpha}(R^2 - R_0^2)} \left[ \left( A_0^{-4/\alpha} \frac{R}{d_0} \right)^2 - \varrho^{-2/\alpha} \right]. \tag{2.23}$$

When $M, K \to \infty$, $P_T^{max}$ also satisfies (2.11) where $\mu_r$ and $\sigma$ can be calculated by using (2.13), (2.12) and (2.14) replacing $H_M(\lambda)$ by $G_P(\varrho)$, with $c \in [0, R_0^\alpha)$. Hence, the probability of the maximum total harvested energy can be given as

$$P_r = F_2\left( \frac{P_T^{max} - M\mu_r}{M^{1/3\sigma}} \right). \tag{2.24}$$

The results (2.20) and (2.24) can be used to calculate the probability of $P_T^{max}$ in clustered networks and uniformly distributed networks respectively. Numerical results for such networks are given in section 2.6.

## 2.5 Asymptotic of the Mean

In this section, we consider the limit of the maximum total harvested energy when the number of transmit antennas $M$ and users $K$ are large, i.e., we look at the behaviour of the largest eigenvalue $\lambda_1$ of the Hermitian matrix $\mathbf{H}^\dagger \mathbf{D}^2 \mathbf{H}$ when $M, K \to \infty$.

### 2.5.1 Users Equidistant from Transmitter

We use the theorem developed in [37],[38] which computes the limiting distributions of the largest eigenvalue of a complex Gaussian sample covariance matrix with large dimensions. That is, when elements of $\mathbf{H} \in \mathbb{C}^{M,K}$ are i.i.d. complex Gaussian random variables with $h_{i,j} \sim \mathcal{CN}(0,1)$, $K \to \infty$, $M = M(K)$ and $\frac{K}{M} = \gamma^2$ for some $\gamma^2 \in [0, \infty)$, the largest eigenvalue $\lambda_1$ of the Wishart matrix of the form $\mathbf{S_M} = \frac{1}{M}\mathbf{H}^\dagger\mathbf{H}$ has

limiting value $\lambda_1 \to \left(\frac{1+\gamma}{\gamma}\right)^2$, almost surely. Using this result, the asymptotic behaviour of the maximum total harvested energy when $\mathbf{D}^2 = \mathbf{I}_K$, where $\mathbf{I}_K$ is the $K \times K$ identity matrix, can be given as

$$\frac{P_T^{max}}{M} \to \left(\frac{1+\gamma}{\gamma}\right)^2. \tag{2.25}$$

This indicates that the maximum harvested energy converges to $\left(\frac{1+\gamma}{\gamma}\right)^2$ when $K \to \infty$. Hence, if the ratio $K/M = \gamma^2$ of a large system is known, the amount of harvested energy can be estimated without any prior knowledge on CSI. However, this result holds when $\mathbf{D}^2 = \mathbf{I}_K$ or in other words all the users are located at an equal distance from the power transmitter. This may not be the case in real networks. Thus, we next focus on the case where $\mathbf{D}^2 \neq \mathbf{I}_K$.

### 2.5.2 General Case

In this subsection, we further analyse the theorem used in Section 2.4 in order to obtain the distribution of the Maximum total harvested energy and then states the asymptotic of the mean of the maximum total harvested energy.

In [31], Theorem 1 gives the asymptotic behaviour of the largest eigenvalue of sample covariance matrix $\mathbf{W} = \mathbf{X}^\dagger\mathbf{X}$ where $\mathbf{X}$ is a $n \times p$ matrix with i.i.d. complex normal rows with zero mean and $\mathbf{\Sigma}_p$ covariance matrix, i.e., $\{\mathbf{X}_k\}_{k=1,\cdots,n} \sim \mathcal{CN}(0, \mathbf{\Sigma}_p)$. The largest eigenvalue and the spectral distribution of $\mathbf{\Sigma}_p$ are $\lambda_1$ and $H_p$, respectively. Assuming that $n/p$ $(\geq 1)$ is uniformly bounded, $\limsup \lambda_1 < \infty$, $\liminf \lambda_p > 0$, and $\limsup \lambda_1 c < 1$, where $c$ is the unique solution in $[0, 1/\lambda_1(\mathbf{\Sigma}_p))$ of the equation

$$c = c(\mathbf{\Sigma_p}, n, p) : \int \left(\frac{\lambda c}{1-\lambda c}\right)^2 dH_p(\lambda) = \frac{n}{p}, \tag{2.26}$$

then, the largest eigenvalue $l_1$ of the Wishart matrix $\mathbf{W}$ follows Tracy-Widom dis-

tribution for Gaussian unitary ensembles ($\mathrm{TW}_2$) [35], [39] such that

$$n, p \to \infty; \ \frac{l_1 - \mu}{\sigma} \Rightarrow \mathrm{TW}_2$$

where

$$\mu = \frac{1}{c}\Big(1 + \frac{p}{n}\int \frac{\lambda c}{1-\lambda c} dH_p(\lambda)\Big), \tag{2.27}$$

$$\sigma^3 = \frac{1}{c^3}\Big(1 + \frac{p}{n}\int \Big(\frac{\lambda c}{1-\lambda c}\Big)^3 dH_p(\lambda)\Big). \tag{2.28}$$

Further, when $n \to \infty$, the largest eigenvalue $l_1$ converges as $l_1/n \to \mu$, almost surely. In [32], this result is extended for $n/p < 1$ case. This is by showing that [31] assumes $n/p \geq 1$ only to be able to utilize Proposition 1.2 in [38], and proving that the proposition is valid for $n/p < 1$. Therefore, the theorem above is valid for $n/p \in (0, \infty)$.

It is worth noting that $\mathbf{H}^{\dagger}\mathbf{D}$ takes the form of $\mathbf{X}$ with the covariance matrix $\mathbf{\Sigma}_p = \mathbf{D^2}$. This enables us to user these results to investigate the behaviour of maximum total harvested energy for a large network size. Therefore, as $M, K \to \infty$, maximum total harvested energy $P_{T,max}$ for a large system converges as $\frac{P_T^{max}}{M} \to \mu$, almost surely.

## 2.6 Numerical and Simulation Results

This section provides numerical results to verify our analytical results obtained in Sections 2.3, 2.4 and 2.5. Our system model is as described in Section 2.2.

Based on the discussion in Section 2.3.1, Figure 2.4 shows the variation of $P_T^{max}$ with number of transmit antennas $M$ when the number of users $K = 10$. As we explain in section 2.3.1, the maximum total harvested energy increases almost linearly when the number of transmit antennas $M$ increases. As a reference, we also consider the equal gain transmitter ( i.e., beamforming vector $\mathbf{u} = \frac{1}{\sqrt{M}}[1, 1, ... , 1]^T$). This beamformer may be applied when the transmitter has no CSI. The total harvested energy from the equal gain transmitter remains constant at 10 for any $M$. Thus, energy beamforming

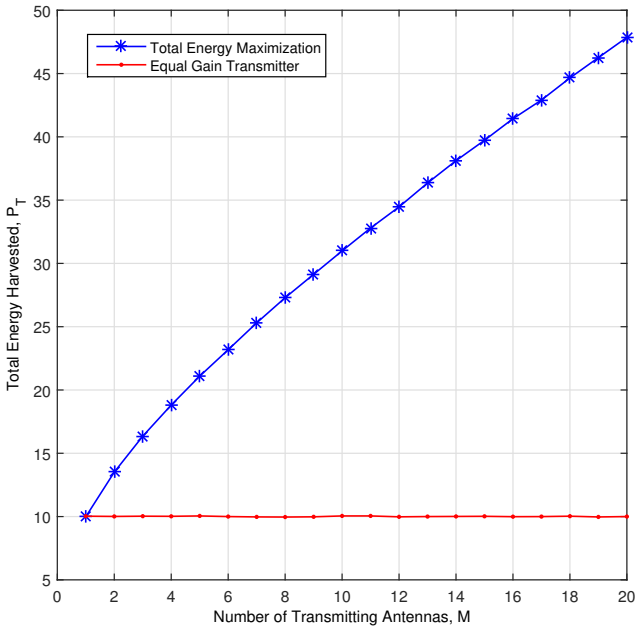


Figure 2.4: Variation of total harvested energy with number of transmit antennas.

scheme outperforms equal grain transmitter, and equality holds when $M = 1$.

Based on the discussion in Section 2.3.2, Figure 2.5 shows the variation of $P_T^{max}$ with number of energy harvesting users $K$ when the number of transmit antennas $M = 20$. With total energy maximization technique, $P_T^{max}$ increases nearly linearly, and with the equal gain transmitter, it also increases but at a slower rate.

Next, we consider the distribution of the maximum total harvested energy as discussed in Section 2.4. We use independent and identically distributed complex Gaussian channels with zero mean and unit variance, i.e., $h_{i,j} \sim \mathcal{CN}(0, 1),\ \forall\, i, j$. Path-loss matrix $\mathbf{D}^2$ is generated according to the Section 2.4.1.

As discussed in Section 2.4.1.1, we consider a network where users are around the power transmitter, in six equally populated clusters ($L = 6$) with path-loss of 1, 0.75, 0.5, 0.25, 0.125 and 0.025. We perform $10^4$ channel realizations and obtain the empirical distribution function of $P_T^{max}$ for $K = M = 30,\ 60,$ and $90$. We plot the corresponding CDFs with $P_{scaled}^{max}$ in Figure 2.6a, where $P_{scaled}^{max}$ is obtained by scaling

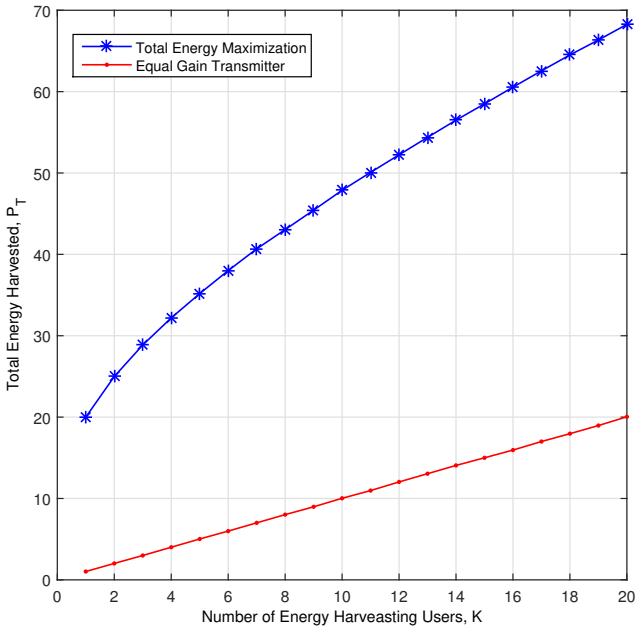


Figure 2.5: Variation of total harvested energy with number of users.

$P_T^{max}$ according to (2.20). We also plot the CDF of standard $\text{TW}_2$. We notice that the CDFs match tightly with $\text{TW}_2$, especially in the tail. Furthermore, $\text{TW}_2$ matching improves when the network size increases.

As discussed in Section 2.4.1.2, we consider a network where users are uniformly located around the power transmitter. We model the path-loss matrix $\mathbf{D^2}$ as given in (2.23) with $R_0$ and $R$ to be $20\,\text{m}$ and $200\,\text{m}$, respectively, with a path-loss exponent of $\alpha = 3$. We perform $10^4$ channel realizations and obtain the empirical distribution of $P_T^{max}$ scaled according to (2.24) for $K = M = 30,\ 60,$ and $90$. We plot the distributions of $P_{scaled}^{max}$ and the CDF of standard $\text{TW}_2$ in Figure 2.6b. Similar to the previous case, we notice that the CDFs match tightly with $\text{TW}_2$, especially in the tail. Furthermore, $\text{TW}_2$ matching improves when the network size increases.

For the uniform network structure of size $K = M = 90$, we increase the transmit power $P_{Tx}$ from $32\,\text{dBm}$ to $35\,\text{dBm}$, and calculate the probability of the maximum total harvested energy being lower than a threshold of $P_T^{th} = -50\,\text{dBm}$. This can be calcu-

lated by using (2.24) as $\mathbb{P}(x < P_T^{th})$. We plot the probability against the transmit power, and compare with the probability calculated from the standard $\text{TW}_2$ in Figure 2.7. We notice that the simulation results matches the theoretical results calculated from the standard $\text{TW}_2$ distribution.

We now discuss the limit of $P_T^{max}$ for large network sizes in Section 2.5.1. For example, we calculate $P_T^{max}/M$ when $M$ varies from 10 to 1000 maintaining $K/M = 1$. We perform 50 channel realizations with $h_{i,j} \sim \mathcal{CN}(0,1)$ and $\mathbf{D}^2 = \mathbf{I}_K$, and plot them in Figure 2.8 ($P_T^{max}/M$ verses $M$), which shows each realization. According to the analysis, $P_T^{max}/M \to \left(\frac{1+\gamma}{\gamma}\right)^2 = 4$. It is important to note that simulated values also approach 4 when $M$ increases, (i.e., $M \to \infty$). This is also illustrated by using cumulative distribution functions (CDFs) of normalized $P_T^{max}/M$ (i.e., $P_T^{max}/(\mu M)$ where $\mu$ is in (2.27)) in Figure 2.9. We use different $M$ values such as $M = 50, 100, 500, 1000$ with $\gamma^2 = 1$. CDFs become steeper while the means reach the theoretical value, i.e., $P_T^{max}/M = 4$.

Next, we discuss the limit of $P_T^{max}$ for large network sizes in Section 2.5.2. For example, we calculate $P_T^{max}/M$ when $M$ varies from 10 to 1000 maintaining $K/M = 1$. We perform 50 channel realizations with $h_{i,j} \sim \mathcal{CN}(0,1)$. The path loss matrix $\mathbf{D}^2$ is obtained by placing users randomly with a radius $r$ from the power transmitter followed by $\varrho = r^{-\alpha}$ transformation. Then, we plot $P_T^{max}/M$ verses $M$ in Figure 2.10, which shows each realization. According to the analysis, $P_T^{max}/M \to \mu$ where $\mu = 1.663$ is obtained as in Section 2.5.2. It is also important to note that the simulated values approach 1.663 when $M$ increases, (i.e., $M \to \infty$). This is also illustrated by using CDFs of normalized $P_T^{max}/M$ (i.e., $P_T^{max}/(\mu M)$ ) in Figure 2.11 for different $M$ values such as $M = 50, 100, 500, 1000$ with $\gamma^2 = 1$. CDFs become steeper while the means reach the theoretical value, i.e., $P_T^{max}/M = 1.663$. When we compare Figure 2.9 and Figure 2.11 for two cases discussed in Section 2.5, we observe a fast convergence of $P_T^{max}/M$ for $\mathbf{D}^2 = \mathbf{I}_K$ compared with locating users uniformly around the power transmitter. For example, when $M = 50$, the normalized mean for the case of $\mathbf{D}^2 = \mathbf{I}_K$

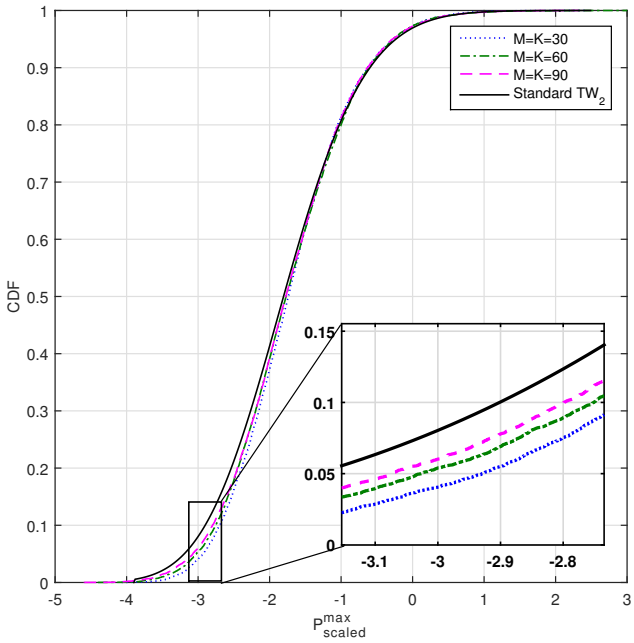


(a)

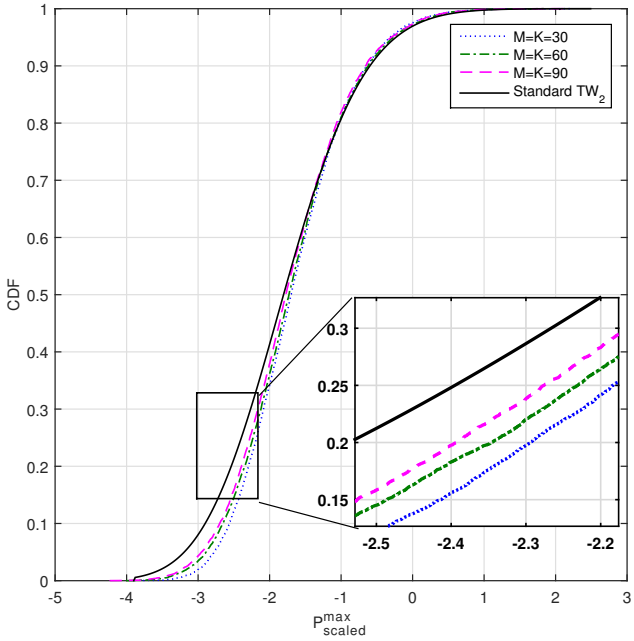


(b)

Figure 2.6: The CDF of scaled total harvested energy for a network with: (a) users clustered at different locations; and (b) uniformly distributed users

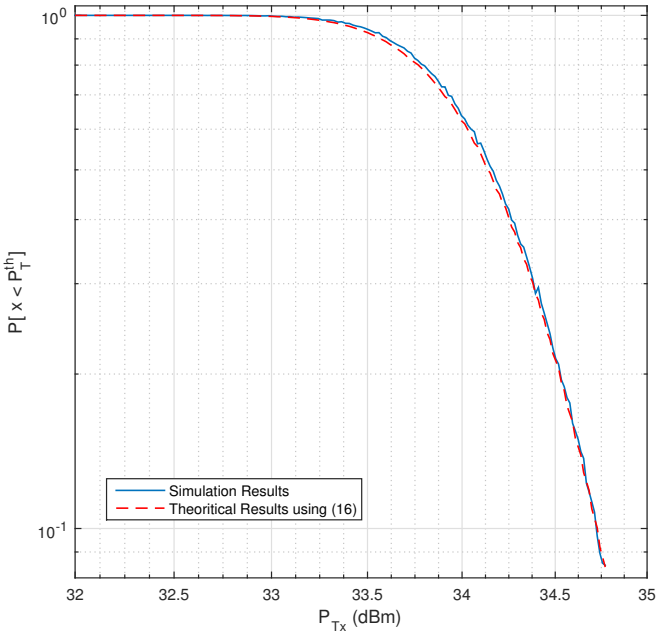


Figure 2.7: Variation of the probability of harvested energy being lower than the threshold $-50\,\mathrm{dBm}$ against the transmit power for users uniformly distributed around the power transmitter.

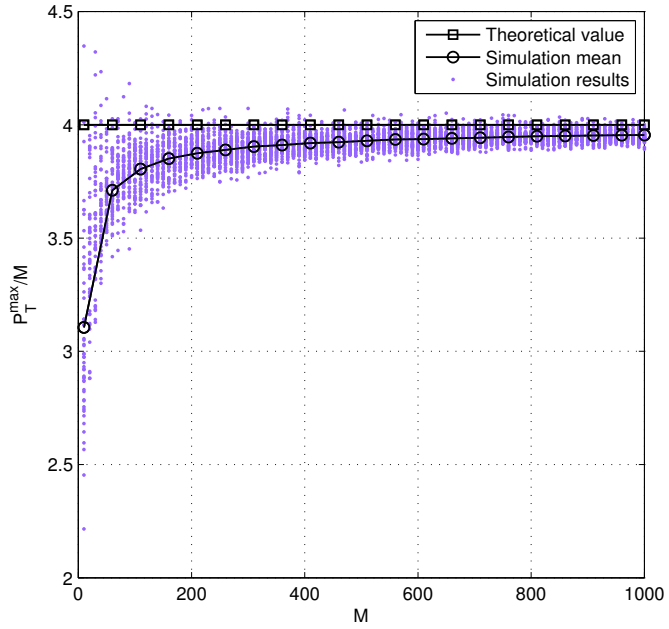


Figure 2.8: Convergence of $P_T^{max}/M$ for $\gamma^2 = 1$ when $\mathbf{D}^2 = \mathbf{I}_K$.

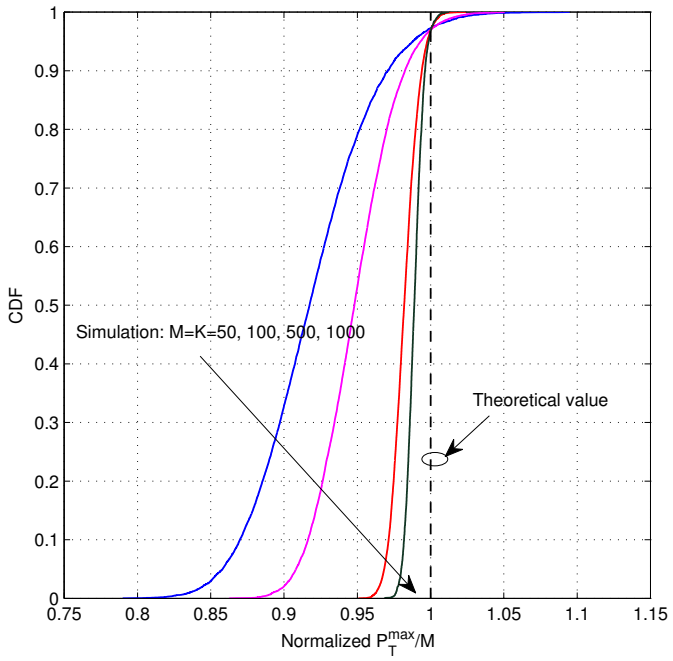


Figure 2.9: CDFs of of $P_T^{max}/M$ with $\gamma^2 = 1$ for various $M$ when $\mathbf{D}^2 = \mathbf{I}_K$.

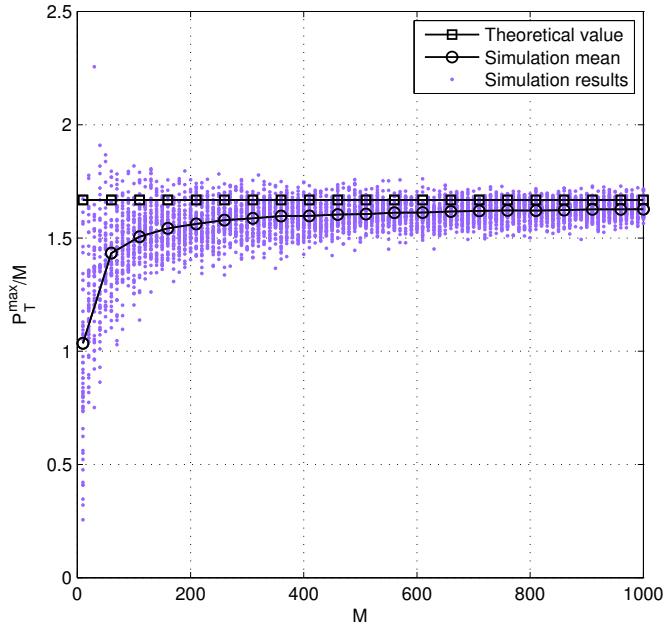


Figure 2.10: Convergence of $P_T^{max}/M$ for $\gamma^2 = 1$ when users are uniformly located around the transmitter.

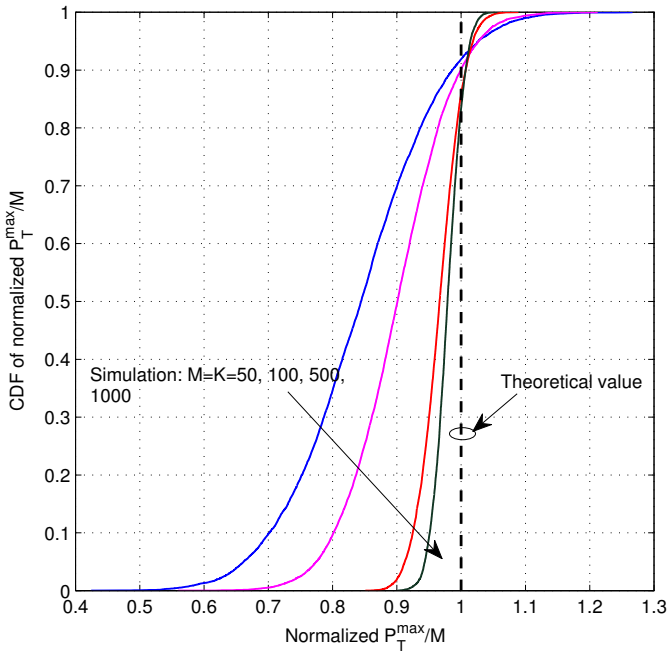


Figure 2.11: CDFs of of $P_T^{max}/M$ with $\gamma^2 = 1$ for various $M$ when users are located uniformly around the power transmitter.

is $0.9175$ while for uniformly distributed users the normalized mean is only $0.8452$.

## 2.7 Conclusion

In this chapter, we consider transmit energy beamforming for multi-user communication networks. Specifically, we study the total harvested energy maximization scheme. We analyse the effect of the network size, i.e., number of transmitters and receivers, on the maximum total harvested energy. we analyse the distribution of the total harvested energy from large networks. We conclude that, with proper scaling the distribution of the total harvested energy follows the standard Tracy-Widom distribution of Type 2. We further discuss the asymptotic behaviour of maximum total harvested energy. Since the asymptotic behaviour does not depend on the particular realization of the channels for infinite network size, this can be used as a CSI-invariant estimate of total harvested energy from a network.

# Chapter 3

# Energy Beamforming for Total Active User Energy Maximization in MISO Networks

*In this chapter, we study MU-MISO network and investigate on how to maximize the total energy harvested by the users that meet the minimum energy requirements. We formulate the optimization and prove its non-convexity. We then solve the convex approximated problem using a gradient projection based algorithm. We compare the performance of the proposed algorithm by using an exhaustive search algorithm using SDP.*

## 3.1 Introduction

Wireless energy transfer undergoes significant path loss with the transmission distance. In the state-of-the-art, in order to improve the end-to-end power transfer efficiency, researchers' efforts were focused on enhancing the transmit efficiency, the receive efficiency, or both. To obtain higher transmit efficiency, the transmit antenna beamforming can be utilized with multi-antenna systems [40].

Different beamforming schemes have been explored in the literature. In [22], a MIMO wireless network is considered with an energy harvesting receiver and an information receiver, when RF signals are transmitted from a common transmitter. For

perfect channel state information (CSI), the beamforming vector at the transmitter is designed to maximize the energy harvested at the energy harvesting receiver with no information receiver. In [23], this result is extended to a multi-user scenario in order to maximize the total harvested energy from the entire network by using multiple beamforming vectors. In [24], a multi-user MIMO network is also considered for weighted sum of energy maximization by introducing a single bit feedback scheme which reduces energy for channel estimation. In Chapter 2, we focused on beamforming scheme to maximize the total harvested energy subjected to the transmit power constraint. However, this design may lead to unfairness in terms of the energy levels of individual users. For example, while users near the power transmitter or with good channel quality harvest much more energy, users far away from the transmitter or with bad channel quality harvest less energy. It is important to note that these users may not harvest their minimum required energy. This may lead the corresponding users to be inactive. In such cases, including the energy harvested by such inactive users for the total harvested energy may be inaccurate. This is because such users may not find the harvested energy levels useful. Therefore, in this chapter we focus on the maximizing the total energy harvested by users who can achieve their minimum energy requirements.

The rest of this chapter is organized as follows. Section 3.2 formulates the total energy harvested by active users maximization problem. Section 3.3 describes the convex approximation of the problem. Section 3.4 gives the gradient projection based algorithm to obtain approximate beamforming algorithm. Section 3.5 discusses a special case of the problem when all the users are able to achieve their minimum energy requirement. Section 3.6 presents numerical results comparing the beamforming algorithm with CVX based algorithm implemented using semidefinite relaxation (SDR) of the problem for each subset of the users. Finally, concluding remarks is given in Section 3.7.

## 3.2 Problem Formulation

In this section, we consider the MU-MISO wireless communication network discussed in Section 2.2. We formulate the sum energy maximization problem of adequately charged users subject to the total power budget at the transmitter. The objective function is given by

$$P_T = \sum_{i=1}^{K} \rho^2 \mathbf{w}^\dagger \mathbf{h}_i^\dagger \mathbf{h}_i \mathbf{w} \mathbb{1}(\rho^2 \mathbf{w}^\dagger \mathbf{h}_i^\dagger \mathbf{h}_i \mathbf{w} - \eta_i) \tag{3.1}$$

where $\mathbb{1}(.)$ denotes the unit step function and $\eta_i$ denotes minimum energy required by the $i$th user. Therefore, the optimization problem can be formulated as

$$\begin{aligned} &\max_{\mathbf{w}\in\mathbb{C}^M} \quad \sum_{i=1}^{K} \rho^2 \mathbf{w}^\dagger \mathbf{h}_i^\dagger \mathbf{h}_i \mathbf{w} \mathbb{1}(\rho^2 \mathbf{w}^\dagger \mathbf{h}_i^\dagger \mathbf{h}_i \mathbf{w} - \eta_i) \\ &\text{s. t.} \quad \mathbf{w}^\dagger \mathbf{w} \leq 1. \end{aligned} \tag{3.2}$$

We reformulate this problem as a minimization problem as

$$\begin{aligned} &\min_{\mathbf{w}\in\mathbb{C}^M} \quad -\sum_{i=1}^{K} \rho^2 \mathbf{w}^\dagger \mathbf{h}_i^\dagger \mathbf{h}_i \mathbf{w} \mathbb{1}(\rho^2 \mathbf{w}^\dagger \mathbf{h}_i^\dagger \mathbf{h}_i \mathbf{w} - \eta_i) \\ &\text{s. t.} \quad \mathbf{w}^\dagger \mathbf{w} \leq 1. \end{aligned} \tag{3.3}$$

The objective function in (3.3) is not smooth. Therefore, it is not continuously differentiable. This is because the unit step function is piece-wise continuous. Further, the objective function is non-convex. In order to prove the non-convexity, consider the function $f_i(\mathbf{w})$ given as,

$$f_i(\mathbf{w}) = -\rho^2 \mathbf{w}^\dagger \mathbf{h}_i^\dagger \mathbf{h}_i \mathbf{w} \mathbb{1}(\rho^2 \mathbf{w}^\dagger \mathbf{h}_i^\dagger \mathbf{h}_i \mathbf{w} - \eta_i). \tag{3.4}$$

We choose $\mathbf{w}$ such that $\mathbb{1}(\rho^2 \mathbf{w}^\dagger \mathbf{h}_i^\dagger \mathbf{h}_i \mathbf{w} - \eta_i) = 0$, and $\alpha > 1$ such that $\mathbb{1}(\alpha^2 \rho^2 \mathbf{w}^\dagger \mathbf{h}_i^\dagger \mathbf{h}_i \mathbf{w} - \eta_i) = 1$. Therefore, the function $f_i(\mathbf{w})$ in (3.4) takes the values $0$ and $-\alpha^2 \rho^2 \mathbf{w}^\dagger \mathbf{h}_i^\dagger \mathbf{h}_i \mathbf{w}$ at $\mathbf{w}$ and $\alpha\mathbf{w}$, respectively. This means that the function $f_i(\mathbf{w})$ transitions from dis-

satisfying the minimum energy requirement to achieving adequate energy in the region $[\mathbf{w}, \alpha\mathbf{w}]$. By considering a scalar $\theta \in [0, 1]$, we have

$$\begin{aligned} f_i\left(((1-\theta(\alpha-1))\mathbf{w}\right) = \\ -(1-\theta(\alpha-1))^2\rho^2\mathbf{w}^\dagger\mathbf{h}_i^\dagger\mathbf{h}_i\mathbf{w}\mathbb{1}((1-\theta(\alpha-1))^2\rho^2\mathbf{w}^\dagger\mathbf{h}_i^\dagger\mathbf{h}_i\mathbf{w}-\eta_i), \end{aligned} \tag{3.5}$$

and

$$(1-\theta)f_i(\mathbf{w}) + \theta f_i(\alpha\mathbf{w}) = -\alpha^2\rho^2\mathbf{w}^\dagger\mathbf{h}_i^\dagger\mathbf{h}_i\mathbf{w}. \tag{3.6}$$

As $\alpha$ was chosen such that the unit step function transitions from $0$ to $1$ in the region $[\mathbf{w}, \alpha\mathbf{w}]$, for a subset of $\theta$ denoted as $\mathcal{A}$, the unit step function in (3.5) becomes zero. Therefore, from (3.5) and (3.6) we have $f_i\left(((1-\theta(\alpha-1))\mathbf{w}\right) > (1-\theta)f_i(\mathbf{w}) + \theta f_i(\alpha\mathbf{w})$ for $\theta \in \mathcal{A}$. This means that the definition of convexity is violated as a section of the secant between $\mathbf{w}$ and $\alpha\mathbf{w}$ lies below the graph of $f_i(\mathbf{w})$. As the objective function in (3.3) is the summation of such non-convex functions, the objective function is non-convex.

## 3.3 Problem Solution

In this section, we approximate the problem in Section 3.2 as a convex optimization problem and derive an algorithm to obtain approximate solution. In order to approximate the objective function using a convex function, we consider a certain beamforming vector $\mathbf{w}$ and a scaling factor $\alpha \in [0, 1]$ similar to Section 3.2. By using the beamforming vector $\alpha\mathbf{w}$, the $i$th user receives $f(\alpha\mathbf{w}) = \alpha^2\rho^2\mathbf{w}^\dagger\mathbf{h}_i^\dagger\mathbf{h}_i\mathbf{w}$. Since the direction of the beamforming vector is fixed along $\mathbf{w}$, the function reduces to a quadratic equation of the variable $\alpha$. Figure 3.1 shows the harvested energy by the $i$th user given as $f(\alpha\mathbf{w})$, Energy considering the minimum energy requirements given in (3.4), and the convex approximation. It can be clearly seen from Figure 3.1 that the function with minimum energy requirement is non-convex. We obtain the approximate function given in the figure by using a line with gradient equal to the instantaneous gradient of the function

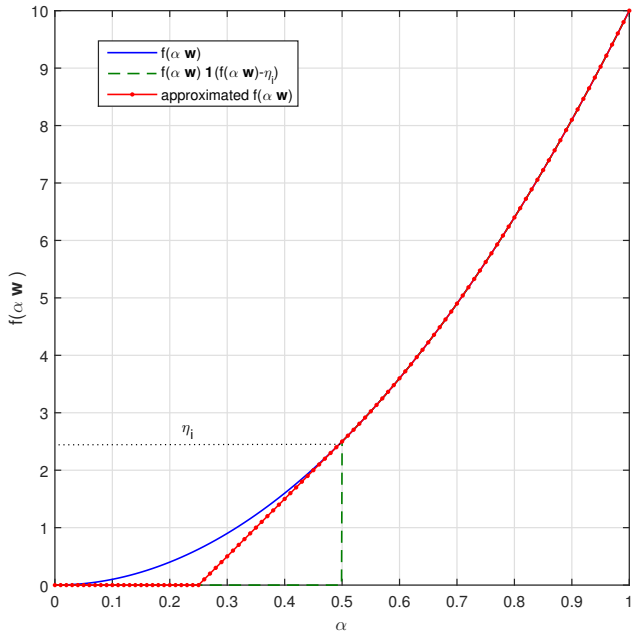


Figure 3.1: Variation of energy harvested by the $i$th user using $\alpha\mathbf{w}$ beamforming vector.

$f(\alpha\mathbf{w})$ at the point that achieves minimum energy requirement. Hence, the approximated convex function for (3.4) can be given as

$$f_i(\mathbf{w}) \approx \begin{cases} -\rho^2\mathbf{w}^\dagger\mathbf{h}_i^\dagger\mathbf{h}_i\mathbf{w}, & \text{for } \rho^2\mathbf{w}^\dagger\mathbf{h}_i^\dagger\mathbf{h}_i\mathbf{w} > \eta_i \\ \min\left(0, \eta_i - 2\rho\sqrt{\eta_i\mathbf{w}^\dagger\mathbf{h}_i^\dagger\mathbf{h}_i\mathbf{w}}\right), & \text{otherwise.} \end{cases} \tag{3.7}$$

The convex approximated optimization problem can be given as

$$\begin{aligned} \min_{\mathbf{w}\in\mathbb{C}^M} \quad & -\sum_{i=1}^{K} f_i(\mathbf{w}) \\ \text{s. t.} \quad & \mathbf{w}^\dagger\mathbf{w} \leq 1, \end{aligned} \tag{3.8}$$

where $f(\mathbf{w})$ is given in (3.7). We implement a gradient projection based algorithm to solve the convex problem. First, we reformulate the problem such that the problem can be solved in real domain. For this purpose, we re-write the complex beamforming

vector $\mathbf{w}$ by using $\mathbf{x} \in \mathbb{R}^{2M}$ as given in (3.19), and the $i$th complex channel vector by $\tilde{\mathbf{h}}_i = [\Re(\mathbf{h}_i) \;\; \Im(\mathbf{h}_i)]$. For presentation simplicity, we denote the matrix $\rho^2 \tilde{\mathbf{h}}_i^{\mathbf{T}} \tilde{\mathbf{h}}_i$ by $\mathbf{Q}_i \in \mathbb{R}^{2M \times 2M}$. It is worth noting that $\mathbf{Q}_i$ is a positive semidefinite matrix, i.e. $\mathbf{Q}_i \succeq 0$ and with rank 1. Then the optimization problem can be given by

$$\begin{aligned} \min_{\mathbf{x} \in \mathbb{R}^{2M}} \quad & -\sum_{i=1}^{K} f_i(\mathbf{x}) \\ \text{s. t.} \quad & \mathbf{x}^T \mathbf{x} \leq 1, \end{aligned} \tag{3.9}$$

where $f_i(\mathbf{x})$ is given as

$$f_i(\mathbf{x}) \approx \begin{cases} -\mathbf{x}^T \mathbf{Q}_i \mathbf{x}, & \text{for } \mathbf{x}^T \mathbf{Q}_i \mathbf{x} > \eta_i \\ \min\left(0, \eta_i - 2\sqrt{\eta_i \mathbf{x}^T \mathbf{Q}_i \mathbf{x}}\right), & \text{otherwise.} \end{cases} \tag{3.10}$$

## 3.4 Gradient Projection Based Algorithm

In this section, we adopt a well known gradient projection algorithm to solve the convex optimization problem in (3.9). This algorithm has two main steps: i) takes a step towards the steepest descent direction; and ii) projects the step onto the feasible region. This means that in each iteration, it is required to solve a sub-problem given by

$$\min_{\mathbf{x} \in \mathcal{X}} \; \|\mathbf{x} - \mathbf{z}\|_2, \tag{3.11}$$

where, $\mathbf{x}$ is the next step and $\mathbf{z}$ is the point obtained from taking a step towards the steepest descent direction. In order to achieve efficiency of the algorithm, this sub-problem must be easily solvable. Hence, such gradient projection algorithm may be efficiently used for optimization problems with simple constraints such as bound constraint. Due to the form of the constraint in problem (3.9), the optimum solution to the sub-problem reduces to normalizing the point $\mathbf{z}$, i.e., $\mathbf{x}^* = \mathbf{z}/\|\mathbf{z}\|$. Thus, a gradient projection based algorithm is suitable to efficiently solve the optimization problem in (3.9). The subse-

quent subsections discuss the algorithm in detail.

### 3.4.1 Projection Step

In this section, we discuss the projection step of the algorithm. Figure 3.2 shows the projection arc of the optimization problem. Since the total energy constraint is a Euclidean norm ball, the feasible set is illustrated as a circle in the figure. In order to obtain the next step, at a given point $\mathbf{x}$, we get the steepest descent direction $\mathbf{x} - \alpha\nabla f(\mathbf{x})$ where $\alpha$ is a variable step length. Then, if the resultant point is in the exterior of the feasible set, we project the point onto the feasible set such the Euclidean distance between the in-feasible point and the projected result is minimized. The set of such points obtained by using different $\alpha$ is known as the projection arc, $\mathbf{x}(\alpha)$ illustrated in red in the figure. As the feasible set is a unit norm ball, the projection arc can be given as

$$\mathbf{x}(\alpha) = \begin{cases} \mathbf{x} - \alpha \sum_{i=1}^{K} \nabla f_i(\mathbf{x}), & \text{for } \mathbf{x}^T\mathbf{x} \leq 1 \\ \frac{\mathbf{x} - \alpha \sum_{i=1}^{K} \nabla f_i(\mathbf{x})}{\|\mathbf{x} - \alpha \sum_{i=1}^{K} \nabla f_i(\mathbf{x})\|}, & \text{otherwise,} \end{cases} \tag{3.12}$$

where $\nabla f_i(\mathbf{x})$ is given by

$$\nabla f_i(\mathbf{x}) = \begin{cases} -2\mathbf{Q}_i\mathbf{x}, & \text{if } \mathbf{x}^T\mathbf{Q}_i\mathbf{x} > \eta_i \\ -2\sqrt{\frac{\eta_i}{\mathbf{x}^T\mathbf{Q}_i\mathbf{x}}}\mathbf{Q}_i\mathbf{x}, & \text{if } 4\mathbf{x}^T\mathbf{Q}_i\mathbf{x} < \eta_i \\ 0, & \text{otherwise.} \end{cases} \tag{3.13}$$

The projection arc, $\mathbf{x}(\alpha)$, consists of all the possible next iterates parameterised by $\alpha$. Further, it is important to ensure that all the steps taken are along a descent direction unless the algorithm has converged to the optimal point.

### 3.4.2 Descent Properties of the Algorithm

In this section, we show that every step taken until convergence is along a descent direction. We consider any point in the feasible region as $\tilde{\mathbf{x}}$ in Figure 3.2. As the feasible set is closed and convex, the angle between $\mathbf{x} - \alpha\nabla f(\mathbf{x}) - \mathbf{x}(\alpha)$ and $\tilde{\mathbf{x}} - \mathbf{x}(\alpha)$ is always

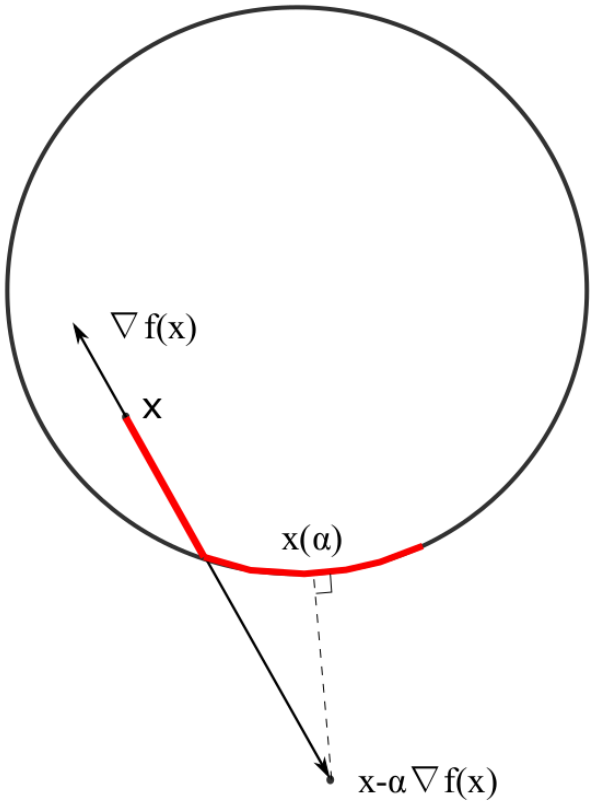


Figure 3.2: The projection arc for the optimization problem.

greater than $\pi/2$. Therefore, we have

$$(\mathbf{x} - \alpha\nabla f(\mathbf{x}) - \mathbf{x}(\alpha))^T (\tilde{\mathbf{x}} - \mathbf{x}(\alpha)) < 0. \tag{3.14}$$

When $\tilde{\mathbf{x}} = \mathbf{x}$, the inequality in (3.14) reduces to $(\mathbf{x} - \alpha\nabla f(\mathbf{x}) - \mathbf{x}(\alpha))^T (\mathbf{x} - \mathbf{x}(\alpha)) < 0$. By rearranging the terms, we have

$$\nabla f(\mathbf{x})^T(\mathbf{x}(\alpha) - \mathbf{x}) \leq -\frac{1}{\alpha}\|\mathbf{x}(\alpha) - \mathbf{x}\|^2. \tag{3.15}$$

This means that $\nabla f(\mathbf{x})^T(\mathbf{x}(\alpha) - \mathbf{x}) < 0$ for every $\mathbf{x}(\alpha) \neq \mathbf{x}$. Therefore, $\mathbf{x}(\alpha) - \mathbf{x}$ is a feasible descent direction for all $\alpha$.

### 3.4.3 Selection of Step Length

In this section, we discuss the procedure for choosing the step length for each iteration. In particular, we use the Armijo-like rule for choosing the step length. That is, at each step, we search for a sufficient decrease by checking steps $1, \beta, \beta^2, \cdots$ along the descent direction obtained for next step for $\beta \in (0, 1)$. In other words, we obtain the smallest $n$ such that

$$f(\mathbf{x} + \beta^n\mathbf{d}) \leq f(\mathbf{x}) + \beta^n\nabla f(\mathbf{x})^T\mathbf{d} \tag{3.16}$$

is satisfied. Here, the descent direction for next step $\mathbf{d}$ is given as $\mathbf{d} = \mathbf{x} - \mathbf{x}(\alpha)$ for a given $\alpha$.

## 3.5 Special Case when all users satisfy the minimum energy requirement

When all the users are in good radio conditions and/or the minimum energy requirement is low, all users may satisfy the minimum energy requirement. In such cases the optimization problem can be reduced as

Table 3.1:
Gradient projection algorithm for the optimization problem.

Select the parameters $\beta \in (0,1)$, $\alpha$ and $\tau_R$.
Initialize $\mathbf{x}_0$.
Set $k \leftarrow 0$ and $n \leftarrow 0$.

**Repeat** until $\left\|\mathbf{x}^+ - \mathbf{x}\right\| \geq \tau_R$
  Compute $\mathbf{d} \leftarrow \mathbf{x}(\alpha) - \mathbf{x}$ using (3.12)
  Set $n \leftarrow 0$
  **Repeat** until (3.16) does not hold
    Set $n \leftarrow n + 1$
  **end**
  Set $\mathbf{x}^+ \leftarrow \mathbf{x} + \beta^n \mathbf{d}$;
  Set $k \leftarrow k + 1$;
**end**

$$\begin{aligned} \max_{\mathbf{w}\in\mathbb{C}^M} \quad & \mathbf{w}^\dagger \mathbf{H}^\dagger \mathbf{D}^2 \mathbf{H} \mathbf{w} \\ \text{s. t.} \quad & \rho^2 \mathbf{w}^\dagger \mathbf{h}_i^\dagger \mathbf{h}_i \mathbf{w} \geq \eta_i \ \ \forall i \in [1, K], \\ & \mathbf{w}^\dagger \mathbf{w} \leq 1. \end{aligned} \tag{3.17}$$

This problem is a quadratically constrained quadratic program (QCQP). Since the matrix $\mathbf{H}^\dagger \mathbf{D}^2 \mathbf{H}$ is positive semidefinite, the objective function denoted as $f(\mathbf{w})$ is convex as,

$$\nabla^2 f(\mathbf{w}) = \mathbf{H}^\dagger \mathbf{D}^2 \mathbf{H} \succeq 0. \tag{3.18}$$

However, the minimum energy requirement inequality constraints are not convex. This is because the feasible set is the exterior of each ellipsoid given by $\rho^2 \mathbf{w}^\dagger \mathbf{h}_i^\dagger \mathbf{h}_i \mathbf{w} / \eta_i = 1$. Hence, care should be taken when implementing the algorithm to solve the optimization problem. The received energy at users is proportional to the transmit power. Therefore, the constraint $\mathbf{w}^\dagger \mathbf{w} \leq 1$ should be met with equality at the optimum.

### 3.5.1 Algorithm

In this section, we implement an algorithm based on well known interior point methods. First, we reformulate the problem such that the problem can be solved in real domain. For this purpose we re-write the beamforming vector, $\mathbf{x} \in \mathbb{R}^{2M}$ as

$$\mathbf{x} = \begin{bmatrix} \Re(\mathbf{w}) \\ \Im(\mathbf{w}) \end{bmatrix} \tag{3.19}$$

where $\Re(.)$ and $\Im(.)$ denote the real and imaginary components. Similarly, the $i$th channel vector can be re-written as $\tilde{\mathbf{h}}_i = [\Re(\mathbf{h}_i) \quad \Im(\mathbf{h}_i)]$. Furthermore, we re-write the channel matrix $\tilde{\mathbf{H}} \in \mathbb{R}^{2K \times 2M}$ as

$$\tilde{\mathbf{H}} = \begin{bmatrix} \Re(\mathbf{H}) & -\Im(\mathbf{H}) \\ \Im(\mathbf{H}) & \Re(\mathbf{H}) \end{bmatrix}. \tag{3.20}$$

For presentation simplicity, we denote the matrix $\rho^2 \tilde{\mathbf{h}}_i^{\mathbf{T}} \tilde{\mathbf{h}}_i$ by $\mathbf{Q}_i \in \mathbb{R}^{2M \times 2M}$. It is worth noting that $\mathbf{Q}_i$ is a positive semidefinite matrix, i.e. $\mathbf{Q}_i \succeq 0$ and with rank 1. Furthermore, we denote $\tilde{\mathbf{H}}^T \mathbf{D}^2 \tilde{\mathbf{H}} = \sum_{i=1}^{K} \mathbf{Q}_i$ as $\mathbf{Q}_T \in \mathbb{R}^{2M \times 2M}$. The optimization problem can be reformulated using slack variables $s_i, \ \forall i \in [1, K]$ as

$$\begin{aligned} \min_{\mathbf{x} \in \mathbb{R}^{2M}, s_i} \quad & -\mathbf{x}^T \mathbf{Q}_T \mathbf{x} \\ \text{s. t.} \quad & \mathbf{x}^T \mathbf{Q}_i \mathbf{x} - s_i = \eta_i \ \ \forall i \in [1, K], \\ & \mathbf{x}^T \mathbf{x} = 1, \ \ s_i \geq 0. \end{aligned} \tag{3.21}$$

Since the linear independence constraint qualifications (LICQ) holds at a point $\mathbf{x}$ (proof can be found in Appendix 3.8), the perturbed Karush-Kuhn-Tucker (KKT) conditions

for the problem can be written as

$$-2\left(\mathbf{Q}_T + \sum_{i=1}^{K} z_i \mathbf{Q}_i + y\mathbf{I}\right)\mathbf{x} = 0 \tag{3.22a}$$

$$\mathbf{x}^T\mathbf{Q}_i\mathbf{x} - \eta_i - s_i = 0 \ \ , \forall i \in [1, K] \tag{3.22b}$$

$$\mathbf{x}^T\mathbf{x} - 1 = 0 \tag{3.22c}$$

$$\mathbf{Z}\mathbf{s} = \mu\mathbf{e} \tag{3.22d}$$

where $z_i$ and $y$ are the Lagrange multipliers of the $i$th inequality constraint with $z_i \geq 0$, and equality constraint, respectively. We define the diagonal matrix $\mathbf{Z}$ as $\mathbf{Z} = \text{diag}\left([z_1, \cdots, z_K]\right)$ and $\mathbf{s} = [s_1, \cdots, s_K]^T$ with $\mathbf{s} \geq 0$, identity matrix as $\mathbf{I}$ and $\mathbf{e} = [1, \cdots, 1]^T$.

#### 3.5.1.1 Computing the Direction

By applying the Newton's method to the nonlinear system (3.22), in the variables $\mathbf{x}, \mathbf{s}, y, \mathbf{z}$, we have

$$\begin{bmatrix} -2\mathbf{A} & \mathbf{0} & -2\mathbf{x} & -2\mathbf{B} \\ \mathbf{0} & \mathbf{Z} & \mathbf{0} & \mathbf{S} \\ 2\mathbf{x}^T & \mathbf{0} & 0 & \mathbf{0} \\ 2\mathbf{B}^T & -\mathbf{I} & \mathbf{0} & \mathbf{0} \end{bmatrix} \begin{bmatrix} \mathbf{p}_x \\ \mathbf{p}_s \\ p_y \\ \mathbf{p}_z \end{bmatrix} = - \begin{bmatrix} -2\mathbf{A}\mathbf{x} \\ \mathbf{S}\mathbf{z} - \mu\mathbf{e} \\ \mathbf{x}^T\mathbf{x} - 1 \\ \mathbf{x}^T\mathbf{Q}_i\mathbf{x} - \eta_i - s_i \end{bmatrix} \tag{3.23}$$

where $\mathbf{A} = \left(\mathbf{Q}_T + \sum_{i=1}^{K} z_i\mathbf{Q}_i + y\mathbf{I}\right)$ and $\mathbf{B} \in \mathbb{R}^{2M \times K}$ is defined as $\mathbf{B} = [\mathbf{x}^T\mathbf{Q}_1, \cdots, \mathbf{x}^T\mathbf{Q}_K]^T$. The system (3.23) is known as the primal-dual system. Furthermore, by using

$$\mathbf{\Sigma} = \mathbf{S}^{-1}\mathbf{Z} \tag{3.24}$$

we re-write the system in the symmetric form as

$$\begin{bmatrix} -2\mathbf{A} & \mathbf{0} & 2\mathbf{x} & 2\mathbf{B} \\ \mathbf{0} & \mathbf{\Sigma} & \mathbf{0} & -\mathbf{I} \\ 2\mathbf{x}^T & \mathbf{0} & 0 & \mathbf{0} \\ 2\mathbf{B}^T & -\mathbf{I} & \mathbf{0} & \mathbf{0} \end{bmatrix} \begin{bmatrix} \mathbf{p}_x \\ \mathbf{p}_s \\ -p_y \\ -\mathbf{p}_z \end{bmatrix} = - \begin{bmatrix} -2\mathbf{A}\mathbf{x} \\ \mathbf{z} - \mu\mathbf{S}^{-1}\mathbf{e} \\ \mathbf{x}^T\mathbf{x} - 1 \\ \mathbf{x}^T\mathbf{Q}_i\mathbf{x} - \eta_i - s_i \end{bmatrix}. \tag{3.25}$$

#### 3.5.1.2 Handling Nonconvexity

The linear system (3.25) can be solved in order to obtain the next step $\mathbf{p} = (\mathbf{p}_x, \mathbf{p}_s, p_y, \mathbf{p}_z)$. However, due to the non-convexity of the problem discussed in Section 3.5, the direction obtained by solving the linear system may not always be productive because it seeks to locate only KKT points. Therefore, it can move towards a maximizer or other stationary points. The step $\mathbf{p}$ is a descent direction if the sub-matrix

$$\begin{bmatrix} -2\mathbf{A} & \mathbf{0} \\ \mathbf{0} & \mathbf{\Sigma} \end{bmatrix} \tag{3.26}$$

is positive definite on the null space of the constraint matrix

$$\begin{bmatrix} 2\mathbf{x}^T & \mathbf{0} \\ 2\mathbf{B}^T & -\mathbf{I} \end{bmatrix}. \tag{3.27}$$

In [41], Lemma 16.3 states that the positive definiteness condition holds if the inertia of the primal-dual matrix in (3.25) is given by $(2M + K, K + 1, 0)$, i.e., the matrix has $2M + K$ positive, $K + 1$ negative, and no zero eigenvalues. Therefore, we modify the primal-dual matrix as

$$\begin{bmatrix} -2\mathbf{A} + \delta\mathbf{I} & \mathbf{0} & 2\mathbf{x} & 2\mathbf{B} \\ \mathbf{0} & \mathbf{\Sigma} & \mathbf{0} & -\mathbf{I} \\ 2\mathbf{x}^T & \mathbf{0} & 0 & \mathbf{0} \\ 2\mathbf{B}^T & -\mathbf{I} & \mathbf{0} & \mathbf{0} \end{bmatrix} \tag{3.28}$$

where $\delta \geq 0$ is chosen such that the required inertia is obtained. Table 3.2 gives an

Table 3.2:
Inertia correcting Algorithm.

Factor (3.28) with $\delta = 0$. Select $\delta > 0$ and $m > 1$.

**if** the inertia of (3.28) is $(2M + K, K + 1, 0)$
  **stop**;
**else**
  **while** the inertia of (3.28) is not $(2M + K, K + 1, 0)$
    Set $\delta \leftarrow m\delta$;
  **end**
**end**

algorithm to select $\delta$ such that the required inertia is obtained. With this inertia modification, we can compute the next direction by replacing the primal-dual matrix in (3.25) with (3.28).

#### 3.5.1.3 Updating Variables

Once the direction is obtained as in Section 3.5.1.2, we then obtain suitable step lengths. By using the *fraction to the boundary rule*, we have

$$\alpha_s = \max\{\alpha \in (0, 1] : \mathbf{s} + \alpha \mathbf{p}_s \geq (1 - \tau)\mathbf{s}\}, \tag{3.29a}$$

$$\alpha_z = \max\{\alpha \in (0, 1] : \mathbf{z} + \alpha \mathbf{p}_z \geq (1 - \tau)\mathbf{z}\}, \tag{3.29b}$$

with $\tau \in (0, 1)$. A typical value of $\tau$ is 0.995. The conditions in (3.29) allow us to choose a step length such that the variables $\mathbf{s}, \mathbf{z}$ do not approach to zero prematurely. Now we compute the next iterate $(\mathbf{x}^+, \mathbf{s}^+, y^+, \mathbf{z}^+)$ as

$$\mathbf{x}^+ = \mathbf{x} + \alpha_s \mathbf{p}_x, \;\; \mathbf{s}^+ = \mathbf{s} + \alpha_s \mathbf{p}_s, \tag{3.30a}$$

$$y^+ = y + \alpha_z p_y, \;\; \mathbf{z}^+ = \mathbf{z} + \alpha_z \mathbf{p}_z. \tag{3.30b}$$

The barrier parameter $\mu$ is also needed to be updated. We fix $\mu$ for a series of iterations until the KKT conditions in (3.22) are achieved to a certain accuracy. In other words, if the error function is given by

$$\begin{aligned} E(\mathbf{x}, \mathbf{s}, y, \mathbf{z}; \mu) = \max \Big\{ & \|2\mathbf{A}\|, \|\mathbf{x}^T \mathbf{Q}_i \mathbf{x} - \eta_i - s_i\|, \\ & \|\mathbf{x}^T \mathbf{x} - 1\|, \|\mathbf{Z}\mathbf{s} - \mu \mathbf{e}\| \Big\}, \end{aligned} \tag{3.31}$$

the barrier parameter is fixed for a series of iterations such that $E(\mathbf{x}, \mathbf{s}, y, \mathbf{z}; \mu) > \mu$. Once this condition is violated, we update the barrier parameter as $\mu^+ = \sigma\mu$ for some $\sigma \in (0, 1)$.

#### 3.5.1.4 Terminating Conditions

It can be clearly seen from Section 3.5.1.3 that the algorithm has two nested loops as given in Table 3.3. Hence, we need two termination conditions for two loops. The inner loop termination condition is given by $E(\mathbf{x}, \mathbf{s}, y, \mathbf{z}; \mu) \leq \mu$. Thus, the inner loop will be terminated when the KKT conditions are satisfied with a certain accuracy. Next, we update the barrier parameter according to Section 3.5.1.3. The outer loop must be terminated when the algorithm has converged. Thus, we terminate the outer loop with the condition $\left| f(\mathbf{x}^+) - f(\mathbf{x}) \right| < \tau_R$, with $\tau_R \ll 1$.

#### 3.5.1.5 Initial Point

Since the optimization problem is nonconvex there may be more than one stationary point. The Theorem 19.1 in [41] states that if the algorithm in Table 3.3 converges and LICQ holds, the limit point satisfies the first-order optimal conditions. However, we cannot guarantee the limit point given by the algorithm to be a global minimum. The limit point may depend on the initial point and therefore the algorithm is not globally convergent. By using the structure of the optimization problem, we initialize $\mathbf{x}$ with the principal eigenvector of the matrix $\mathbf{Q}_T$, i.e., $\mathbf{x}_0 = \mathbf{v}_1$. We choose the eigenvector $\mathbf{v}_1$ because when we relax the inequality constraints of the problem (3.21), we have

Table 3.3:
MU-MISO Beamforming Algorithm.

Select the initial barrier parameter $\mu_0 > 0$ and parameters $\sigma, \tau$, and $\tau_R \in (0, 1)$.
Initialize $(\mathbf{x}_0, \mathbf{s}_0, y_0, \mathbf{z}_0)$ according to Section 3.5.1.5.
Set $k \leftarrow 0$.

**Repeat** until $\left|f(\mathbf{x}^+) - f(\mathbf{x})\right| \geq \tau_R$
  **Repeat** until $E(\mathbf{x}_k, \mathbf{s}_k, y_k, \mathbf{z}_k) \geq \mu_k$
    Correct inertia of primal-dual matrix with the algorithm in Table 3.2;
    Solve (3.25) to obtain the direction $\mathbf{p} = (\mathbf{p}_x, \mathbf{p}_s, p_y, \mathbf{p}_z)$;
    Compute $(\mathbf{x}_{k+1}, \mathbf{s}_{k+1}, y_{k+1}, \mathbf{z}_{k+1})$ using (3.29) and (3.30);
    Set $\mu_{k+1} \leftarrow \mu_k$ and $k \leftarrow k + 1$;
  **end**
  Choose $\mu_k \in (0, \sigma\mu_k)$;
**end**

$$\begin{aligned} \min_{\mathbf{x}\in\mathbb{R}^{2M}} \quad & -\mathbf{x}^T\mathbf{Q}_T\mathbf{x} \\ \text{s. t.} \quad & \mathbf{x}^T\mathbf{x} = 1. \end{aligned} \tag{3.32}$$

The optimum of the problem (3.32) is the largest eigenvalue, $\lambda_1$, which is obtained by using the principal eigenvector of $\mathbf{Q}_T$, i.e., $\mathbf{x}^* = \mathbf{v}_1$. This means that the total energy harvested is maximized by using $\mathbf{v}_1$. Thus, $\mathbf{x}_0 = \mathbf{v}_1$ may be the best initial point we can choose. This can also be seen as warm starting of the algorithm. We further initialize $\mathbf{S}$ by $\mathbf{S}_0 = \mathbf{I}$ and from (3.22d) we have $\mathbf{Z}_0 = \mu\mathbf{I}$. Therefore, from (3.22a) we initialize $y$ as $y_0 = -(1 + \mu)\lambda_1$.

## 3.6 Numerical and Simulation Results

In this section, we obtain numerical results for the optimization problem to evaluate the performance of the algorithm. We assume independent and identically distributed (i.i.d.)

complex Gaussian channels with zero mean and unit variance, i.e.,$h_{ij} \sim \mathcal{CN}(0,1)$. Further, we assume $\rho_i = 1$ and $\eta = 0.7, \forall i \in [1, K]$.

Next, we consider networks consisting two transmit antennas ($M = 2$) and $K = 2, 4, 6$ and $8$ single antenna users. We implement the algorithms given in Table 3.2 and Table 3.1 and obtain the approximate solution $\mathbf{x}^*$.

In order to verify and compare the results using a benchmark, we solve the optimization problem using the CVX toolbox. However, in order to handle the non-convexity of the problem we use SDR to approximately solve the problem. For this purpose, by defining $\mathbf{X} = \mathbf{x}\mathbf{x}^\dagger$, we rewrite the problem in (3.17) as

$$\begin{aligned} \min_{\mathbf{X} \in \mathbb{C}^{M \times M}} \quad & -\operatorname{Tr}\left(\mathbf{H}^\dagger \mathbf{H} \mathbf{X}\right) \\ \text{s. t.} \quad & \operatorname{Tr}\left(\mathbf{h}_i^\dagger \mathbf{h}_i \mathbf{X}\right) \geq \eta_i \ \ \forall i \in [1, K], \\ & \operatorname{Tr}\left(\mathbf{X}\right) = 1, \\ & \operatorname{Rank}\left(\mathbf{X}\right) = 1, \quad \mathbf{X} \succeq 0, \end{aligned} \tag{3.33}$$

where $\operatorname{Tr}(.)$ denotes the trace operator. Although the non-convex minimum energy constraints in (3.17) are transformed into linear trace constraints, the transformation $\mathbf{X} = \mathbf{x}\mathbf{x}^\dagger$ requires the additional rank constraint which is non-convex. Thus, we relax the problem by removing the rank constraint as

$$\begin{aligned} \min_{\mathbf{X} \in \mathbb{C}^{M \times M}} \quad & -\operatorname{Tr}\left(\mathbf{H}^\dagger \mathbf{H} \mathbf{X}\right) \\ \text{s. t.} \quad & \operatorname{Tr}\left(\mathbf{h}_i^\dagger \mathbf{h}_i \mathbf{X}\right) \geq \eta_i \ \ \forall i \in [1, K], \\ & \operatorname{Tr}\left(\mathbf{X}\right) = 1, \quad \mathbf{X} \succeq 0. \end{aligned} \tag{3.34}$$

In order to compensate for the relaxation, the solution obtained from the CVX toolbox, $\mathbf{X}_{opt}$ is post-processed to obtain a rank one solution. This process is known as the *randomization*. This allows us to generate a set of candidate vectors, and then, the

best approximate solution can be selected from that set of candidate vectors [42]–[45]. We focus on three randomization techniques that are available in the literature: *randA, randB* and *randC* [42], [43].

- *randA*: we calculate the eigen-decomposition of $\mathbf{X}_{opt} = \mathbf{U}\mathbf{\Sigma}\mathbf{U}^{\dagger}$, where $\mathbf{\Sigma}$ is the diagonal eigenvalue matrix $\mathbf{U}$ is the eigenvector matrix. Then we generate a set of candidate vectors $\{\mathbf{w}_c\}$ such that $\mathbf{w}_c = \mathbf{U}\mathbf{\Sigma}^{1/2}\mathbf{v}_c$ where $\mathbf{v}_c \in \mathbb{C}^M$ is a vector of independent random variables which are uniformly distributed on the unit circle in the complex plane. This technique ensures that the trace constraint in (3.34) is satisfied for any realization of $\mathbf{v}_c$.

- *randB*: we generate a set of candidate vectors $\{\mathbf{w}_c\}$ such that $[\mathbf{w}_c]_i = \sqrt{[\mathbf{X}_{opt}]_{ii}}[\mathbf{v}_c]_i$.

- *randC*: we generate $\{\mathbf{w}_c\}$ such that $\mathbf{w}_c = \mathbf{U}\mathbf{\Sigma}^{1/2}\mathbf{g}_c$, where $\mathbf{g}_c$ is a vector of zero mean and unit variance complex circularly symmetric uncorrelated Gaussian random variables such that $\mathbb{E}[\mathbf{w}_c\mathbf{w}_c^{\dagger}] = \mathbf{X}_{opt}$. The resulting $\{\mathbf{w}_c\}$ must be normalized to meet the power budget $\|\mathbf{w}_c\|^2 = 1$.

We generate $100$ candidate vectors per randomization technique and the best solution of these three randomization techniques, $\mathbf{w}_{\mathbf{c}}^*$, can be selected such that it yields the largest value for the objective function in (3.34).

### 3.6.1 Results for special Case

We use above technique to find the approximate solution using the CVX toolbox and compare it against the results of the beamforming algorithm in Section 3.5.1. We generate 1000 channel matrices $\mathbf{H}$ for each network size, i.e., $M = 2$ and $K = 2, 4, 6, 8,$ and 10.

Figure 3.3 shows the times taken for the beamforming algorithm in Section 3.5.1 and the CVX together with randomization for each instant of the channel $i$ for $K = 2, 4, 6, 8$ and 10, in shades of blue and red, respectively. The minimum time taken for the beamforming algorithm for $K = 2$ to $K = 10$ is $0.2\,\mathrm{ms}$ to $6\,\mathrm{ms}$ while for the CVX

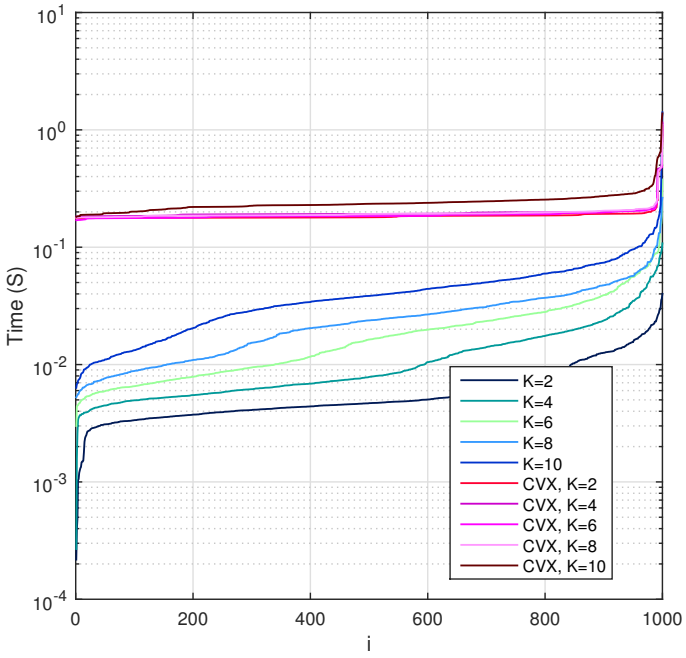


Figure 3.3: The solving time for the two algorithms for different network sizes.

based algorithm the time taken is $0.17\,\mathrm{s}$ to $0.18\,\mathrm{s}$. It can be clearly seen that the time taken for the beamforming algorithm is much smaller than the time taken for the CVX based algorithm.

Figure 3.4 illustrates the minimum Energy harvested by users for each instant of the channel $i$ for $K = 2, 4, 6, 8$ and 10, using the beamforming algorithm and the CVX based algorithm, in shades of blue and red, respectively. For each network size, the channel instances $i$ are sorted such that the minimum energy harvested by using the beamforming algorithm is in ascending order. It can be seen that the minimum energy levels obtained using the two algorithms are approximately the same, with the minimum energy level harvested using the beamforming algorithm slightly outperform the CVX based algorithm. However, when the network size increases, e.g., $K = 8$ and 10, the CVX result has not been able to match the beamforming algorithm. In these situations, the energy levels obtained by the CVX based algorithm is lower than the energy level obtained using the beamforming algorithm, sometimes even below the minimum

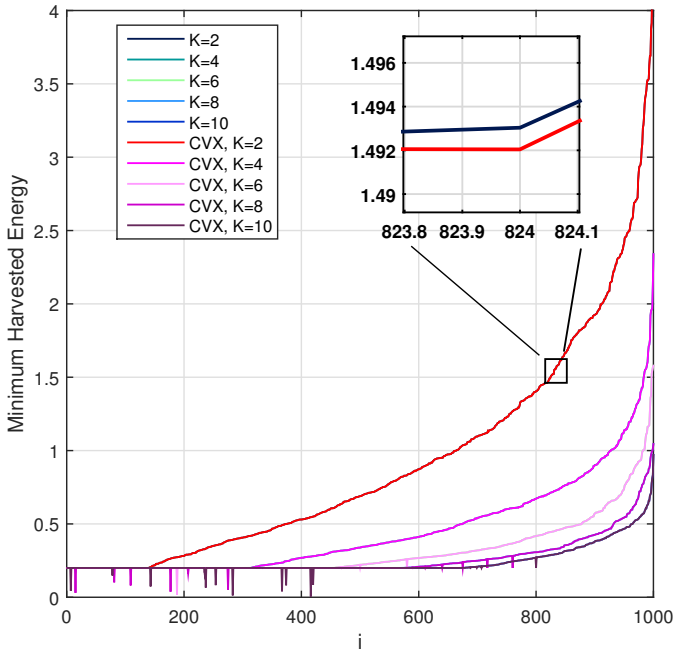


Figure 3.4: Minimum energy levels harvested by using the two algorithms.

threshold $\eta = 0.2$. For example at the channel instant $i = 109$, the minimum energy levels obtained by the beamforming algorithm and the CVX based algorithm is $0.2$ and $0.0805$, respectively. The latter violates the minimum energy constraint. This is because the randomization techniques have not been designed to ensure that all the solutions are feasible. We can impose constraints such that the best candidate vector is in feasible region. However, this may further decrease the efficiency of the CVX based algorithm.

Figure 3.5 shows the total energy harvested by using the two algorithms for 1000 channel instances with network sizes $M = 2$ and $K = 2, 4, 6, 8$ and 10. For each network size, the channel instances $i$ are sorted such that the total energy harvested by using the beamforming algorithm (illustrated in shades of blue) is in ascending order. The corresponding results for the CVX based algorithm is illustrated in shades of red. It can be seen that most of the energy levels obtained from the two algorithms are approximately equal except for some finite occasions. These spurious results correspond to the channel instances where the CVX based algorithm failed to satisfy the minimum

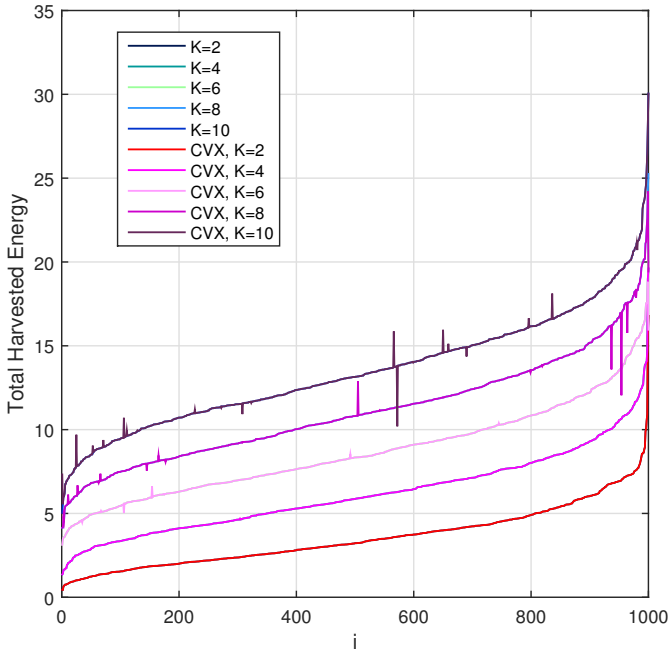


Figure 3.5: The total energy harvested by using the two algorithms.

energy constraints.

Figure 3.6 shows the time taken by the two algorithms averaged over the 1000 instances with the number of users (network size with $M = 2$). The average time taken for 2 users using the beamforming algorithm and the CVX based algorithm are, $6.32\,\mathrm{mS}$ and $0.18\,\mathrm{S}$, respectively. This means that in this case, the beamforming algorithm is approximately 29 times faster than the CVX base algorithm. Furthermore, it can be seen that the average run time increases with the network size.

### 3.6.2 Results for General Case

In this section we focus on the general case of the problem where all users may not be able to harvest their minimum energy requirement. We implement the algorithms given in Table 3.1 and obtain the approximate solution $\mathbf{x}^*$. In order to verify and compare the results using a benchmark, we solve the optimization problem discussed in section 3.5 using the CVX algorithm for each and every subset of users. We consider the solutions

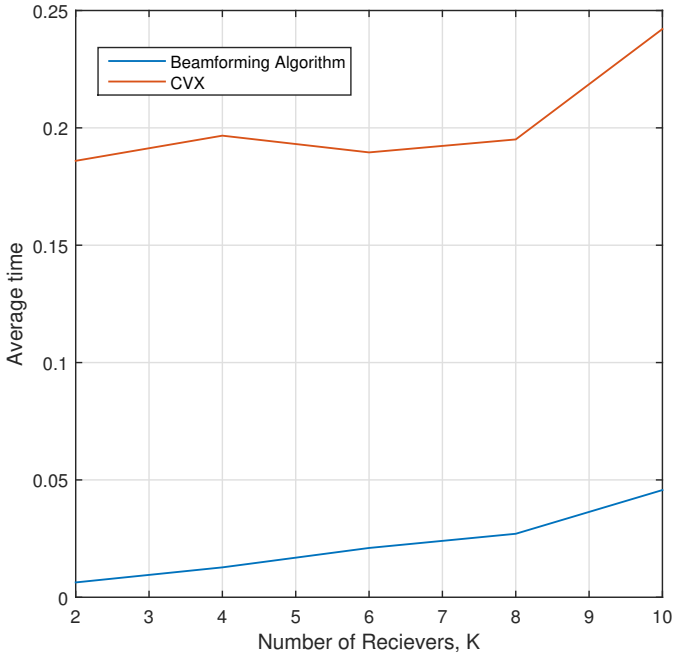


Figure 3.6: Average run time of the two algorithms with the number of users.

obtained for each subset as the candidate solution set for the problem in concern. Then, we choose the optimum solution as the maximum value from the candidate set and consider the corresponding set of users as the active users. We name this method as the exhaustive SDP algorithm.

Figure 3.7 shows the total energy harvested by the active users by using the two algorithms for different number of users. We apply both algorithms for 1000 set of channel realizations. The solutions obtained for these realizations are sorted into ascending order to achieve clarity of the figure. We note that the exhaustive SDP algorithm outperforms the proposed algorithm. This is because the proposed algorithm merely gives an approximate solution due to convex approximation of the objective function. When $K = 2$, we can see that both algorithms have resulted in zero harvested energy for the case when $i < 65$. This is because when the number of users is small, the probability of at least one user may be able to achieve its minimum energy requirement is low. Therefore, for $65$ instances out of the $1000$ considered, both users are inactive. Further,

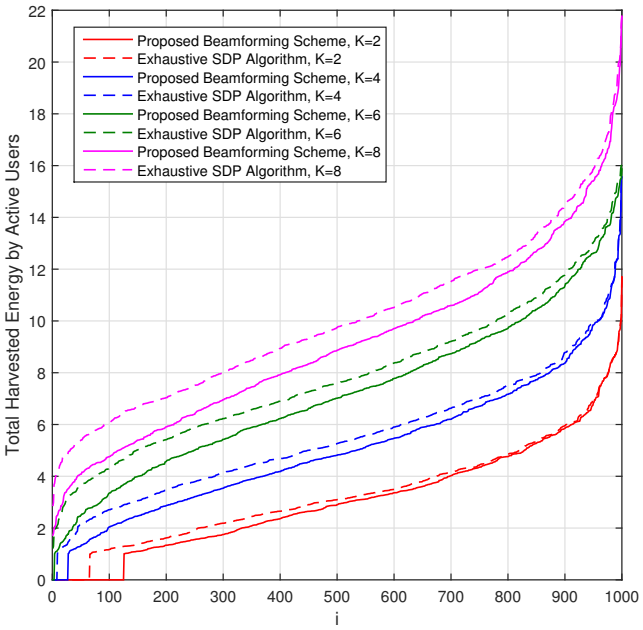


Figure 3.7: The total energy harvested by the active users for different number of users for the two algorithms.

in case $K = 2$, we note that when $65 \leq i < 125$, the total energy harvested by the active users is zero for the proposed algorithm while the exhaustive SDP algorithm produces a positive value. This is also because of the convex approximation. As the sudden change in step function is replaced by a smooth approximation, the proposed algorithm has converged at a point in the smooth transition. However, when we post process the solution to obtain the users with minimum energy, both users are not active, Therefore, the solution is zero. The same effect can be seen for the case $K = 4$ when $8 \leq i < 27$.

Figure 3.8 shows the execution times taken by the algorithms for different number of users. We see that the execution times taken by the exhaustive SDP algorithm is remarkably higher compared to the proposed algorithm.

## 3.7 Conclusions

In this chapter, we study the problem of maximizing the total energy harvested by users satisfying the minimum energy constraint. We formulate the non-convex problem and

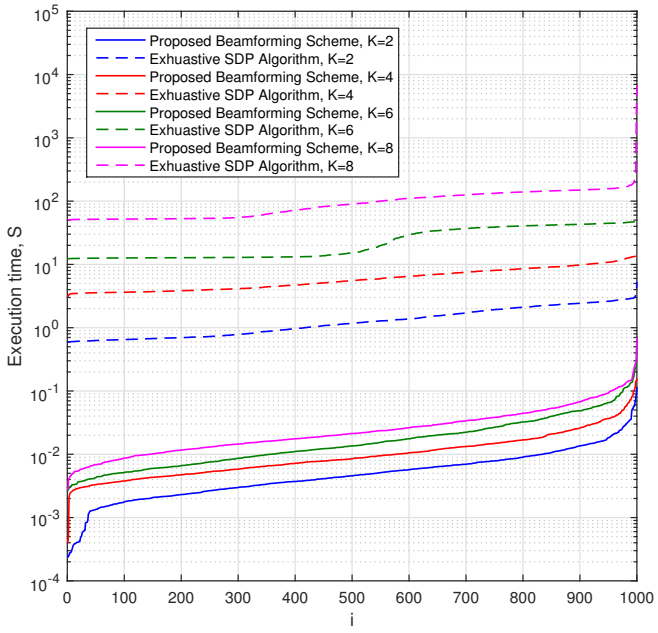


Figure 3.8: The execution times taken by the two algorithms for different number of users.

approximately solve for the beamforming vector by using a gradient projection based algorithm on the convexified problem. We identify that in good radio conditions and/or low minimum energy requirements, all users may harvest their minimum energy requirements. For this case, we obtain the optimum energy beamforming design such that the total harvested energy of the network is maximized while the minimum energy requirement of each user in the network is achieved. We implement an IPM based algorithm to obtain the optimum beamforming vector. We verify and compare the results of the algorithm by using the results obtained by performing SDR to the problem and solving the SDP using CVX toolbox. These results indicate that the accuracy and the speed of the beamforming algorithm outperforms the CVX based algorithm. For the general problem, we solved the optimization problem discussed in section 3.5 for every subset of the users, and obtained the maximum total harvested energy. This can be used as a performance benchmark. These results indicate that the speed of the proposed al-

gorithm outperforms the exhaustive SDP algorithm although the accuracy is affected by the convex approximation.

## 3.8 Appendix

The channels $h_{i,j}$ can be modeled as continuous random variables. Therefore, the probability of the channel being a constant $a$ where $a \in \mathbb{C}$ is zero, i.e., $\mathbb{P}[h_{i,j} = a] = 0$. Since, $\mathbf{Q}_i = \rho^2 \tilde{\mathbf{h}}_i^T \tilde{\mathbf{h}}_i, \ \forall i \in [1, K]$, the $i$th users channel matrix $\mathbf{Q}_i$ consists of continuous random variables. Therefore, $\mathbb{P}[a_l \mathbf{Q}_l + a_n \mathbf{Q}_n = 0] = 0$ for $a_l, a_n \in \mathbb{R}$, $l, n \in [1, K]$ and $l \neq n$. In other words, the users $l$ and $n$ have linearly independent channel matrices almost surely (with probability one).

Considering the constraints of the problem given in (3.21), $c_i(\mathbf{x}) = \mathbf{x}^T \mathbf{Q}_i \mathbf{x} - s_i - \eta_i = 0 \ \ \forall i \in [1, K]$, and $c_p(\mathbf{x}) = \mathbf{x}^T \mathbf{x} - 1$ we have

$$\nabla c_i(\mathbf{x}) = 2\mathbf{Q}_i \mathbf{x}, \ \ \forall i \in [1, K] \tag{3.35a}$$

$$\nabla c_p(\mathbf{x}) = 2\mathbf{x}. \tag{3.35b}$$

Since all the constraints are equality constraints, for a given feasible point $\mathbf{x}$ all the constraints are in the active set $\mathcal{A}(\mathbf{x})$. As $\mathbf{Q}_i \ \forall i \in [1, K]$ are lineally independent almost surely, the gradients of the constraints given in (3.35) are linearly independent almost surely. This means LICQ holds for any feasible point $\mathbf{x}$ almost surely.

# Chapter 4

# Energy Beamformer Design for Minimum Harvested Energy Maximization.

*In this chapter, we consider energy harvesting in a multi-user multi-input single-output (MU-MISO) network, and investigate two energy beamforming schemes which ensure fairness among the energy levels harvested by all users in the network. In particular, we investigate how to maximize the minimum harvested energy in the network by using i) a single beamforming vector; and ii) multiple beamforming vectors. We solve these problems by using semidefinite programming. The performance of different beamforming techniques is discussed with the aid of numerical simulations.*

## 4.1 Introduction

There has been a recent growing interest in studying wireless powered communication networks (WPCNs), where energy harvested from radio frequency (RF) signals is used to power wireless terminals in the network [17], [46]. This becomes a promising alternative for prolonging the lifetime of conventional battery powered wireless devices [17], [22], [23], [47]. For instance, use of energy harvesting in wireless sensor networks (WSNs) can mitigate the inconvenient or even in some cases infeasible battery replace-

ment process [22], [23], [48]. However, harvested energy at the receiver may depend on several parameters such as transmit power, wavelength, distance, efficiency of the antennas, etc. Among them, a key concern in RF energy harvesting is the propagation path loss with the transmission distance.

In information transmission, beamforming techniques are used to improve the received signal-to-noise ratio (SNR) at the receiver. A similar concept can be applied in energy harvesting, but to improve the received energy level. Although information beamforming has been investigated extensively in the literature, energy beamforming is still relatively new to the research community. Advanced energy beamforming techniques can improve the energy transfer efficiency significantly [24]. By carefully shaping the transmit waveform at each antenna, energy beamforming can control the collective behaviour of the radiated waveforms causing them to coherently combine at a specific receiver. Further, compared to single antenna omni-directional transmission, using multi-antenna transmission with beamforming, energy transfer efficiency can be further improved without additional bandwidth or increased transmit power [19].

Different beamforming designs have been explored to transmit RF energy towards receivers with different information and/or energy requirements. In [49], a beamforming design is proposed for a multi-antenna power transmitter to energize single-antenna users. Then, users utilize all harvested energy to transmit their individual information to a single-antenna sink based on the time-division-multiple-access (TDMA) scheme. For perfect channel state information (CSI), the beamforming vector at the transmitter is designed in order to maximize the sum-throughput. However, solutions are not in closed form. Imperfect CSI is considered in [50]–[52] where optimizing time for channel state estimation and energy transfer are discussed for different objectives. In [53], a multi-user multi-input single-output (MU-MISO) network which has one information receiver (IR) and multiple energy harvesting receivers (ERs) operating simultaneously is considered for i) maximizing the secrecy rate for the IR subject to individual harvested energy constraints of ERs; and ii) maximizing the weighted sum-energy transferred to ERs

subject to a secrecy rate constraint for IR. When there is no IR, the second optimization problem reduces to a fair energy allocation scheme (weighted sum maximization) for multiple ERs. For this problem, the optimum beamforming vector is obtained by using eigen analysis. However, weighted sum maximization is not the only scheme that can be used to achieve fairness. Hence, in this chapter, we focus on different schemes that can achieve fairness among the energy levels of the users.

We study a WPCN with a fixed power supply which coordinates the wireless energy transmissions to a set of distributed users. All users have rechargeable batteries that are assumed to have no other energy sources. Unlike works on simultaneous wireless information and power transfer (SWIPT) ([24]–[28]), which focused on the simultaneous energy and information transmissions to users, in this chapter, we consider a setup where the transmitter broadcasts only wireless energy to all users. This set up can be applied for several applications: i) In sensor networks, the users transmit their independent information using their individually harvested energy to a remote data centre [54]–[56]; ii) In "harvest-then-transmit" protocol, the transmitter (access point) first broadcasts wireless energy to all users in the downlink, and then the users forward their information to the access point (e.g., by TDMA) [57], [58]; and iii) In other wireless networks, the energy harvesting users can support their own secondary network in cognitive radio networks [59], or can act as cooperative/intermediate nodes in relay networks [60]–[62].

Therefore, it is an interesting problem to analyse how fairness can be achieved when transmitter broadcasts only wireless energy to all users. To fill this research gap, in this paper, we propose two energy beamforming designs for MU-MISO networks to achieve fairness by using max-min criterion:

- *Single beamforming vector* which is used for the entire charging time to maximize the minimum harvested energy among all users in the network.

- *Multiple beamforming vectors* which are used in different times to maximize the minimum harvested energy among all users in the network.

Further, our optimization problem which maximize the minimum harvested energy can overcome the near-far problem with user locations. Different from [53], these beamforming designs achieve fairness without the need of knowing the weights to be used to achieve fairness. Since there are more degrees of freedom with multiple beamformers, in terms of time (use of different time slots) and space (use of different beamforming vectors), the worst user achieves higher energy levels than in the single beamforming case.

The rest of this chapter is organized as follows. Section 4.2 develops the proposed approach to maximize the minimum harvested energy using a single beamforming vector. Section 4.3 extends the beamforming design for multiple beamforming vectors at different times. Section 4.4 presents numerical and simulation results followed by concluding remarks in Section 4.5.

## 4.2 Max-Min Fair Energy Beamforming

In this section, we consider the MU-MISO wireless communication network discussed in Section 2.2. We use the max-min criterion to achieve fairness among users, i.e., this criterion maximizes the minimum energy level of all users. However, this does not guarantee that we maximize the total harvested energy. Thus, the energy harvesting problem can be formulated as

$$\begin{aligned} &\max_{\mathbf{w}\in\,\mathbb{C}^M} \min_{i\in[1,K]} \quad P_i = \rho_i^2 \mathbf{h}_i \mathbf{w}\mathbf{w}^\dagger \mathbf{h}_i^\dagger \\ &\text{subject to } \ \|\mathbf{w}\|^2 \leq 1. \end{aligned} \tag{4.1}$$

The received energy at users is proportional to the transmit power. Therefore, the constraint $\|\mathbf{w}\|^2 \leq 1$ should be met with equality at an optimum. Hence, we re-write the optimization problem in (4.1) as

$$\begin{aligned} &\max_{\mathbf{w}\in\,\mathbb{C}^M} \min_{i\in[1,K]} \quad P_i = \rho_i^2 \mathbf{h}_i \mathbf{w}\mathbf{w}^\dagger \mathbf{h}_i^\dagger \\ &\text{subject to } \ \|\mathbf{w}\|^2 = 1. \end{aligned} \tag{4.2}$$

A similar problem is considered to maximize the multicast channel capacity in [42], [63]. For the special case of two transmit antennas ($M = 2$) a prune and search algorithm (PASA) is developed to find the global optimal beamforming vector in [63]. However, due to the complexity of this optimization problem, it cannot be solved analytically for a closed form solution. Thus, we consider the special case of two transmit antennas and two energy harvesting users ($\text{Rx}_1$ and $\text{Rx}_2$), i.e., $M = K = 2$. This may help for a better understanding of the general problem ($M, K > 2$).

### 4.2.1 Special Case (M=K=2)

From $P_i = \rho_i^2 \|\mathbf{h}_i \mathbf{w}\|^2 = \rho_i^2 \mathbf{h}_i \mathbf{w}\mathbf{w}^\dagger \mathbf{h}_i^\dagger$, we can notice that the energy harvested by $\text{Rx}_i$ is the square of the vector projection of the channel vector $\mathbf{h}_i$ onto the beamforming vector $\mathbf{w}$. Hence, to obtain the optimum solution, $\mathbf{w}$ must be selected such that the minimum vector projection of $\mathbf{h}_i$ onto $\mathbf{w}$ is maximized. When $M = K = 2$, consider the user with smaller channel norm. If it so happens that the magnitude on the inner product of the other user's channel with the smaller channel is bigger than the norm of the smaller channel, then the optimal beamforming vector must simply be in the direction of the smaller channel. Otherwise, the beamforming vector should be rotated to the point where the projections of both vectors onto the beamformer are equal (and so the harvested energy is equal). Unfortunately this simple reasoning does not extend to the general case.

### 4.2.2 General Case (M,K>2)

Although, this problem can be solved simply for $M = K = 2$, it may be difficult to solve in closed form for the general case. Further, when we increase the number of users $K$, the computational complexity also increases (e.g. we need longer computation time), because the general case is an NP-hard optimization problem [42], [63]. Therefore, we find an approximate solution by using a relaxed problem. Further, a similar problem is analysed in [42] in which a two-step approach has been proposed to formulate a problem which can be solved using semidefinite programming. Thus, we define our problem as

follows. In the first step, the original problem is reformulated as

$$\begin{aligned} \max_{\mathbf{X}\in\mathbb{C}^{M\times M}} \quad & \min_{i\in[1,K]} \quad \mathrm{Tr}(\mathbf{X}\mathbf{Q}_i) \\ \text{s. t.} \quad & \mathrm{Tr}(\mathbf{X}) = 1, \\ & \mathbf{X} \succeq 0, \\ & \mathrm{Rank}(\mathbf{X}) = 1, \end{aligned} \tag{4.3}$$

where $\mathrm{Tr}(.)$ is the trace operator, $\mathbf{Q_i}$ and $\mathbf{X}$ are defined as $\mathbf{Q}_i := \rho_i^2 \mathbf{h}_i^\dagger \mathbf{h}_i$ and $\mathbf{X} := \mathbf{w}\mathbf{w}^\dagger$ respectively. By relaxing the non-convex rank constraint, $\mathrm{Rank}(\mathbf{X}) = 1$, and introducing an additional variable $t \in \mathbb{R}$, the relaxed problem can be given as

$$\begin{aligned} \min_{\mathbf{X}\in\ \mathbb{C}^{M\times M},\ t\in\mathbb{R}} \quad & -t \\ \text{subject to} \quad & \mathrm{Tr}(\mathbf{X}\mathbf{Q}_i) \geq t, \forall i \in [1, K], \\ & \mathrm{Tr}(\mathbf{X}) = 1, \\ & \mathbf{X} \succeq 0. \end{aligned} \tag{4.4}$$

This problem can be solved using standard semidefinite program solvers such as CVX [64]. Since the rank constraint is removed, the solution $\mathbf{X}_{opt}$ may not be rank one in general. Therefore, as the second step, the solution is post-processed to achieve a rank-one solution. This process is known as randomization. This allows us to generate a set of candidate vectors from which the best approximate solution can be selected ([42]–[45]).

## 4.3 Max-Min Fair Multiple Beamforming

In Section 4.2, we obtained an approximate beamforming vector such that the minimum harvested energy is maximized. This beamforming vector is used to deliver energy to all users for the entire charging time $T_c$. We now extend this problem by allowing use of multiple beamforming vectors within $T_c$. As shown in Figure 4.1a, each beamfoming vector is used for time duration $T_c/r$ where $r$ denotes the number of beamforming vectors used. Therefore, the extended optimization problem can be given as

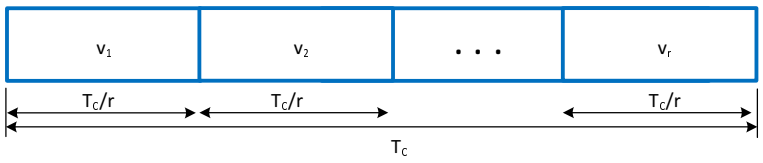


(a)

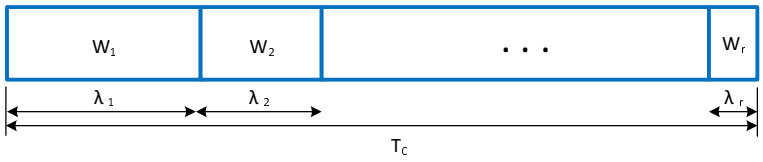


(b)

Figure 4.1: Time-slot allocation for multiple beamforming scheme using (a) equal durations; and (b) different durations.

$$\begin{aligned} \max_{\{\mathbf{v}_l\}} \quad & \min_{i\in[1,K]} \quad P_i = \sum_{l=1}^{r} \rho_i^2 \mathbf{h}_i \mathbf{v}_l \mathbf{v}_l^\dagger \mathbf{h}_i^\dagger \\ \text{subject to} \quad & \sum_{l=1}^{r} \|\mathbf{v}_l\|^2 = 1. \end{aligned} \tag{4.5}$$

The constraint $\sum_{l=1}^{r} \|\mathbf{v}_l\|^2 = 1$ ensures that the power budget at the transmitter is met. We solve this problem by using a similar approach to that used in Section 4.2.2. We define $\mathbf{Y} \in \mathbb{C}^{M\times M}$ as $\mathbf{Y} := \sum_l^r \mathbf{v}_l \mathbf{v}_l^\dagger$.

It is important to note that $\mathbf{Y}$ is a matrix with rank $\min(r, M)$. For the case of $r > M$, the set of beamforming vectors $\{\mathbf{v}_l\}$ are no longer linearly independent to each other. Hence, without loss of generality we can assume that $r \leq M$. Then, we transform problem in (4.5) to a SDP which is given as

$$\begin{aligned} \max_{\mathbf{Y}\in\mathbb{C}^{M\times M}} \quad & \min_{i\in[1,K]} \quad \mathrm{Tr}(\mathbf{Y}\mathbf{Q_i}) \\ \text{subject to} \quad & \mathrm{Tr}(\mathbf{Y}) = 1, \\ & \mathbf{Y} \succeq 0. \end{aligned} \tag{4.6}$$

Note that we do not need a rank constraint in (4.6) as we can select $r$ to be equal to the rank of the optimal $\mathbf{Y}$. Therefore, $\mathbf{Y}_{opt}$ can be obtained by solving the following

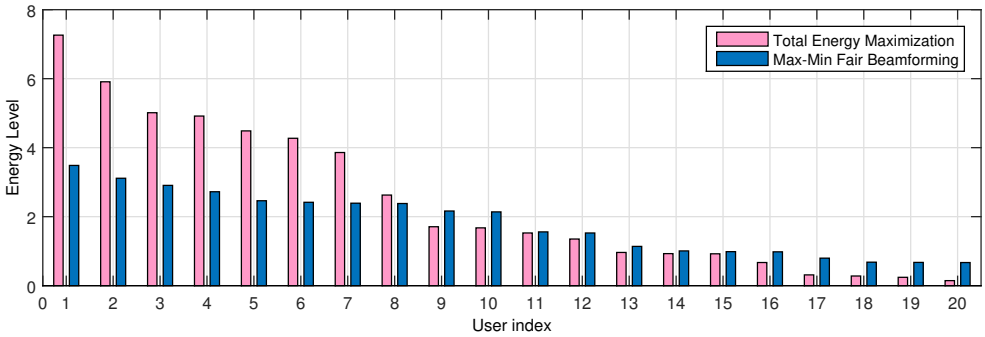


Figure 4.2: Energy harvested by each user for two energy harvesting schemes.

problem:

$$\begin{aligned} \min_{\mathbf{Y}\in\, \mathbb{C}^{M\times M},\, t\in\mathbb{R}} \quad & -t \\ \text{subject to} \quad & \mathrm{Tr}(\mathbf{Y}\mathbf{Q_i}) \geq t, \forall i \in [1,K], \\ & \mathrm{Tr}(\mathbf{Y}) = 1, \\ & \mathbf{Y} \succeq 0. \end{aligned} \tag{4.7}$$

The beamforming vectors $\{\mathbf{v}_l\}$ can be obtained by eigen-decomposition of $\mathbf{Y}_{opt}$. In order to meet the power budget, i.e., $\sum_{l=1}^{r} \|\mathbf{v}_l\|^2 = 1$ , the beamforming vectors $\{\mathbf{v}_l\}$ must be normalized by their corresponding eigenvalues. Hence, the transmitted power during each time sub-slot is different and is given by the corresponding eigenvalue.

Another protocol which can be used to achieve multiple beamforming is to utilize different beamforming vectors, for different durations as shown in Figure 4.1b. In this scenario, the beamforming vectors $\mathbf{w}_l$ and the corresponding times $\lambda_l$ are the eigen-vectors and the corresponding eigenvalues of $\mathbf{Y}_{opt}$ respectively.

## 4.4 Numerical and Simulation Results

In this section, we provide numerical results based on analysis in Sections 4.2 and 4.3, and verify them using simulations. We assume independent and identically distributed (i.i.d.) complex Gaussian channels with zero-mean and unit-variance, i.e., $h_{ij} \sim \mathcal{CN}(0,1)$.

Next, we consider a network consisting ten transmit antennas ($M = 10$) and twenty energy harvesting users ($K = 20$). For a particular channel realization, we solve the

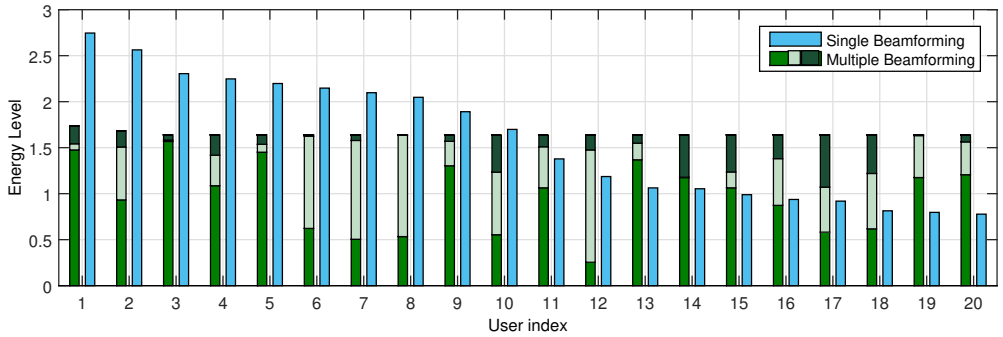


Figure 4.3: Energy harvested by each user by single beamforming (rank-1) and multiple beamforming (3 vectors).

optimization problem in (4.3) using the CVX toolbox. In order to obtain the optimum beamforming vector $\mathbf{w}_{opt}$, we use *randc* randomization process [42]. In this method, we calculate the eigen-decomposition of $\mathbf{X}_{opt} = \mathbf{U}\mathbf{\Sigma}\mathbf{U}^{\dagger}$, and generate $10,000$ candidate solutions for $\mathbf{w}_c = \mathbf{U}\mathbf{\Sigma}^{\mathbf{1/2}}\mathbf{v}_c$, where $\mathbf{v}_c \in \mathbb{C}^M$ is a vector of zero-mean and unit-variance complex circularly symmetric uncorrelated Gaussian random variables. It is important to note that $\|\mathbf{w}_c\|^2$ depends on the particular realization of $\mathbf{v}_c$. Hence, it is crucial to normalize the set of candidate vectors $\{\mathbf{w}_c\}$ in order to satisfy the power budget at the transmitter. Then, we choose $\mathbf{w}_{opt}$ that yields the largest minimum harvested energy. We sort users in descending order according to the amount of harvested energy by each user. We calculate the harvested energy of each user by using both max-min fair energy beamforming scheme and total energy maximization scheme. Then, we plot these energy levels according to the sorted order in Figure 4.2. The harvested energy for each user with the total energy maximization scheme varies between $0.2$ and $7.1$, and with the harvested energy using the max-min fair beamforming varies between $0.7$ and $3.2$. Then, the minimum energy level with max-min fair beamforming, i.e., $0.7$, is significantly improved more than three times with comparing the minimum energy level harvested with total energy maximization, i.e., $0.2$. Therefore, max-min fair beamforming introduce more fairness among the energy levels of users.

Now, we consider multiple beamforming vectors as discussed in Section 4.3, and compare the results with a single beamforming vector. For a particular realization of the

channel matrix, we use the CVX toolbox to obtain the optimum solution $\mathbf{Y}_{opt}$ (which in this case has an effective rank of three after neglecting eigenvalues less than $10^{-5}$). Figure 4.3 shows the energy harvested by each user with the three beamforming vectors (energy harvested by each beamforming vector shown in different shades are stacked together in one bar). For comparison, we also plot the energy harvested by each user with rank-1 beamforming (i.e., a single beamforming vector). The minimum harvested energy in multiple beamforming and single beamforming are $1.5$ and $0.8$, respectively. Thus, utilization of multiple beamforming vectors outperforms single beamforming vector. According to this example, it has almost $100\%$ energy improvement.

In order to compare the performance of different schemes, i.e., i) equal gain transmission; ii) max-min fair single beamforming; and iii) max-min fair multiple beamforming, we consider a network with $M = 10$ and $K = 20$. Therefore, the channel matrix is $\mathbf{H} \in \mathbb{C}^{10\times 20}$. For equal gain transmission, the beamforming vector is $\mathbf{w} = \frac{1}{\sqrt{M}}[1, 1, \cdots, 1]$. Equal gain transmitters can be utilized when CSI is not known. Since we have already compared the user who has minimum energy level for a particular realization of the channel, now we compare the average energy level of the users. We consider $10,000$ channel realizations in the simulation.

Figure 4.4 shows the average energy harvested per user for three different beamforming techniques. The average harvested energy varies from $3.61$ to $0.05$ with equal gain transmitter and from $3.88$ to $0.82$ with max-min fair energy beamforming. These results show that max-min fair beamforming outperforms equally weighted transmission in terms of fairness among users and average energy per user. The average energy harvested using max-min fair multiple beamforming varies from $2.80$ to $1.57$. It can be seen that 13 users (out of all 20) harvest similar energy levels. This demonstrates the high fairness achieved by multiple beamforming when compared with both equal gain transmission and max-min fair beamforming. The reason behind obtaining better results for multiple beamforming compared with single beamforming is that the *randomization* process moves the solution away from the optimum point. Thus, solution

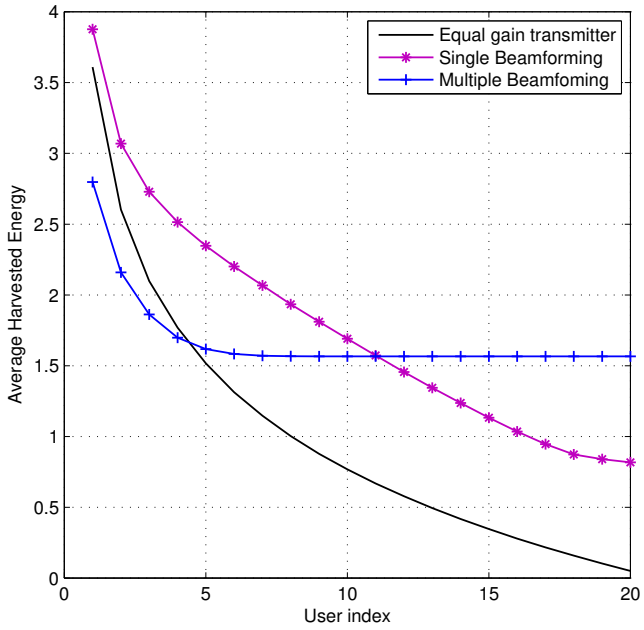


Figure 4.4: Average energy harvested for three schemes.

for single beamforming is approximate. However, with multiple beamforming we are able to obtain the exact solution leading to better results compared to single beamforming scheme.

## 4.5 Conclusion

In this chapter, we study transmit energy beamforming designs for a MU-MISO communications system with energy harvesting capability. We design beamforming vectors to maximize the energy level of the minimum harvested user. Such schemes provide fairness among users in the network. We propose a beamforming design which utilizes multiple beamforming vectors for max-min energy beamforming. We formulated the design problem under the transmit power budget and solved the problem using SDP. Such beamforming designs can be used practically in slowly changing wireless environments.

# Chapter 5

# Beamforming for Wireless Energy Harvesting Networks with Throughput Fairness

*In this chapter, we consider a multi-user multi-input single-output (MU-MISO) wireless communication network. A* harvest-then-transmit *protocol is considered where a hybrid-access point (H-AP) with a co-located antenna array transfers energy to all users via the downlink (DL), and then all users transmit their individual information back to the H-AP via the uplink (UL) by using a time-division-multiple-access (TDMA) scheme. We propose two energy beamforming schemes which ensure the throughput fairness among all users. In particular, we investigate how to maximize the minimum throughput of the network by using: i) a single beamforming vector; and ii) multiple beamforming vectors. Further, we analyse the optimal time allocations for the DL and UL transmissions. Instead of a co-located multi-antenna H-AP, we also consider distributed single-antenna H-APs, in which individual transmit power constraints are assumed for each antenna. We compare the performance of different beamforming schemes and network scenarios by using numerical examples.*

## 5.1 Introduction

Wireless energy transfer has gained a significant research interest during the past few years, especially, in far-field energy transfer which can be utilized in wireless communication networks. This technology greatly benefits the advancement of wireless sensor networks [65]. At sensor nodes, energy is scarce, and replenishment of energy may be an expensive or impossible task [13], [21], [66]. For example, we can consider personnel health monitoring systems in wireless body area networks in which bio-signals are acquired using implanted invasive sensors and wearable non-invasive sensors. Since battery replacement is difficult for implanted sensors, energy harvesting techniques may be a desirable technique to maintain a quality service of health care systems [67]–[69]. For such networks, a protocol called *harvest-then-transmit* allows sensors to first harvest energy from a dedicated power transmitter via the downlink (DL), and then to transmit individual information to a sink via the uplink (UL) [17], [49], [50], [52], [70], [71].

One of the major challenges in wireless energy transfer is propagation path-loss with transmission distance, which has a worse impact on a network with a single omni-directional antenna. However, the path-loss effect can be mitigated by using multi-antenna arrays together with beamforming which does not need additional bandwidth or increased transmit power [19], [22], [51]. A properly designed beamforming vector allows shaping of the transmit waveform at each antenna such that transmit signals can be coherently combined at the receiver in order to acquire adequate energy levels for the successful information communications. However, in multi-user networks, beamforming vectors may be designed in order to ensure that each user can communicate with a fair throughput rate. This may also be called throughput fairness, e.g., maximization of minimum throughput [70]. Such energy beamforming is especially important in the harvest-then-transmit protocol because the UL throughput depends on the harvested energy levels via the DL [17], [50].

### 5.1.1 Related Work

Energy harvesting in a multi-user single-input single-output (SISO) network is considered in [17]. All users harvest energy from a hybrid-access point (H-AP)[1], and transmit information back to the H-AP using a time division multiple access (TDMA) scheme. The sum throughput is maximized by jointly optimizing the time allocations for the DL and the UL transmissions for a given total time constraint. This optimization can result in a severe throughput unfairness among users because users located far from the H-AP not only harvest low energy levels via the DL but also undergo worse path-loss in the UL compared to users located closer to the H-AP. This effect is called as the *doubly near-far* effect. Therefore, the common throughput is maximized by assuming that each user has same rate regardless of their distances from the H-AP. Instead of multi-user single-antenna transmission [17], a network with multi-antenna power transmitter and a single-antenna energy harvesting receiver is considered in [50]. The harvested energy is maximized by balancing the time for channel estimation and the time used for energy transfer. An optimal energy beamforming scheme is derived when we use: i) a fixed preamble length obtained by solving an offline optimization; and ii) a variable preamble length obtained online by solving a dynamic program.

A multi-antenna power transmitter and multiple single-antenna users are considered in [49]. Utilizing the harvested energy, the users transmit information to a dedicated information sink using a TDMA scheme. This work shows that the sum throughput can be improved by using multi-antenna transmission with energy beamforming, compared to a single antenna power transmitter used in [17]. The sum throughput is maximized by optimizing the joint time allocation for the UL and DL transmissions, and energy beamforming by assuming perfect and imperfect channel state information (CSI) at the transmitter.

In [70], a multi-user multi-input single-output (MU-MISO) network is considered

[1]Since the access point serves as a power transmitter and an information receiver, we call it a hybrid-access point (H-AP).

when users transmit information simultaneously. The minimum throughput among all users is maximized by a joint design of the DL and UL time allocations, the DL energy beamforming, the UL transmit power allocation, and receive beamforming for minimum mean square error (MMSE) and zero forcing (ZF) receivers. A two-step approach is used to solve nonconvex optimization problems: i) for a given set of DL and UL times, the minimum throughput is maximized with respect to the UL power allocation, and transmit/receive beamforming vectors; and ii) the optimal UL and DL time allocations are obtained by one-dimensional search for the UL and DL time allocations. The search for optimal UL and DL time allocations is exhaustive. Thus, a suboptimal solution is proposed when the number of users is no larger than the number of antennas at the H-AP. This is one limitation and a drawback of this paper.

### 5.1.2 Motivation

A single-user network is one of the simplest networks for which to design energy beamforming vectors because all transmit power can be focused on the single user. However, future wireless networks consist of multiple users. Since a single-user beamforming vector may not be readily used in multi-user networks, it is required to design different beamforming schemes for multi-user networks [17], [49]. One such scheme is sum-throughput maximization, e.g. [17], [49], however, due to the doubly near-far effect, this scheme causes unfairness for the far users in terms of throughput [17]. Therefore, it is crucial to design schemes which allow sufficient energy harvesting for distant users. This problem can be addressed by maximizing the minimum throughput. The literature on maximizing the minimum throughput resorts to suboptimal solutions because the network size limits the capability of finding efficient optimal solutions [70]. In reality, not all communication networks satisfy the network size constraints posed in [70]. Thus, in this research, we focus on obtaining optimal solutions for MU-MISO networks without posing any constraints of the network size. We use the TDMA scheme for the UL information transmission which mitigates the user interference. Therefore, the optimal solutions can be achieved for MU-MISO networks without any network limitations

nor exhaustive search for the UL and DL time allocations.

### 5.1.3 Contribution

In Chapter 4, we obtain fair beamforming schemes for energy harvesting, in which we maximize the minimum harvested energy in a MU-MISO network with the total transmit energy constraint. We also propose single beamforming and multiple beamforming schemes. However, we merely focus on the harvested energy, but not for the information transmission.

This chapter proposes beamforming schemes for the harvest-then-transmit protocol. We maximize the minimum throughput of all users by jointly optimizing the beamforming vectors and the DL and UL time allocations. We use the TDMA scheme in UL to avoid the user interference. This chapter provides three main contributions:

- We propose two energy beamforming schemes: i) a single beamforming scheme; and ii) multiple beamforming scheme. For both schemes, we solve the optimization problem by using semidefinite programming (SDP).

- We provide an analytical framework to calculate the optimal DL and UL time allocations which is a novel result.

- We consider distributed single-antenna H-APs, and design single and multiple beamforming vectors by maximizing the minimum throughput when each H-AP has an individual transmit power constraint.

Our performance comparison shows that utilization for distributed single-antenna H-APs outperforms the centralized multi-antenna H-AP.

The rest of this chapter is organized as follows. Section 5.2 discusses the system model for the multi-user energy harvesting networks. Section 5.3 and Section 5.4 develop the optimizing framework for co-located and distributed antenna systems, respectively. Section 5.6 presents numerical and simulation results, followed by concluding remarks in Section 5.7. Related proofs are provided in the Appendix 5.8.

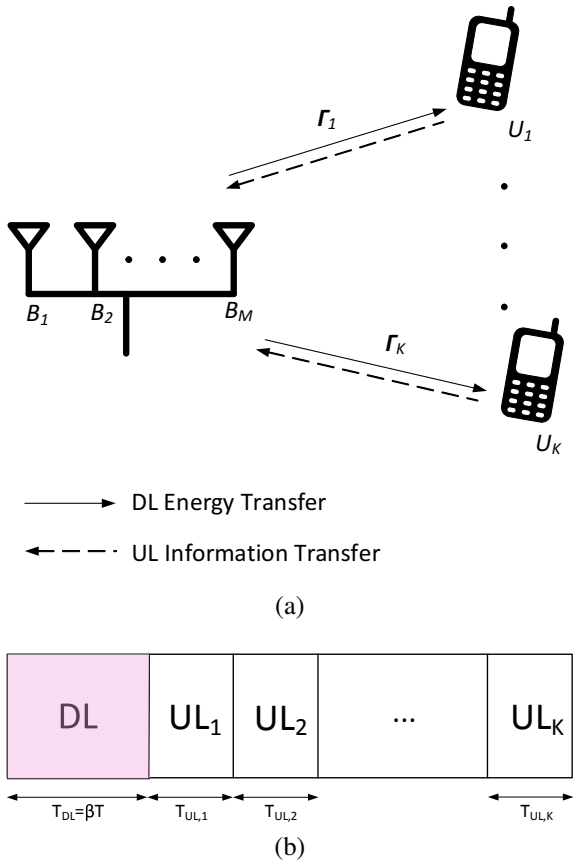


Figure 5.1: (a) MU-MISO network with co-located multi-antenna H-AP; and (b) TDMA scheme used for energy and information transfer.

## 5.2 System Model

We consider a wireless powered communication network with $K$ single antenna users connected to a H-AP which consists of $M$ co-located antennas as shown in Figure 5.1a. The users denoted by $U_i,\ i = 1, \cdots, K$, harvests energy from the signals transmitted from the H-AP via the DL transmission. Then, each user transmits its individual information back to the H-AP via the UL transmission utilizing all the harvested energy, which is the harvest-then-transmit protocol. Figure 5.1b shows the TDMA scheme used for the UL information transfer. All users harvest energy for a period of $T_{DL} = \beta T$, and then each $U_i$ transmits information back for a period of $T_{UL,i} = (1 - \beta)T/K$.

Further, we make the following assumptions. The H-AP and all the users are op-

erating in the same frequency band. The users have no other energy sources[2]. Both DL and UL transmissions take place within a coherence time. Thus, the fading channel between $i$th user, $U_i$, and $j$th antenna of the H-AP, $B_j$, denoted as $h_{ij}$ is same for both UL and DL transmissions. Since the distance between $U_i$ and $B_j$ is $d_{ij}$, the distance dependent path-loss factor is $\rho_{ij} = 1/\sqrt{d_{ij}^{\alpha}}$ where $\alpha$ is the path-loss exponent. For a co-located H-AP, we have $\rho_i = \rho_{i,j}, \forall j$. Thus, the effective channel between $U_i$ and $B_j$ including path-loss fading can be given as $\gamma_{ij} = \rho_{ij} h_{ij}$. Further, the H-AP has perfect CSI knowledge.

### 5.2.1 Downlink Energy Harvesting

The DL transmission is only for energy harvesting. The received signal at $U_i$ can be given as

$$y_i = \mathbf{\Gamma}_i \mathbf{w} s_i + n_i \tag{5.1}$$

where the effective channel vector is $\mathbf{\Gamma}_i = [\gamma_{i1}, \cdots, \gamma_{iM}]$, the beamforming vector of the H-AP is $\mathbf{w} = [w_1, \cdots, w_M]^T$, a random transmit signal is $s_i$, and the received additive white Gaussian noise is $n_i$. Since this noise is independent from the beamforming vector $\mathbf{w}$, we cannot improve the power of the received signal $y_i$ by adjusting the beamforming vector. Hence, we can neglect the noise term as it does not affect the objective function. Thus, the harvested energy by $U_i$ can be given as

$$E_i = \|y_i\|^2 T_{DL} = \eta_i \beta T \mathbf{w}^{\dagger} \mathbf{\Gamma}_i^{\dagger} \mathbf{\Gamma}_i \mathbf{w}, \tag{5.2}$$

where $\eta_i$ is conversion efficiency of $U_i$, which accounts for the energy consumption for processing and running the circuitry, and $^{\dagger}$ denotes the conjugate transpose. This harvested energy is used for the information transmission.

[2]Although, the formulation of the problem presented assumes zero initial energy at all users, the problem can be altered to handle initial energy conditions by changing the objective function in (5.7) to $\mathrm{Tr}(\mathbf{Q}_i)\big[\mathrm{Tr}(\mathbf{X}\mathbf{Q}_i) + e_i\big]$ where $e_i$ denotes the initial energy of the $i$th user.

### 5.2.2 Uplink Information Transfer:

The UL transmission is only for the information transfer. After the energy harvesting period, the users subsequently transmit their information back to the H-AP. Due to the very low energy transfer efficiency in WET, the amount of energy harvested by each user may be very low. Therefore, it is highly likely that the users may have more information to be transmitted than what the harvested amount of energy allow them to transfer. Therefore, it is reasonable to assume that all the harvested energy is utilized by the subsequent information transmission. Then, the average transmit power of $U_i$ can be given as

$$P_{s_i} = \frac{E_i}{T_{UL,i}} = \eta_i K \left( \frac{\beta}{1-\beta} \right) \mathbf{w}^\dagger \mathbf{\Gamma}_i^\dagger \mathbf{\Gamma}_i \mathbf{w}. \tag{5.3}$$

Assuming the received noise power at the H-AP to be additive white Gaussian with zero mean and unit variance, i.e., $n_i \sim \mathcal{CN}(0,1)$, and that H-AP uses the maximum ratio combining (MRC), the signal-to-noise-ratio (SNR) due to $U_i$ transmission is $\mathbf{\Gamma}_i \mathbf{\Gamma}_i^\dagger P_{s_i}$. Therefore, the achievable throughput of $U_i$ is

$$R_{s_i} = \frac{(1-\beta)}{K} \log_2 \left[ 1 + \frac{K\beta}{1-\beta} \eta_i \mathbf{w}^\dagger \left( \mathbf{\Gamma}_i \mathbf{\Gamma}_i^\dagger \right) \mathbf{\Gamma}_i^\dagger \mathbf{\Gamma}_i \mathbf{w} \right]. \tag{5.4}$$

It is worth noting that the users with weak channels, i.e., small $\mathbf{\Gamma}_i$, may have low throughput while the users with strong channels may achieve high throughput. For example, we consider a user located far away from all $M$ antennas of the H-AP. Due to distance-dependent path-loss, the far user harvests less energy as (5.2), and the far user requires more transmit power for sufficient SNR. Both these factors are taken into account in (5.4). This is known as the *doubly near-far* effect.

## 5.3 Maximization of the Minimum Throughput

In this section, we consider maximizing the minimum throughput among all users. This optimization problem, called as the max-min problem, can be formulated as

$$\begin{aligned} \max_{\mathbf{w},\,\beta} \quad & \min_{i\in[1,K]} \quad R_{s_i} \\ \text{s. t.} \quad & \|\mathbf{w}\|^2 \leq 1, \\ & \beta \in [0,1] \end{aligned} \tag{5.5}$$

where $R_{s_i}$ is the throughput of $U_i$ in (5.4). The constraint $\|\mathbf{w}\|^2 \leq 1$ ensures that the total transmit power at the H-AP is within its power budget. This constraint is important as we cannot supply infinite transmit power, and must be met with an equality for the optimum solution, i.e., $\|\mathbf{w}\|^2 = 1$. Since equal time durations are allocated for all users, the problem can be solved in two stages: i) by keeping the energy harvesting time factor $\beta$ constant, we find the optimum beamforming vector in order to maximize the minimum throughput; and ii) for the given beamforming vector, we find the optimum energy harvesting time factor $\beta^*$.

### 5.3.1 Optimum Beamforming Vector

As the first stage, we solve the optimization problem with respect to the beamforming vector $\mathbf{w}$, while keeping the energy harvesting time factor $\beta$ constant. Since the function $\log_2(1+ax)$ is a monotonically increasing function with $x$ for any positive constant $a$, we can rewrite (5.5) for a given $\beta$ as

$$\begin{aligned} \max_{\mathbf{w}} \quad & \min_{i\in[1,K]} S_i = \eta_i \mathbf{w}^\dagger \big(\mathbf{\Gamma}_i \mathbf{\Gamma}_i^\dagger\big) \mathbf{\Gamma}_i^\dagger \mathbf{\Gamma}_i \mathbf{w} \\ & \text{s. t.} \|\mathbf{w}\|^2 = 1. \end{aligned} \tag{5.6}$$

In general, this is a NP-hard optimization problem [42], [63]. Therefore, we find an approximate solution by using a relaxed problem. A similar problem is analysed in [42] in which a two-step approach is proposed to find an approximate solution by using semidefinite programming (SDP). To apply the similar technique, we can define the above problem as follows.

In the first step, the original problem (5.6) can be given as

$$\begin{aligned} \max_{\mathbf{X}\in\mathbb{C}^{M\times M}} \ \min_{i\in[1,K]} \ & \mathrm{Tr}(\mathbf{Q}_i)\mathrm{Tr}(\mathbf{X}\mathbf{Q}_i) \\ \text{s. t.} \quad \mathrm{Tr}(\mathbf{X}) &= 1, \\ \mathbf{X} &\succeq 0, \\ \mathrm{rank}(\mathbf{X}) &= 1, \end{aligned} \tag{5.7}$$

where $\mathrm{Tr}(.)$ denotes the trace function, $\mathbf{Q}_i = \sqrt{\eta_i}\mathbf{\Gamma}_i^{\dagger}\mathbf{\Gamma}_i$ and $\mathbf{X} = \mathbf{w}\mathbf{w}^{\dagger}$. By relaxing the nonconvex rank constraint, i.e. $\mathrm{rank}(\mathbf{X}) = 1$, and introducing an additional variable $t \in \mathbb{R}$, the relaxed problem can be given as

$$\begin{aligned} \min_{\mathbf{X}\in\ \mathbb{C}^{M\times M},\ t\in\mathbb{R}} \ & -t \\ \text{s. t.} \quad \mathrm{Tr}(\mathbf{Q}_i)\mathrm{Tr}(\mathbf{X}\mathbf{Q_i}) &\geq t, \quad \forall i \in [1, K], \\ \mathrm{Tr}(\mathbf{X}) &= 1, \\ \mathbf{X} &\succeq 0. \end{aligned} \tag{5.8}$$

This problem can be solved by using standard SDP solvers such as CVX [64]. Since the rank constraint is removed, the solution for $\mathbf{X}$, $\mathbf{X}_{opt}$, may not be rank one in general. Thus, the second step rectifies this issue.

In the second step, the solution $\mathbf{X}_{opt}$ is post-processed to achieve a rank-one solution. This process is called as *randomization*. This allows us to generate a set of candidate vectors, and then, the best approximate solution can be selected from that set of candidate vectors [42]–[45]. Three randomization techniques are available in the literature: *randA, randB* and *randC* [42], [43], [72], [73].

- *randA*: we calculate the eigen-decomposition of $\mathbf{X}_{opt} = \mathbf{U}\mathbf{\Sigma}\mathbf{U}^{\dagger}$, where $\mathbf{\Sigma}$ is the diagonal eigenvalue matrix $\mathbf{U}$ is the eigenvector matrx. Then we generate a set of

candidate vectors $\{\mathbf{w}_c\}$ such that $\mathbf{w}_c = \mathbf{U}\mathbf{\Sigma}^{1/2}\mathbf{v}_c$ where $\mathbf{v}_c \in \mathbb{C}^M$ is a vector of independent random variables which are uniformly distributed on the unit circle in the complex plane. This technique ensures that the trace constraint in (5.8) is satisfied for any realization of $\mathbf{v}_c$.

- *randB*: we generate a set of candidate vectors $\{\mathbf{w}_c\}$ such that $[\mathbf{w}_c]_i = \sqrt{[\mathbf{X}_{opt}]_{ii}}[\mathbf{v}_c]_i$.
- *randC*: we generate $\{\mathbf{w}_c\}$ such that $\mathbf{w}_c = \mathbf{U}\mathbf{\Sigma}^{1/2}\mathbf{g}_c$, where $\mathbf{g}_c$ is a vector of zero mean and unit variance complex circularly symmetric uncorrelated Gaussian random variables such that $\mathbb{E}[\mathbf{w}_c\mathbf{w}_c^{\dagger}] = \mathbf{X}_{opt}$. The resulting $\{\mathbf{w}_c\}$ must be normalized to meet the power budget $\|\mathbf{w}_c\|^2 = 1$.

The best solution of these three randomization techniques, $\mathbf{w}_\mathbf{c}^*$, can be selected from the set of candidate vectors $\{\mathbf{w}_c\}$ such that it yields the largest value for the objective function, $S_i$, in (5.6).

### 5.3.2 Optimum Energy Harvesting Time

We denote the optimum value for the objective function in (5.6) as $S_{i^*}$ where $i^*$ is the corresponding user. With the aid of (5.5), for a known $S_{i^*}$, we can find the optimum energy harvesting time factor $\beta^*$ as

$$\beta^* = \arg \max_{\beta \in [0,1]} \frac{(1-\beta)}{K} \log_2 \left[1 + \frac{\beta K}{(1-\beta)} S_{i^*}\right]. \tag{5.9}$$

This objective function has the form $f(x) = (1-x)\ln\left[1 + \frac{bx}{1-x}\right]$. We note that when $x \to 0$ the function $f(0) \to 0$, and when $x \to 1$ the function $f(1) \to 0$. Further, $f(x) > 0$ for $x \in (0,1)$. Since the second derivative of the function $f(x)$ which is $f''(x) = \frac{-b^2}{(1-x)[1+(b-1)x]^2}$ is negative for $x \in (0,1)$, the function $f(x)$ is a concave function. Hence, the objective function has only one maximum in $[0,1]$ and the optimum value $\beta^*$ can be given as

$$\beta^* = \frac{1}{(KS_{i^*}-1)}\left[\frac{KS_{i^*}}{1+\mathcal{W}\left(\frac{KS_{i^*}-1}{e}\right)}-1\right] \tag{5.10}$$

where $\mathcal{W}(.)$ denotes the LambertW function [74]. Proof is given in Appendix 5.8.

With the beamforming vector design in Section 5.3.1 and the energy harvesting time factor design discussed in this subsection, an approximate solution for the maximization of the minimum throughput is then achieved by using the optimum beamforming vector, $\mathbf{w_c^*}$, and the optimum energy harvesting time factor $\beta^*$.

## 5.4 Utilizing Multiple Beamforming Vectors

In Section 5.3, we obtain a beamforming vector $\mathbf{w_c^*}$, such that the minimum throughput is maximized. In this section, we extend the problem by allowing the H-AP to use multiple beamforming vectors within a coherence time. We subdivide the DL energy harvesting time into $N$ sub-time slots in which different beamforming vectors are used at the H-AP, i.e., the beamforming vector in the $n$th sub-time-slot is $\mathbf{w}_n$, $n \in [1, N]$. We investigate whether we can further improve the minimum throughput.

With $N$ beamforming vectors, the average transmit power of $U_i$ can be given as

$$P_{m_i} = \eta_i K \left(\frac{\beta}{1-\beta}\right) \sum_{n=1}^{N} \mathbf{w}_n^\dagger \mathbf{\Gamma}_i^\dagger \mathbf{\Gamma}_i \mathbf{w}_n. \tag{5.11}$$

After MRC at the H-AP, the SNR due to $U_i$ transmission is $\mathbf{\Gamma_i \Gamma_i^\dagger} P_{m_i}$. Therefore, the achievable throughput of $U_i$ is

$$R_{m_i} = \frac{(1-\beta)}{K}\log_2\left[1+\eta_i K \left(\frac{\beta}{1-\beta}\right) \sum_{n=1}^{N} \mathbf{w}_n^\dagger \left(\mathbf{\Gamma}_i \mathbf{\Gamma}_i^\dagger\right) \mathbf{\Gamma}_i^\dagger \mathbf{\Gamma}_i \mathbf{w}_n\right]. \tag{5.12}$$

Thus, the problem of maximization of the minimum throughput can be given as

$$\begin{aligned} \max_{\{\mathbf{w}_n\},\, \beta} \quad & \min_{i\in[1,K]} \quad R_{m_i} \\ \text{s. t.} \quad & \sum_{n=1}^{N} \|\mathbf{w}_n\|^2 = 1, \\ & \beta \in [0,1]. \end{aligned} \tag{5.13}$$

This problem can be solved by using the similar approach applied in Section 5.3. We define $\mathbf{Y} \in \mathbb{C}^{M\times M}$ such that $\mathbf{Y} = \sum_{n=1}^{N} \mathbf{w}_n \mathbf{w}_n^{\dagger}$. The sum of positive semidefinite matrices results in another positive semidefinite matrix, thus, $\mathbf{Y} \succeq 0$ [75], [76]. It is worth noting that unlike $\mathbf{X}_{opt}$ in Section 5.3, the optimum solution $\mathbf{Y}_{opt}$ will no longer need to be rank 1. Moreover, $\mathbf{Y}_{opt}$ is a matrix with rank $\min(N, M)$. For $N > M$, the set of beamforming vectors $\mathbf{w}_n$ is no longer linearly independent to each other. Without loss of generality, we thus assume that $N \leq M$. We reformulate the problem as

$$\begin{aligned} \max_{\mathbf{Y}\in\mathbb{C}^{M\times M}} \quad & \min_{i\in[1,K]} \quad \mathrm{Tr}(\mathbf{Q}_i)\mathrm{Tr}(\mathbf{Y}\mathbf{Q}_i) \\ \text{s. t.} \quad & \mathrm{Tr}(\mathbf{Y}) = 1, \\ & \mathbf{Y} \succeq 0 \end{aligned} \tag{5.14}$$

which can be solved by using SDP because it is a similar problem as (5.7), but without the rank constraint. Thus, the optimum matrix $\mathbf{Y}_{opt}$ can be obtained by using the CVX toolbox as used in Section 5.3. A randomization technique is no longer required as the rank of $\mathbf{Y}_{opt}$ is no longer restricted to be 1. Hence, this is an exact solution. The optimum beamforming vectors can be obtained using eigen-decomposition of $\mathbf{Y}_{opt}$. We denote non-zero eigenvalues and corresponding eigenvectors of $\mathbf{Y}_{opt}$ as $\delta_1 \geq \delta_2 \geq \cdots \geq \delta_N$ and $\mathbf{q}_1, \mathbf{q}_2, \cdots, \mathbf{q}_N$, respectively.

The sub-slots for different beamforming vectors can be chosen in two ways:

- *Equal time division*: The DL time $T_{DL}$ can be equally divided into $N$ sub-slots as given in Figure 5.2a. In this case, beamforming vector to be used in the $n$th

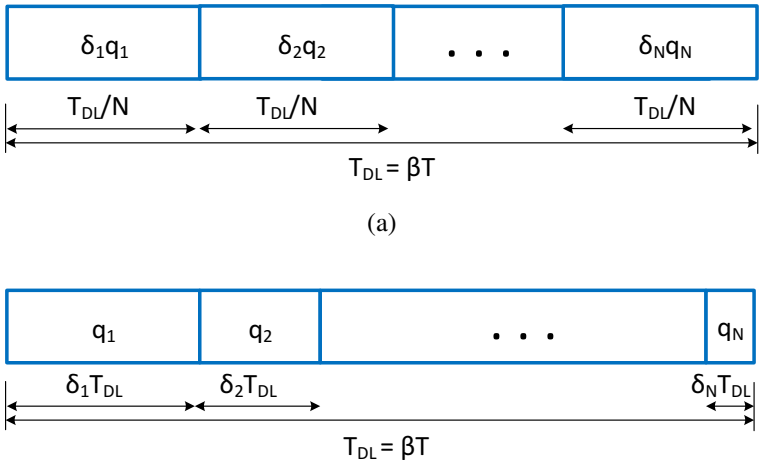


Figure 5.2: Sub-slot allocation for multiple beamforming using (a) equal time division; and (b) unequal time division.

sub-slot is given by $\sqrt{\delta_n}\mathbf{q}_n$. Since the eigenvectors are orthonormal, the factor $\sqrt{\delta_n}$ controls the amount of energy transmitted during the $n$th sub-slot. Hence, the power budget at the H-AP is met, i.e. $\mathrm{Tr}(\mathbf{Y}_{opt}) = \sum_{n=1}^{N} \delta_n = 1$.

- *Unequal time division*: The DL time $T_{DL}$ can be divided into different time durations according to the eigenvalues as given in Figure 5.2b. We do not need to scale the eigenvectors because the duration of the sub-slot ensures the power budget.

As we have obtained the optimum beamforming vectors, the optimum energy harvesting time factor, $\beta_{opt}$ can be calculated as in Section 5.3.

## 5.5 Beamforming for Distributed Antenna System

In this section, we extend these proposed schemes such that they can be applied for: i) multiple single-antenna H-APs; and ii) a distributed antenna array with a single H-AP as shown in Figure 5.3. We assume that all antennas corporate with each other in order to decode the received information in UL transmission. Unlike the previous case, since $B_j$s are placed in different locations, each antenna may have a different power constraint. Hence, we formulate the problem for maximization of the minimum

throughput as follows. It is important to note that we have to control the individual transmit power constraints, i.e. the transmit power constraint of $B_j$ is $\phi_j,\ \forall j$. Then, the optimization problem can be given as

$$\begin{aligned} \max_{\mathbf{w},\,\beta} \quad & \min_{i\in[1,K]} \quad R_i \\ \text{s. t.} \quad & \|\mathbf{w}\|^2 \leq 1, \\ & |w_j|^2 \leq \phi_j,\ \ \forall j, \\ & \beta \in [0,1], \end{aligned} \tag{5.15}$$

where $R_i$ is the throughput of $i$th user in (5.4). We use a similar approach as Section 5.3, i.e., we reformulate the problem as an SDP, solve the relaxed problem without the rank constraint and then post-process the solution using randomization techniques to find the best beamforming vector. The problem can be formulated as an SDP which is given as

$$\begin{aligned} \max_{\mathbf{X}\in\mathbb{C}^{M\times M}} \quad & \min_{i\in[1,K]} \quad \mathrm{Tr}(\mathbf{Q}_i)\mathrm{Tr}(\mathbf{X}\mathbf{Q}_i) \\ \text{s. t.} \quad & \mathrm{Tr}(\mathbf{X}) = 1, \\ & [\mathbf{X}]_{jj} \leq \phi_j \ \ \forall j, \\ & \mathbf{X} \succeq 0. \end{aligned} \tag{5.16}$$

When we relax the rank constraint in (5.16), the optimum solution for $\mathbf{X}$, $\mathbf{X}_{opt}$, may not be rank one in general. Hence, a randomization technique must be applied for the single beamforming scheme. However, it is important to ensure that none of the constraints are violated during the randomization process.

- In randA, as each element of $\{\mathbf{v}_c\}$ is drawn from a uniform distribution on the unit circle, the total transmit power constraint is not violated. However, as randA involves linear combination of eigen-vectors, the individual power constraints may not be satisfied. Therefore, all the candidate vectors generated using randA may not qualify as the beamforming vector.

- In randB, we only use the diagonal elements of $\mathbf{X}_{opt}$. Each diagonal element is multiplied by the corresponding element of $\{\mathbf{v}_c\}$, i.e., $[\mathbf{w}_c]_i = \sqrt{[\mathbf{X}_{opt}]_{ii}}[\mathbf{v}_c]_i$. Hence, both total and individual power constraints are maintained. This enables us to use randB to obtain the best beamforming vector without further checking nor processing of the candidate set.

- In randC, unlike the other two randomization techniques, a vector of zero mean, unit variance complex circularly symmetric uncorrelated Gaussian random variables $\mathbf{g}_c$ is used. Since each element of $\mathbf{g}_c$ is not restricted to be unit magnitude, randC may fail to satisfy both individual power constraints and the total power budget of the H-AP. The latter however, can be easily fixed by normalizing the candidate set as discussed previously in this chapter.

Similar to the co-located H-AP, utilizing multiple beamforming vectors ensure that the optimum throughput is achieved. Since the optimum solution $\mathbf{X}_{opt}$ is Hermitian semidefinite, each diagonal element of $\mathbf{X}_{opt}$ is given by the linear combination of energy transmitted in $N$ sub-slots by the corresponding element of the beamforming vectors, i.e., $[\mathbf{X}_{opt}]_{ii} = \sum_{n=1}^{N} \delta_n |[\mathbf{q}_n]_i|^2$. Therefore, the individual transmit power constraints is maintained during all sub-slots of the DL transmission. Hence, the equal sub-slot allocation scheme shown in Figure 5.2a can be directly applied for the distributed H-AP. However, unequal sub-slot duration scheme shown in Figure 5.2b might cause some antennas to transmit high power which violates the individual constraints in a short duration of time. Thus, we recommend using the equal sub-slot duration scheme for distributed H-AP with individual power constraints.

After the optimum beamforming vector(s) are chosen, optimization over the energy harvesting time can be done the same way as for the co-located H-AP using (5.10). However, all $M$ antennas of the H-AP will have to corporate with each other to decode the information. This, requires each antenna to communicate with a central processor. This procedure is beyond scope of this research.

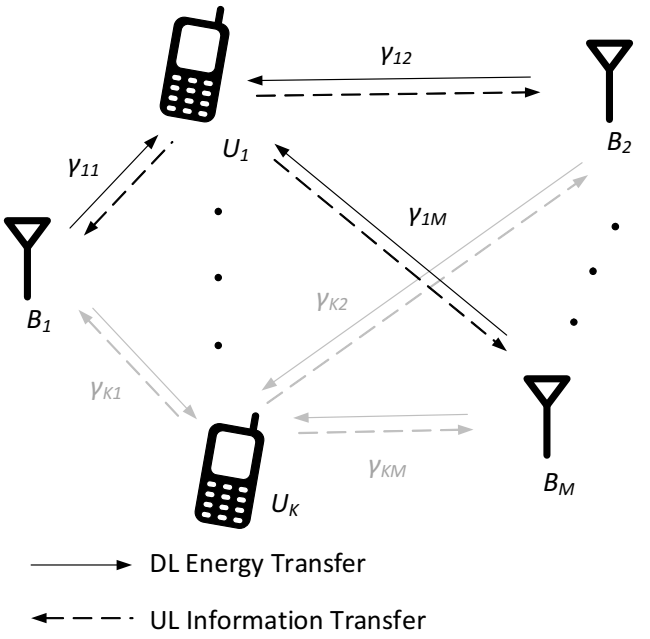


Figure 5.3: Wireless powered communication network with distributed antenna array for H-AP.

## 5.6 Simulation Results

In this section, we provide numerical examples to compare the beamforming schemes for two networks: i) a network with a co-located H-AP; and ii) a network with a distributed antenna system, which are discussed in Section 5.3 and Section 5.4, respectively. As a benchmark, we use an equal-gain transmitter at the H-AP, i.e., the beamforming vector at the transmitter is $\mathbf{w}_{eq} = \frac{1}{\sqrt{M}}[1, 1, \cdots, 1]^T$. This equal-gain beamforming vector can be used when the CSI is not available at the H-AP. For simulations, we use following parameters. The network consists of one hundred energy harvesting users ($K = 100$) with a H-AP (for both co-located and distributed) which has nineteen transmitting antennas ($M = 19$). The perfect RF-DC conversion is possible for all users, i.e., $\eta_i = 1, \forall\, i$. The total transmit power is $10\,\mathrm{W}$ ($40\,\mathrm{dBm}$). The noise power $\sigma^2 = -100\,\mathrm{dBm}$. The communication bandwidth is $25\,\mathrm{MHz}$ at frequency $f_c = 900\,\mathrm{MHz}$.

### 5.6.1 Network with a co-located H-AP

In this case, the slow and fast fading are modelled as follows:

- The slow gain depends on the distance dependent path-loss as

$$\rho_i^2 = A_0 \left( \frac{d_i}{d_0} \right)^{-\alpha} \tag{5.17}$$

  where $A_0 = 10^{-3}$ is the reference path-loss at a reference distance of $d_0 = 1\,\mathrm{m}$ with a path-loss exponent $\alpha = 3$ [70], and $d_i$ is the distance between the $i$th user and the H-AP. All users are uniformly placed on a disc which has radii between $20\,\mathrm{m}$ to $200\,\mathrm{m}$ from the co-located H-AP. Thus, $d_i^2$ is assumed to be a uniform random variable between $400$-$40\,000\,\mathrm{m}^2$. The angle of the user (with reference to $x$-axis) is $\varphi_i$ which is also a uniform random variable between $0$-$2\pi$ radians.

- Since the fast fading may have line-of-sight (LOS) and non-line-of-sight (NLOS) components, it is modelled as a Rician channel which can be given as

$$\mathbf{h}_i = \sqrt{\frac{K_R}{1+K_R}} \mathbf{h}_i^{LOS} + \sqrt{\frac{1}{1+K_R}} \mathbf{h}_i^{NLOS} \tag{5.18}$$

  where $K_R =$ is the Rician factor, and $\mathbf{h}_i^{LOS} \in \mathbb{C}^M$ and $\mathbf{h}_i^{NLOS} \in \mathbb{C}^M$ represent the LOS and NLOS components from the co-located transmitter to the $i$th user, respectively. Further, $\mathbf{h}_i^{LOS} \in \mathbb{C}^M$ follows the far-field uniform linear antenna array model as $\mathbf{h}_i^{LOS} = [1, e^{j\theta_i}, e^{j2\theta_i}, \cdots, e^{j(M-1)\theta_i}]$ with $\theta_i = 2\pi d_t f_c sin(\varphi_i)$, where $d_t$ is the distance between two adjacent antenna elements of the H-AP which is at half wavelength, and $\mathbf{h}_i^{NLOS} \in \mathbb{C}^M$ is a vector of independent and identically distributed (i.i.d.) random variables with $h_{i,j}^{NLOS} \sim \mathcal{CN}(0,1),\ \forall\, i,j$.

For the maximization of the minimum throughput using a single beamforming vector in Section 5.3, we solve the relaxed problem in (5.8) using the CVX toolbox in MATLAB for Rayleigh fading channels ($K_R = 0$) and Rician fading channels with

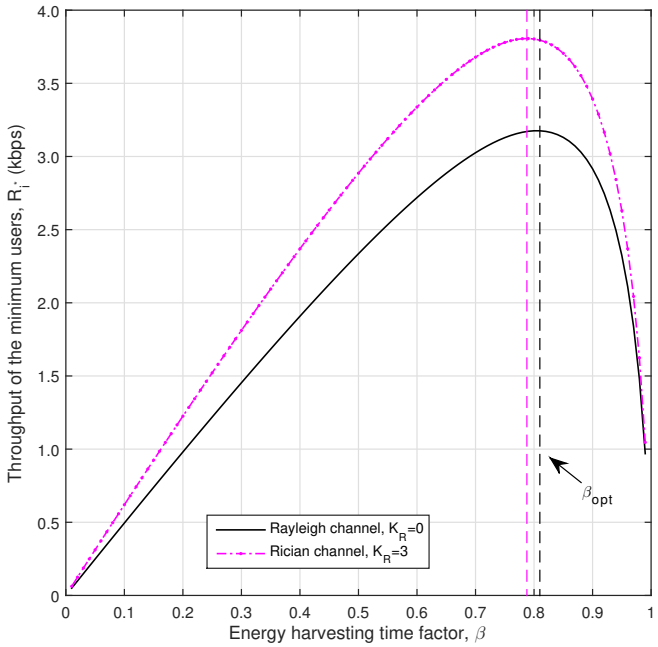


Figure 5.4: Variation of throughput for the minimum throughput user with $\beta$.

$K_R = 3$. We generate a set of 1000 candidate vectors for $\{\mathbf{w}_c\}$ using each randomization technique (randA, randB and randC ). The best beamforming vector among all three sets of candidate vectors is chosen according to the criteria given in Section 5.3. For the maximization of the minimum throughput using multiple beamforming vectors in Section 5.4, we solve the SDP in (5.14) and the beamforming vectors are obtained using eigen-decomposition. For the equal-gain beamforming vector, we use the beamforming vector $\mathbf{w}_{eq} = \frac{1}{\sqrt{19}}[1, 1, \cdots, 1]^T$ at the H-AP.

Figure 5.4 shows the variation of the throughput of the minimum throughput achieving user with the multiple beamforming scheme versus the energy harvesting time $\beta$. We consider single channel realization for each channel - Rayleigh fading channel ($K_R = 0$) which is in solid lines, and Rician fading channel with $K_R = 3$ which is in dotted line. As shown in the figure, the throughput is a concave function with respect to $\beta$, which is also proven in Section 5.3.2. When $\beta = 0$, the throughput is zero because no energy can be harvested, and thus the user has no energy for the information transmission. When

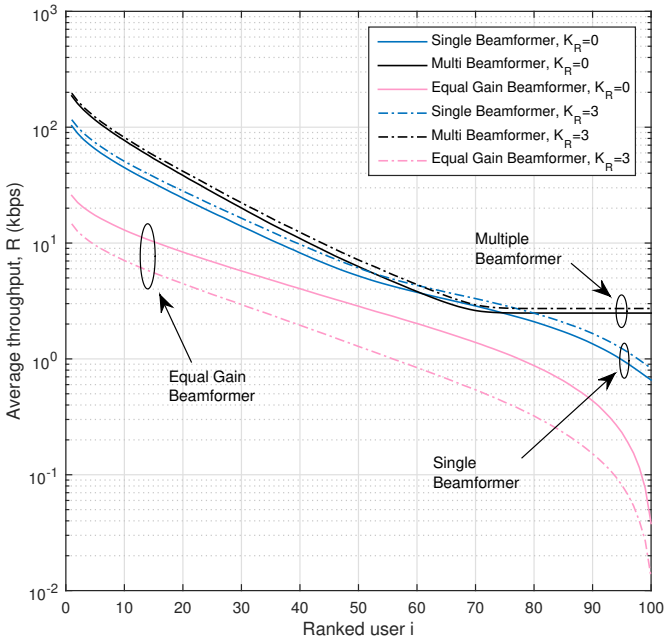


Figure 5.5: Average throughput of each user with a co-located H-AP network.

$\beta = 1$, the throughput is also zero because the entire time is used only for the energy harvesting, and thus no time is available for the information transmission. Since the throughput is a concave function, by proper selection of $\beta$, we can find an optimal $\beta$ value, $\beta_{opt}$, which maximizes the throughput, $R_{i^*,opt}$. This means that we can maximize the minimum throughput. In these particular examples, $\beta_{opt} = 0.81$ and $R_{i^*,opt} = 3.18\,\text{kbps}$ for $K_R = 0$; and $\beta_{opt} = 0.79$ and $R_{i^*,opt} = 3.80\,\text{kbps}$ for $K_R = 3$. In the rest of this section, we calculate the throughput for the optimal $\beta$ value.

Now, we compare the three schemes, i.e., single beamforming vector, multiple beamforming vectors and the equal-gain beamforming vector. First, we find the optimum energy harvesting time, $\beta_{opt}$, for each scheme for a particular channel realization as (5.10). Then, we sort the users according to the descending order of their corresponding throughput, and find the average throughput over $1000$ channel realizations. Figure 5.5 shows the average throughput versus ranked users $i$. The $i$th ranked user means that the user with $i$th highest throughput in all realizations. Thus, $i = 1$ and $i = 100$ represent

| | Rayleigh Channels, $K_R = 0$ | | | Rician Channels, $K_R = 3$ | | |
|---|---|---|---|---|---|---|
| Scheme | Max (kbps) | Min (kbps) | $\frac{\text{Max}}{\text{Min}}$ | Max (kbps) | Min (kbps) | $\frac{\text{Max}}{\text{Min}}$ |
| Single | 103 | 0.66 | 156 | 116 | 0.832 | 140 |
| Multiple | 186 | 2.49 | 75 | 197 | 2.72 | 72 |
| Equal gain | 25.7 | 0.038 | 676 | 14.7 | 0.013 | 1131 |

Table 5.1: The average throughput of the three schemes for co-located H-AP network.

the user with the highest and the lowest throughput, respectively, which are tabulated in Table 5.1 for three beamforming schemes and two fading channels.

We have following observations based on Figure 5.5:

- For single and multiple beamforming techniques, the Rician fading outperforms the Rayleigh fading while for equal-gain beamforming, the Rayleigh fading outperforms the Rician fading. This happens because the Rayleigh fading is scattered in the region while the Rician fading has a dominant LOS component. Therefore, the beams can be focused towards the dominant LOS component which leads to better performance in Rician fading compared to Rayleigh fading with optimally designed single and multiple beamforming vectors. However, for the equal-gain beamforming, the beam pattern is fixed and we may not be able to tune the beam towards the dominant LOS component. Hence, a rich scattered Rayleigh fading may outperform the Rician fading.

- Since the focus of this paper is on minimum throughput, we compare the minimum throughput of three beamforming techniques with Rician channel. The multiple beamforming outperforms both single beamforming and equal-gain beamforming by approximately 3 times and 209 times, respectively. Further, the single beamforming outperforms the equal-gain beamforming by approximately 64 times.

- We also tabulate the ratio between highest and lowest throughput in Table 5.1, which may also be a measure to indicate the fairness among users. The multiple beamforming technique has a lower ratio compared to the other two schemes.

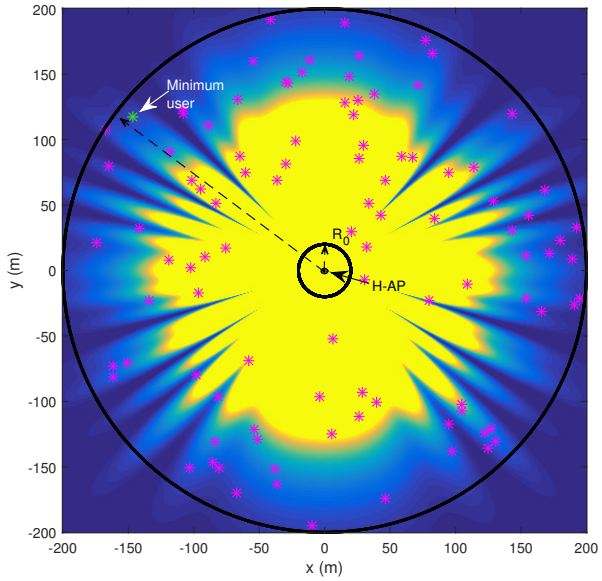


(a)

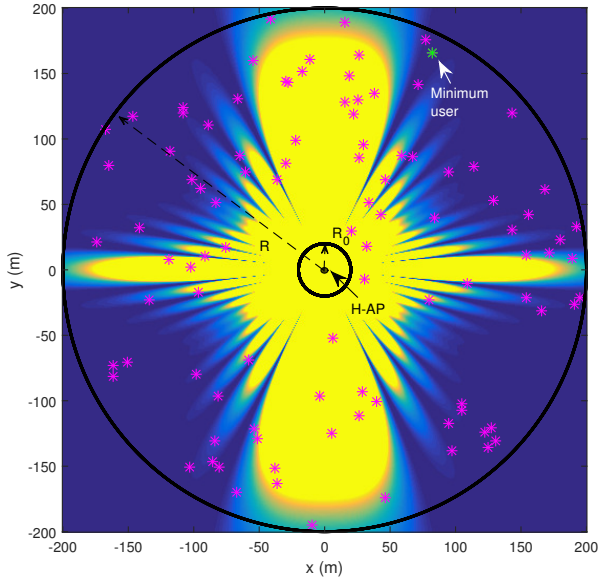


(b)

Figure 5.6: Beam patterns for the co-located H-AP network with pure LOS model: (a) single beamforming; and (b) equal-gain beamforming.

Since the user throughput depends on its available energy (or harvested energy), it is interesting to see how the energy beam pattern is distributed from the transmitter. Figure 5.6 illustrates the beam patterns of the single and equal-gain beamforming techniques for a pure LOS channel model for a particular realization of user locations. Users are denoted with small (red) stars, and the user with minimum throughput is a green star which is also labelled separately. As shown in Figure 5.6a, beam pattern is spread according to the user distribution and their distances which facilitates a fair energy harvesting among users, e.g., many more edged-users may harvest more energy than some of inside users. As shown in Figure 5.6b, beam pattern is not spread according to the user distribution and their distances, however we see strong main lobes and weak side lobes. Thus, users may harvest energy more unevenly. For example, there is a cluster of users at the north-west corner, however, no any stronger energy lobe is focused to that direction.

Figure 5.7 illustrates the beam patterns used in the multiple beamforming scheme for a pure LOS channel model for a particular realization. For this particular realization, the rank of the optimum beamforming matrix $\mathbf{X}_{opt}$ is three. Thus, three distinct beamforming vectors are used in three sub-slots as shown in the figure. Here, we use the unequal time division to obtain the time duration for each sub-slot. This means all three beamforming vectors have unit power and the time duration of the sub-slot is determined by the corresponding eigenvalue. As shown in Figure 5.7a, the first beamforming vector which corresponds to the largest eigenvalue tends to spread the beam pattern according to user distribution and their distances which facilitates a fair energy harvesting among users. In the next sub-slots, which are illustrated in Figure 5.7b and Figure 5.7c, we see more defined lobes compared to the first beamforming vector. This is because these beamforming vectors further improves the users who harvest less energy from the first sub-slot. Hence, these beam patterns are more focused towards some users.

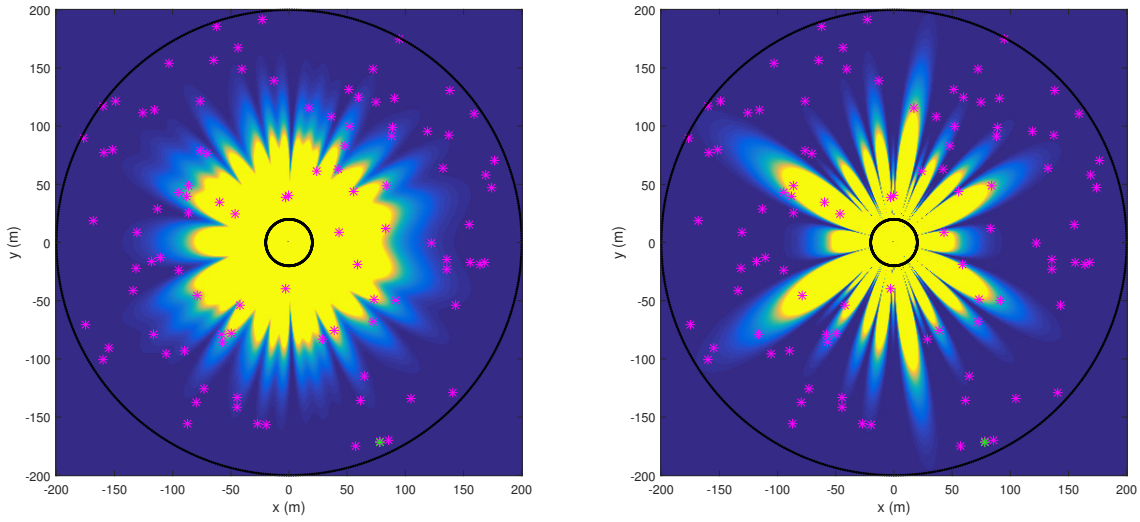


(a)




(b)

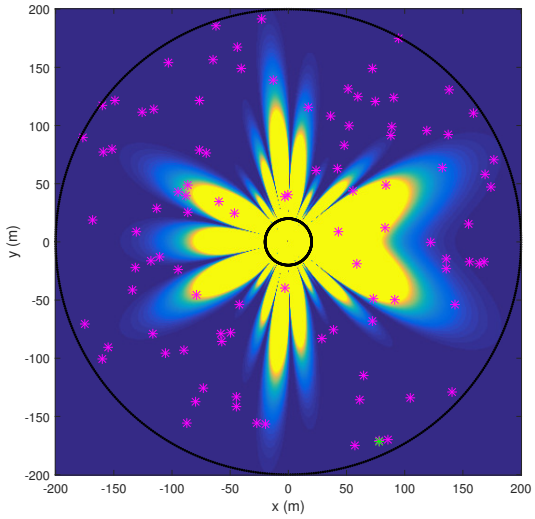


(c)

Figure 5.7: For pure LOS model multiple beamforming scheme's beam patterns used for : (a) the 1st sub-slot; (b) the 2nd sub-slot ; and (c) the 3rd sub-slot.

### 5.6.2 Network with a Distributed Antenna System

In this case, we uniformly locate $19$ antennas of the H-AP in a circular region with radius of $200\,\mathrm{m}$ to form a cellular structure. Similar to the previous case, all users ($K = 100$) are uniformly located on a disc which has radii between $20\,\mathrm{m}$ to $200\,\mathrm{m}$ from the center. Thus, the maximum distance between a user and the closest antenna is $57.7\,\mathrm{m}$ (which may be $200\,\mathrm{m}$ in the co-located H-AP). The slow fading and fast fading are modelled as (5.17) and (5.18), respectively, with $\rho_i,\ d_i,\ h_i,\ h_i^{LOS},\ h_i^{NLOS}$ replaced by $\rho_{ij},\ d_{ij},\ h_{ij},\ h_{ij}^{LOS},\ h_{ij}^{NLOS}$, respectively. Note that subscript $ij$ represents the parameter between the $j$th antenna of the H-AP to the $i$th user. Further, $A_0 = 10^{-3}$, $d_0 = 1\,\mathrm{m}$, $\alpha = 3$, $h_{i,j}^{NLOS} \sim \mathcal{CN}(0,1)$, and $h_{ij}^{LOS} = e^{j\theta_{ij}}$ with $\theta_{ij} = \frac{2\pi}{\lambda}\mathrm{rem}(\frac{d_{ij}}{\lambda})$ where $\mathrm{rem}(.)$ is the remainder of a division. We can calculate the distance $d_{ij}$ for each realization. We set individual transmit power constraints to be equal to $1/\sqrt{19}$ such that it can be compared with the equal-gain transmitter. Similar to the previous case, we sort the users according to the descending order of their corresponding throughput, and find the average throughput over 1000 channel realizations of Rayleigh fading channels ($K_R = 0$) and Rician fading channels with $K_R = 3$. To compare the three schemes, we first find the optimum energy harvesting time, $\beta_{opt}$, for each scheme for a particular channel realization as (5.10). Then, we sort the users according to the descending order of their corresponding throughput, and find the average throughput over $1000$ channel realizations.

For the maximization of the minimum throughput using a single beamforming vector, we solve the problem in (5.16) without the rank constraint by using the CVX toolbox in MATLAB. We generate a set of $1000$ candidate vectors for $\{\mathbf{w}_c\}$ using randB. The best beamforming vector in the set of candidate vectors is chosen according to the criteria given in Section 5.3. For the maximization of the minimum throughput by using multiple beamforming vectors, we solve the SDP in (5.16) without the rank constraint and the beamforming vectors are obtained using eigen-decomposition. For the equal-gain beamforming vector, we use the beamforming vector $\mathbf{w}_{eq} = \frac{1}{\sqrt{19}}[1, 1, \cdots, 1]^T$ at

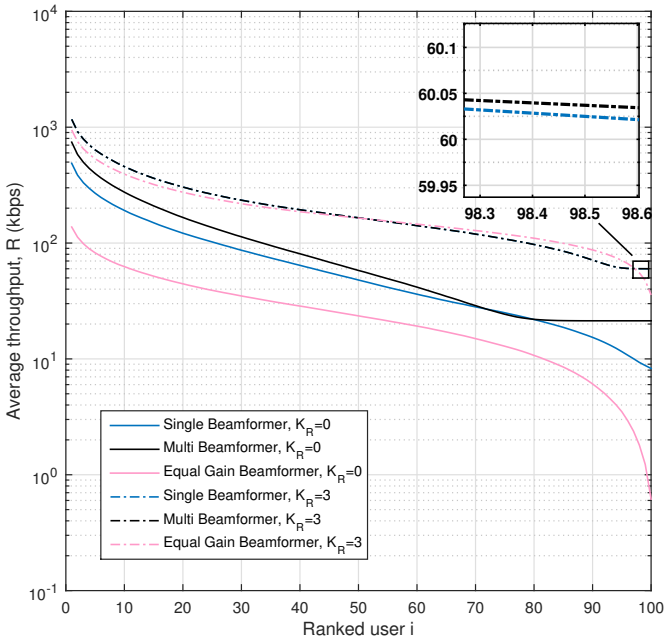


Figure 5.8: Average throughput of ranked users with a distributed H-AP network.

| | Rayleigh Channels, $K_R = 0$ | | | Rician Channels, $K_R = 3$ | | |
|---|---|---|---|---|---|---|
| Scheme | Max (kbps) | Min (kbps) | $\frac{\text{Max}}{\text{Min}}$ | Max (kbps) | Min (kbps) | $\frac{\text{Max}}{\text{Min}}$ |
| Single | 488 | 8.27 | 59 | 1169 | 60.0 | 19 |
| Multiple | 742 | 21.3 | 35 | 1170 | 60.02 | 19 |
| equal-gain | 137 | 0.62 | 221 | 947 | 35.7 | 27 |

Table 5.2: Throughput values obtained from the three schemes for the distributed H-AP network.

the H-AP.

Figure 5.8 shows the average throughput versus ranked users $i$, and the highest and the lowest throughput are tabulated in Table 5.2 for three beamforming schemes over two fading channels. For all three beamforming schemes, the Rician fading outperforms the Rayleigh fading because the beam patterns for all elements of the distributed H-AP are distributed in the area which may improve the dominant LOS component. Unlike, for the co-located H-AP, in distributed H-AP networks Rician fading outperforms Rayleigh fading for the equal-gain beamforming because for distributed H-AP equal-gain beamforming evenly distributed power in the area rather than focusing the

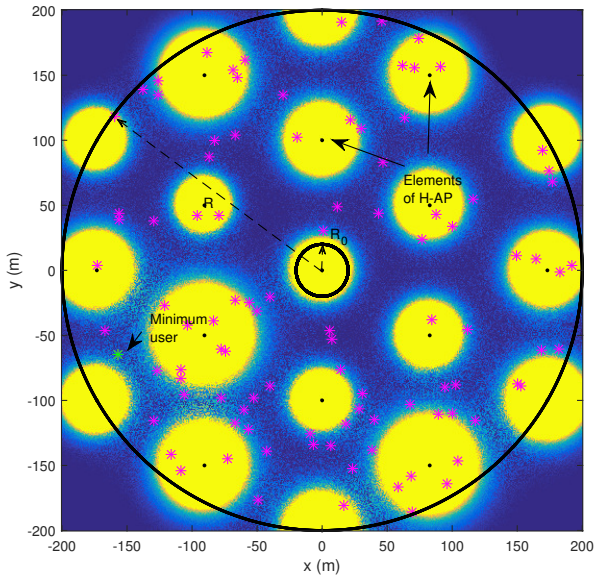


(a)

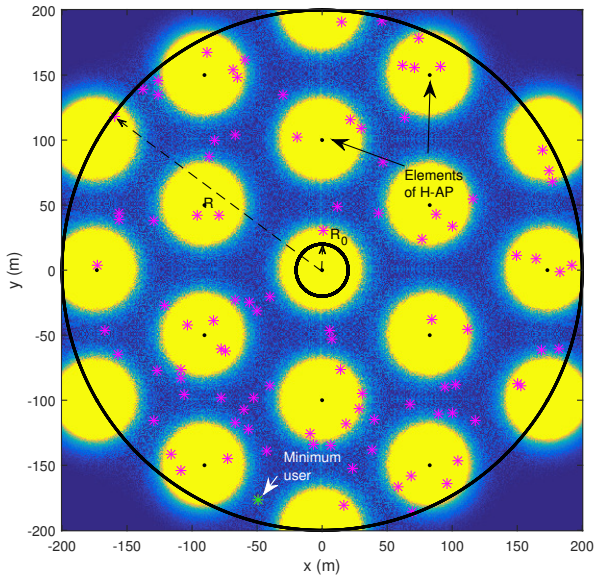


(b)

Figure 5.9: Beam patterns for the distributed H-AP network with pure LOS model: (a) single beamforming; and (b) equal-gain beamforming.

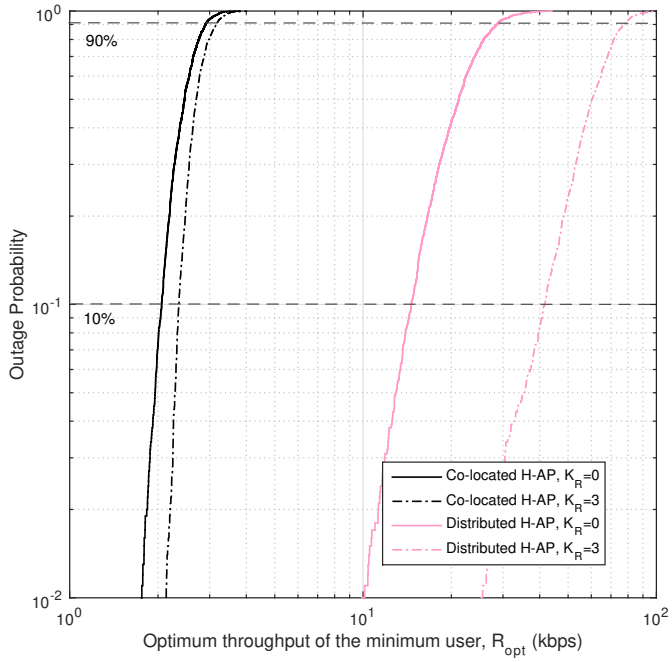


Figure 5.10: The outage probability of the minimum throughput user for co-located and distributed H-AP.

beams to a specific direction in co-located network. The multiple beamforming outperforms both single beamforming and equal-gain beamforming by approximately 3 times and 34 times, respectively. Further, the single beamforming outperforms the equal-gain beamforming by approximately 13 times. We also tabulate the ratio between highest and lowest throughput in Table 5.2. The multiple beamforming technique has a lower ratio compared to the other two schemes.

For Rician fading, the minimum throughput achieved by the single beamforming and multiple beamforming are almost the same. This implies that the optimum solution $\mathbf{X}_{opt}$ has its maximum eigenvalue to be almost 1. Therefore, the approximated rank of $\mathbf{X}_{opt}$ is one. Further, these two schemes outperforms the equal-gain beamforming by approximately 1.7 times.

Figure 5.9 illustrates the beam patterns of the single and equal-gain beamforming techniques for a pure LOS channel model for a particular realization of user locations.

Users are denoted with small (red) stars, and the user with minimum throughput is a green star which is also labelled separately. As shown in Figure 5.9a, the antenna elements located at higher user density areas have large radii of beams with single beamforming. However, as shown in Figure 5.9b, the radii of all antenna elements are equal with equal-gain beamforming because the transmit power is equally divided for the antenna elements. Although for LOS models, the equal-gain beamforming may achieve the fairness, it can be further improved by a properly designed beamforming vectors such as the proposed single beamforming scheme. However, when the number of users is infinitely large, i.e., $K \to \infty$, the users may distribute uniformly over the region, beamforming vectors for single beamforming and the equal-gain beamforming schemes may be the same. Thus, they may have similar performance for a large $K$. This explains the reason for the $\mathbf{X}_{opt}$ to be approximately rank one for Rician channels.

Figure 5.10 shows the outage probability of the minimum throughput of the multiple beamforming scheme for a network over Rayleigh fading channels (in solid lines) and Rician fading channels with $K_R = 3$ (in dashed lines) for $1000$ realizations. For Rayleigh fading channels, the outage probabilities of the user with minimum throughput at $R$ =$2.90\,\mathrm{kbps}$ are 90% and 0% for the co-located H-AP and distributed H-AP, respectively. For Rician fading channels, those values are 73% and 0% for the co-located H-AP and distributed H-AP, respectively. Moreover, if we expect only 10% outage probability, the maximum possible minimum user's throughput of the co-located H-AP and distributed H-AP are $2.35\,\mathrm{kbps}$ and $41.6\,\mathrm{kbps}$, respectively, over Rician fading channels. Thus, the distributed network can improve the performance significantly, which is almost 18 times higher than the co-located H-AP. As shown in the figure, we may also have a significant benefit of the LOS component with the distributed network. For example, at 10% outage probability, the throughput difference between Rayleigh and Rician fading channels is $0.29\,\mathrm{kbps}$ for the co-located H-AP network, however, this value is $37.2\,\mathrm{kbps}$ for the distributed network, This means that the LOS component has a significant impact on the minimum user's throughput with the distributed network.

## 5.7 Conclusion

This paper studies two MU-MISO networks for the DL energy harvesting and the UL information transfer with: i) a co-located multi-antenna H-AP; and ii) distributed single antenna H-APs. We consider two energy beamforming schemes using: i) a single beamforming vector; and ii) multiple beamforming vectors; which maximizes the minimum throughput of the UL information transfer. Further, we derive the optimum energy harvesting time required for the DL transmission. These optimization problems are solved in two stages: i) beamforming vectors are obtained by using SDP; and ii) for the given beamforming vector, the optimum energy harvesting time for DL is obtained. Numerical results show that multiple beamforming scheme outperforms both single and equal-gain beamforming schemes for both networks. Further, utilization of distributed single antenna H-APs improves the throughput fairness among users compared to utilization of a co-located multi-antenna H-APs.

## 5.8 Appendix

We can write the Lagrangian function $L$ of (5.9) as

$$L(\beta, \lambda_1, \lambda_2) = \frac{(1-\beta)}{K}\log_2\left[1 + \frac{\beta K}{(1-\beta)}S_{i^*,opt}\right] + \lambda_1\beta + \lambda_2(1-\beta)$$

where $\lambda_1$ and $\lambda_2$ are Lagrange multipliers. Since $\log_2(x) = \ln(x)/\ln(2)$, we have

$$L(\beta, \lambda_1, \lambda_2) = \frac{(1-\beta)}{K\ln(2)}\ln\left[1 + \frac{\beta K}{(1-\beta)}S_{i^*,opt}\right] + \lambda_1\beta + \lambda_2(1-\beta).$$

By using partial differentiation, we solve the optimization problem of $L(\beta, \lambda_1, \lambda_2)$ with respect to $\beta, \lambda_1$and $\lambda_2$, which are given as

$$\frac{\partial L}{\partial \beta} = \frac{KS_{i^*,opt}}{\big(1-\beta(1-KS_{i^*,opt})\big)} - \ln\left(1 + \frac{\beta}{(1-\beta)}KS_{i^*,opt}\right) + \lambda_1 - \lambda_2 = 0$$

$$\frac{\partial L}{\partial \lambda_1} = \beta = 0$$
$$\frac{\partial L}{\partial \lambda_2} = \beta = 1.$$

It is important to note: i) if $\beta = 0$, there is no time allocation for the DL transmission then we cannot transmit information to the receiver as no energy harvesting is possible. and ii) if $\beta = 1$, the entire time is used for energy harvesting in DL transmission then we cannot transmit information to the receiver as no time left for the UL transmission. Thus, we can consider the equation

$$\frac{\partial L}{\partial \beta} = \frac{KS_{i^*,opt}}{\big(1-\beta(1-KS_{i^*,opt})\big)} - \ln\left(1+\frac{\beta}{(1-\beta)}KS_{i^*,opt}\right) = 0.$$

Which can be rearranged as $Ze^Z = \frac{KS_{i^*,opt}-1}{e}$ where

$$Z = \frac{KS_{i^*,opt}}{1-\beta_{opt}(1-KS_{i^*,opt})} - 1.$$

Hence, the optimum value $\beta_{opt}$ can be derived as

$$\beta_{opt} = \frac{1}{(KS_{i^*,opt}-1)}\left[\frac{KS_{i^*,opt}}{1+\mathcal{W}\left(\frac{KS_{i^*,opt}-1}{e}\right)} - 1\right]$$

where the equality comes from properties of the LambertW function $\mathcal{W}(\cdot)$, i.e., $w(z) = \mathcal{W}(p)$ is the solution of the equation $w(z)e^{w(z)} = p$ [74].

# Part II

# Opportunistic Energy Transmission in Point-to-point Networks

# Chapter 6

# Opportunistic Energy Transfer in Point-to-Point Networks

*This chapter considers a point-to-point network with an energy transmitter and an energy harvesting (EH) user which has a constraint on EH time. We study an opportunistic energy transfer scheme for a block-faded frame structure. In particular, the amount of energy to be transmitted at each frame and the transmit beamforming vector is determined in order to maximize the expected total harvested energy when only the past and present channels are known. We investigate this problem for the case where the energy associated with channel estimation is negligible. We completely solve the optimization problem, and find the optimum threshold of each frame, optimum beamforming vector to be used, and the maximum expected total harvested energy of the network. Further, we discuss special cases of the problem such as utilizing different multi-antenna models and channel models. For these scenarios, we compare the performance of the opportunistic energy transfer scheme with respect to the performance benchmarks provided by the genie-aided energy transfer schemes.*

## 6.1 Introduction

Wireless sensor networks (WSNs) are widely used for sensing in smart environments. These networks are typically battery operated, and highly energy constrained [77]. With the advancement of low power circuitry and development of radio frequency (RF) energy harvesting circuits, significant research attention has been drawn to Wireless Energy Transfer (WET) [19].

Various opportunistic energy transfer schemes are considered in literature for relay networks [78] and cognitive radio networks [27], [79]. However, point-to-point network is the focus of this chapter. Such a network is considered in [80], and two objectives, namely i) maximizing the throughput by a deadline; and ii) minimizing the transmission completion time, are considered. Energy allocation over a finite horizon is considered based on channel conditions and time varying energy sources in [81]. The throughput is maximized by considering causal and non-causal channel state information (CSI). Similar network is considered in [82], in which transmitter is equipped with finite-sized data and energy buffers. The power allocation strategies are considered in order to maximize the long term-average throughput subject to data and energy constraints. Another design of online transmission strategies for slotted energy harvesting is considered in [83]. This work focuses on minimizing the gap between the maximum rate obtained using offline and online policies. These works mainly focus on maximizing throughput. However, in some applications, the sensor nodes may be highly restricted to perform the EH before a given time (i.e., a time deadline) in order to perform a specific task. In such situations maximizing the harvested energy with time constraints may be at high importance. To the best of our knowledge such a problem has not been studied in the literature. Therefore, this chapter focuses on finite horizon WET with transmit energy constraints.

This chapter considers a wireless network with an energy-constrained transmitter and a time-constrained EH user. We study the problem of maximizing the expected total harvested energy over a finite horizon with causal CSI. We formulate the general

problem in order to handle multi-antenna networks with a general channel distribution. We also analyse the genie-aided scheme as a benchmark.

The rest of this chapter is organized as follows. Section 6.2 discusses the system model for the point-to-point network. Section 6.3 formulates the optimization problem followed by the solution in Section 6.4. Section 6.5 disuses various special cases of the problem in which the general optimization problem can be applied. Section 6.6 presents numerical results followed by the concluding remark in Section 6.7.

## 6.2 System Model

This section describes the network model and the corresponding analytical model for a point-to-point wireless network used for EH.

### 6.2.1 Network Model

We consider a point-to-point wireless network as shown in Figure 6.1a. The network consists of a power transmitter with $M$ co-located antennas, and a energy harvesting user with $K$ co-located antennas. The power transmitter has a fixed energy source with a maximum available energy level $P$ which can be used up to $N$ time frames. This means that power transmitter can transmit all $P$ energy to the EH user by using maximum $N$ frames. Then, the EH user can harvest energy within those time frames which are indexed from $j = N - 1$ to $j = 0$ in Figure 6.1b. It is important to note that the indexing of the frames is in the descending order, so that the frame index reveals the number of frames remaining for the future. We denote the block fading channels at the $j$th frame between $m$th transmit antenna $\text{Tx}_m$ and $k$th receiving antenna $\text{Rx}_k$ by $h_j^{m,k}$. We denote the channel matrix at the $j$th frame by $\mathbf{H}_j \in \mathbb{C}^{M \times K}$ which has $h_j^{m,k}$ at $(m, k)$th position.

Since we consider an opportunistic wireless energy transfer, the energy transmitter should know the channel matrix $\mathbf{H}_j$ before energy transfer to the EH user. We assume perfect channel estimation is carried out at EH user. Since the EH user does not have any energy source, at the beginning of each frame, the energy transmitter transmits

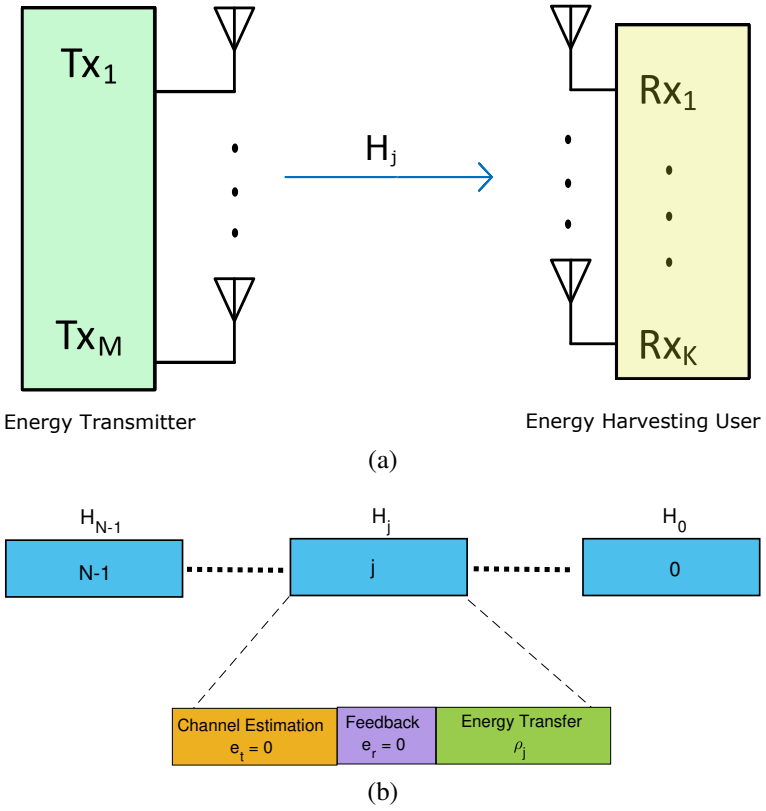


Figure 6.1: (a) A point-to-point SISO wireless network for EH; and (b) Frame structure for the energy transfer protocol.

$e_t$ amount of energy towards EH user for the channel estimation. In this chapter, we assume that the energy associated with channel estimation is negligible, i.e. $e_t = 0$. Using that received signal, the EH user estimates the channel matrix $\mathbf{H}_j$, and calculates the transmit energy required for energy transfer within the same frame denoted as, $\rho_j$ and the normalized beamforming vector which can be used to focus the energy beam towards the EH user for maximum harvested energy. Then, the EH user informs this information to Tx during the feedback phase. We assume that the energy associated in the feedback phase is negligible, i.e., $e_r = 0$, and the EH user is sufficiently charged to perform the feedback. Then, the energy transmitter transmits, $\rho_j$ amount of energy using the beamforming vector provided by the EH user.

### 6.2.2 Analytical Model

Since the energy level for each set of $N$ frames at Tx is limited to $P$, the available energy at Tx at the beginning of frame $j$ which depends on all the transmit energy of previous frames, can be given as $P_{j,(available)} = P - \sum_{i=j+1}^{N-1} \rho_i$. Then, the energy transmitted at the frame $j$, $\rho_j$ also depends on the energy transmitted at the previous frames. Although, this $\rho_j$ may be a function of all previous channel matrices, i.e., $\rho_j(\mathbf{H}_{N-1}, \cdots, \mathbf{H}_{j-1})$, we use $\rho_j$ for the sake of simplicity.

$$E_j = \eta_j \rho_j \mathbf{w}_j^{\dagger} \mathbf{H}_j^{\dagger} \mathbf{H}_j \mathbf{w}_j + \sigma_{n_j}^2 \tag{6.1}$$

where, $\mathbf{w}_j \in \mathbb{C}^M$ denotes the normalized beamforming vector, $\sigma_{n_j}^2$ is the energy associated with received noise, $\eta_j$ is the energy conversion efficiency, and $\dagger$ denotes the conjugate transpose. Hence, the total energy harvested at the end of $N$ frames is given by

$$E_T = \sum_{j=0}^{N-1} \eta_j \rho_j \mathbf{w}_j^{\dagger} \mathbf{H}_j^{\dagger} \mathbf{H}_j \mathbf{w}_j + \sigma_{n_j}^2. \tag{6.2}$$

We assume that the energy associated with noise is negligible, i.e., $\sigma_{n_j}^2 = 0$. It is important to note that the energy conversion efficiency, $\eta_j$ accounts for the energy con-

sumed for processing and running the circuitry [19]. This may depend on the circuitry of the user, and can be considered to be time invariant, i.e., $\eta_j = \eta \; \forall j$. Therefore, we have $E_T = \eta \sum_{j=0}^{N-1} \rho_j \mathbf{w}_j^\dagger \mathbf{H}_j^\dagger \mathbf{H}_j \mathbf{w}_j$. For presentation simplicity, we assume perfect energy conversion efficiency, i.e., $\eta = 1$. Then, the expected total harvested energy for $N$ frames can be given as

$$\tilde{E}_T = \sum_{j=0}^{N-1} \mathbb{E}_{\mathbf{H}_j} \Big[ \rho_j \mathbf{w}_j^\dagger \mathbf{H}_j^\dagger \mathbf{H}_j \mathbf{w}_j \Big], \tag{6.3}$$

where $\mathbb{E}_{\mathbf{H}_j}(.)$ is the expectation operation with respect to $\mathbf{H}_j$. We can achieve maximum harvested energy within $N$ frames by maximizing $\tilde{R}_T$. This can be done by optimizing the energy transfer, $\rho_j$ and the normalized beamforming vector, $\mathbf{w}_j$ to be used at each frame, based on the past and present channel knowledge only, i.e., $\mathbf{H}_i \; i \in [N-1, j]$. However, knowledge of the future channels, i.e., $\mathbf{H}_i \; i \in [j-1, 0]$, are unknown. This procedure may be called as *opportunistic* energy transfer which is discussed in detail in the next section.

## 6.3 Problem Formulation

In this section, we study the problem of maximizing the expected total harvested energy during given $N$ frames under the total transmit energy constraint. Specifically, we optimize the amount of energy to be transmitted in each time frame, i.e., $\rho_j, \forall j \in [0, N-1]$. This optimization problem can be formulated as

$$\begin{aligned} \max_{\rho_j, \, \mathbf{w}_j \in \mathbb{C}^M, \, \forall j \in [0, N-1]} \quad & \mathbb{E}\left[ E_{total} = \sum_{j=0}^{N-1} \rho_j \mathbf{w}_j^\dagger \mathbf{H}_j^\dagger \mathbf{H}_j \mathbf{w}_j + \sigma_{n_j}^2 \right] \\ \text{s. t.} \quad & \sum_{j=0}^{N-1} \rho_j \leq P, \\ & \rho_j \geq 0 \;\; \forall j \in [0, N-1]. \end{aligned} \tag{6.4}$$

It is worth noting that we cannot increase the energy associated with noise $\sigma_{n_j}^2$ by

varying transmit energy $\rho_j$ nor the beamforming vector $\mathbf{w}_j$. Hence, without changing the objective we can simply disregard all $\sigma_{n_j}^2$s. Further, we note at the optimum point the total transmit energy constraint should be met with an equality. Because otherwise the $\rho_j$s can be scaled such that the equality condition is met. However, this will contradict the optimality. Hence, the optimization problem reduces to

$$\begin{aligned} \max_{\rho_j,\ \mathbf{w}_j \in \mathbb{C}^M,\ \forall j \in [0,N-1]} \quad & \mathbb{E}\left[ E_{total} = \sum_{j=0}^{N-1} \rho_j \mathbf{w}_j^{\dagger} \mathbf{H}_j^{\dagger} \mathbf{H}_j \mathbf{w}_j \right] \\ \text{s. t.} \quad & \sum_{j=0}^{N-1} \rho_j = P, \\ & \rho_j \geq 0 \ \ \forall j. \end{aligned} \tag{6.5}$$

We note that $\rho_j$s are sequential. Thus, the optimization problem in (6.5) needs to be reformulated to obtain a recursive formula.

## 6.4 Optimum Solution

In this section, we consider the problem in (6.5) and reformulate the problem such that it can be solved recursively. We denote the optimum value of the objective function in (6.5) as $R_{N-1}(P)$. Hence, the optimization problem can be reformulated as

$$\begin{aligned} R_{N-1}(P) = \max_{\rho_{N-1},\ \mathbf{w}_{N-1} \in \mathbb{C}^M} & \mathbb{E}\left[ \rho_{N-1} \mathbf{w}_{N-1}^{\dagger} \mathbf{H}_{N-1}^{\dagger} \mathbf{H}_{N-1} \mathbf{w}_{N-1} \right] \\ & + R_{N-2}(P - \rho_{N-1}) \\ \text{s. t.} \quad & 0 \leq \rho_{N-1} \leq P \end{aligned} \tag{6.6}$$

It is worth noting that the problem in (6.6) has the recursive structure and the number of decision variables has reduced to two, which are the energy transmitted and the beamforming vector used at the frame $N-1$, i.e., $\rho_{N-1}$ and $\mathbf{w}_{N-1}$. Since the beamforming vector, $\mathbf{w}_{N-1}$ represents the proportions of the transmit energy to be distributed over the transmit antennas, $\mathbf{w}_{N-1}$ is independent form the total transmit energy of all antennas at the frame $N-1$, $\rho_{N-1}$ and the beamforming vectors used and the total transmit

energy at the other frames. Thus, we can solve for the optimum beamforming vector, $\mathbf{w}_{N-1}^{*}$ independent form $\rho_j,\ \forall j \in [0, N-1]$ and $\mathbf{w}_j,\ \forall j \in [0, N-2]$. In order to solve for the optimum beamforming vector, we consider the problem

$$\begin{aligned} &\max_{\mathbf{w}_j \in \mathbb{C}^M} \mathbb{E}\left[\mathbf{w}_j^{\dagger}\mathbf{H}_j^{\dagger}\mathbf{H}_j\mathbf{w}_j\right] \\ &\text{s. t.} \quad \|\mathbf{w}_j\|^2 = 1. \end{aligned} \tag{6.7}$$

We note that the harvested energy is non-negative. Thus, we can simply omit the expectation function, $\mathbb{E}(.)$ without changing the objective function. Therefore, the problem can be reduced to

$$\begin{aligned} &\max_{\mathbf{w}_j \in \mathbb{C}^M} \mathbf{w}_j^{\dagger}\mathbf{H}_j^{\dagger}\mathbf{H}_j\mathbf{w}_j \\ &\text{s. t.} \quad \|\mathbf{w}_j\|^2 = 1. \end{aligned} \tag{6.8}$$

This is a well studied problem for which the optimum beamforming vector is given by $\mathbf{w}_j^{*} = \mathbf{v}_1(\mathbf{H}_j^{\dagger}\mathbf{H}_j)$ and the optimum harvested energy is given by $\lambda_1(\mathbf{H}_j^{\dagger}\mathbf{H}_j)$, where $\lambda_1(\mathbf{A})$ and $\mathbf{v}_1(\mathbf{A})$ denotes the principle eigenvalue and the corresponding eigen-vector of a matrix $\mathbf{A}$, respectively, [22], [84], [85]. Hence, the problem in (6.6) can be given as

$$\begin{aligned} R_{N-1}(P) = \max_{\rho_{N-1}} &\mathbb{E}\left[\rho_{N-1}\lambda_1(\mathbf{H}_{N-1}^{\dagger}\mathbf{H}_{N-1})\right] \\ &+ R_{N-2}(P-\rho_{N-1}) \\ \text{s. t.} \quad &0 \leq \rho_{N-1} \leq P \end{aligned} \tag{6.9}$$

Theorem 1 gives the optimum policy and the optimum harvested energy for the problem in (6.8).

**Theorem 1.** *When the channel estimation energy is negligible ($e_t = 0$), the optimum expected total harvested energy using $N$ frames over block faded i.i.d. channels is*

$$R_{N-1}(P) = P\sum_{j=0}^{N-1} c_j \tag{6.10}$$

*where,*

$$c_j = \begin{cases} \int_0^{\infty} x f(x) dx, & j = 0 \\ \int_{\sum_{i=0}^{j-1} c_i}^{\infty} \left( x - \sum_{i=0}^{j-1} c_i \right) f(x) dx, & j > 0 \end{cases} \tag{6.11}$$

*and $f(x)$ denotes the probability density function (PDF) of the largest eigenvalue of the matrix $\mathbf{H}^{\dagger}\mathbf{H}$. Furthermore, the optimum transmit energy at the $j$th frame is given by*

$$\rho_j^* = \begin{cases} P, & \lambda_1(\mathbf{H}_j^{\dagger}\mathbf{H}_j) \geq R_{j-1}(P), \sum_{i=j+1}^{N-1} \rho_i = 0, \\ 0, & \textit{otherwise} \end{cases} \tag{6.12}$$

*Proof.* We use method of induction to prove Theorem 1.

Base Case: For one frame ($N = 1$), the problem in (6.6) reduces to

$$R_0(P) = \max_{\rho_0, \mathbf{w}_0 \in \mathbb{C}^M} \mathbb{E}\left[ \rho_0 \mathbf{w}_0^{\dagger} \mathbf{H}_0^{\dagger} \mathbf{H}_0 \mathbf{w}_0 \right]$$
$$\text{s. t.} \quad 0 \leq \rho_0 \leq P.$$

By using the optimum beamforming vector discussed in Section 6.4, the above problem can be given as

$$R_0(P) = \max_{\rho_0} \int_o^{\infty} \rho_0 x f(x) dx$$
$$\text{s. t.} \quad 0 \leq \rho_0 \leq P.$$

where $f(x)$ denotes the probability density function (PDF) of $\lambda_1(\mathbf{H}_0^{\dagger}\mathbf{H}_0)$. Clearly, the optimum transmit energy $\rho_0^*$ is $P$. In other words, if there is only one frame to transmit energy, all the energy will be transmitted in that frame regardless the quality of channel. Therefore, $R_0(P) = Pc_0$, where $c_0 = \int_0^{\infty} x f(x) dx$. It is worth noting that $c_0$ is the mean of the largest eigenvalue distribution, $\lambda_1(\mathbf{H}^{\dagger}\mathbf{H})$.

Inductive hypothesis: Assume that the solution in (6.10) is true for $N = n + 1$.

Then, we have

$$R_n(P) = P\sum_{j=0}^{n} c_j. \tag{6.13}$$

where, the terms $c_j$ and $\rho_j^*$ are given by (6.11) and (6.12), respectively.

Inductive Step: Consider the case of $N = n + 2$. The objective function in (6.9) can be written as

$$\begin{aligned} R_{n+1}(P) = \max_{\rho_{n+1}} & \mathbb{E}\left[\rho_{n+1}\lambda_1(\mathbf{H}_{n+1}^{\dagger}\mathbf{H}_{n+1})\right] \\ & + R_n(P - \rho_{n+1}) \\ \text{s. t.} \quad & 0 \leq \rho_{n+1} \leq P \end{aligned}$$

By substituting (6.13) we have

$$\begin{aligned} R_{n+1}(P) = \max_{\rho_{n+1}} & \mathbb{E}\left[\rho_{n+1}\lambda_1(\mathbf{H}_{n+1}^{\dagger}\mathbf{H}_{n+1})\right] \\ & + \mathbb{E}\left[(P - \rho_{n+1})\sum_{j=0}^{n} c_j\right] \\ \text{s. t.} \quad & 0 \leq \rho_{n+1} \leq P. \end{aligned}$$

By rearranging the terms and using $\mathbb{E}[g(x)] = \int g(x)f(x)dx$, we get

$$\begin{aligned} R_{n+1}(P) = \max_{\rho_{n+1}} & \int_0^{\infty} \rho_{n+1}\Big(x - \sum_{j=0}^{n} c_j\Big)f(x)dx + P\sum_{j=0}^{n} c_j \\ \text{s. t.} \quad & 0 \leq \rho_{n+1} \leq P. \end{aligned}$$

In order to maximize the total expected harvested energy, it is clear that $\rho_n + 1$ must be zero if $\lambda_1(\mathbf{H}_{n+1}^{\dagger}\mathbf{H}_{n+1}) < \sum_{j=0}^{n} c_j$, and $\rho_n + 1 = P$ otherwise. Therefore, it can be given as

$$R_{n+1}(P) = P\int_{\sum_{j=0}^{n} c_j}^{\infty} \Big(x - \sum_{j=0}^{n} c_j\Big)f(x)dx + P\sum_{j=0}^{n} c_j$$

It is worth noting that $\int\limits_{\sum_{j=0}^{n} c_j}^{\infty} \Big(x - \sum_{j=0}^{n} c_j\Big) f(x)dx = c_{n+1}$ as given in (6.11). Hence, we can see that

$$R_{n+1}(P) = P \sum_{j=0}^{n+1} c_j$$

where,

$$c_j = \begin{cases} \int\limits_{0}^{\infty} x f(x)dx, & j = 0 \\ \int\limits_{\sum_{i=0}^{j-1} c_i}^{\infty} \Big(x - \sum_{i=0}^{j-1} c_i\Big) f(x)dx, & j > 0 \end{cases} \tag{6.14}$$

Based on the rule of induction, Theorem 1 is true for all $N > 0$. This completes the proof. □

This means, the optimum transmit energy at each frame is given by a threshold policy. Specifically, at the time frame $j$, if the eigenvalue $\lambda_1(\mathbf{H}_j^{\dagger}\mathbf{H}_j)$ is greater than the threshold $\gamma_j$ given by

$$\gamma_j = \sum_{i=0}^{j-1} c_i, \tag{6.15}$$

all the available energy $\rho_j^* = P$ will be transmitted at the $j$th frame using the optimum beamforming vector, $\mathbf{v}_1(\mathbf{H}_j^{\dagger}\mathbf{H}_j)$.

If we are able to foresee all the channels matrices, it is obvious that by choosing the frame $j^*$ that yields the largest $\lambda_1(\mathbf{H}_j^{\dagger}\mathbf{H}_j)$, i.e. $j^* = \arg\max_j \lambda_1(\mathbf{H}_j^{\dagger}\mathbf{H}_j)$, we can maximize the expected harvested energy. Unfortunately, we do not have the luxury of seeing into the future. Therefore, we will use this method (addressed as genie aided method hereafter) as an upper bound of the proposed algorithm.

## 6.5 Special Cases of the Problem

In this section, we study the opportunistic energy transfer problem in scenarios where we assume Rayleigh fading channels for MIMO, multi-input single-output (MISO), and single-input single-output (SISO) networks.

### 6.5.1 Point-to-point MIMO Network with Rayleigh fading

In this section, we analyse the opportunistic wireless transfer problem for a point-to-point MIMO network with Rayleigh faded channels. We assume the block fading channel at the $j$th frame between $m$th transmit antenna $Tx_m$ and $k$th receiving antenna $Rx_k$, denoted by $h_j^{m,k}$ to be a complex Gaussian random variable with zero mean and unit variance, i.e., $h_j^{m,k} \sim \mathcal{CN}(0,1)$. Hence, the matrix $\mathbf{H}^\dagger\mathbf{H}$ is in the form of a Wishart matrix. The properties of of the eigenvalues of Wishart matrices is a well studied problem, and the PDF of the largest eigenvalue is given in [86] as

$$f(x) = \frac{1}{\prod_{i=1}^{K}(K-i)!(M-i)!}\frac{d}{dx}\det(\mathbf{S}(x)) \tag{6.16}$$

where $\mathbf{S}(x)$ is $K \times K$ Hankel matrix with $[\mathbf{S}(x)]_{k,l}$ at the $(k,l)$th position with

$$[\mathbf{S}(x)]_{k,l} = \gamma(M-K+k+l-1,x) \tag{6.17}$$

and $\gamma(t,x)$ denotes the lower incomplete gamma function which can be given by $\gamma(t,x) = \int_0^x u^{(t-1)}e^{-u}du$.

### 6.5.2 Point-to-point MIMO Network with Rician Fading

Practically, wireless energy transfer in limited to short range transmission (few meters) due to the path loss. Therefore, a significant line of sight component may exist in the wireless channels. This means it is acceptable to assume Rician faded channels. In this section, we model the channel matrix as

$$\mathbf{H} = \sqrt{\frac{K_R}{1+K_R}} + \sqrt{\frac{1}{1+K_R}}\mathbf{H}^N \tag{6.18}$$

where, $K_R$ denotes the Rician factor and the non-line of sight (NLOS) components of the channel matrix is given by $\mathbf{H}^N \in \mathbb{C}^{M,K}$, which can be models as i.i.d. complex Gaussian random variables with zero mean and unit variance, i.e., $h_{m,k}^N \sim \mathcal{CN}(0,1)$. In

this case, the PDF of $\lambda_1(\mathbf{H}^\dagger\mathbf{H})$ is given in [87] as

$$f(x) = \frac{e^{-\lambda_1} \times |\mathbf{\Psi}(x)| \mathrm{Tr}\left(\mathbf{\Psi}^{-1}(x)\mathbf{\Phi}(x)\right) \mathrm{U}(x)}{\Gamma(t-s+1)\lambda_1^{s-1} \prod_{k=1}^{s-1} \Gamma(t-k)\Gamma(s-k)} \tag{6.19}$$

where, $s = \min(M, K)$, $t = \max(M, K)$, $\lambda_1 = stK_R$, $\mathrm{U}(.)$ is the unit step function, $\mathrm{Tr}(.)$ and $|.|$ denotes the trace function and the determinant, respectively. The $s \times s$ matrix $\mathbf{\Phi}(x)$ has the $(i, j)$th element given as

$$[\mathbf{\Phi}(x)]_{i,j} = x^{t-i}\, e^{-x}\, {}_0\mathrm{F}_1\left(t-s+1; x\lambda_1\right) \tag{6.20}$$

where, ${}_0\mathrm{F}_1(.;.)$ is the generalized hyper-geometric function given by ${}_p\mathrm{F}_q(a_1, \cdots, a_p; b_1, \cdots, b_q; z)$ with $p = 0$ and $q = 1$ [88]. The $s \times s$ matrix $\mathbf{\Psi}(x)$ has the $(i, j)$th element given as

$$[\mathbf{\Psi}(x)]_{i,j} = \int_0^x y^{t-i} e^{-y} {}_0\mathrm{F}_1\left(t-s+1; y\lambda_1\right) dy. \tag{6.21}$$

For the elements other than the first column, i.e. $i = 1, \cdots, s$ and $j = 2, \cdots, s$, the equation in 6.21 reduces to $[\mathbf{\Psi}(x)]_{i,j} = \gamma(t-s+i+j-1, x)$.

### 6.5.3 Point-to-point MISO Network with Rayleigh Fading

In this section, we analyse the opportunistic wireless transfer problem for a point-to-point MISO network with Rayleigh faded channels. In other words, the network consists of a power transmitter with $M$ antennas and a single antenna user. In this case, the channel matrix at the frame $j$, $\mathbf{H}_j$ reduces to a vector $\mathbf{h}_j$. Therefore, the optimum beamforming vector discussed in Section 6.4, i.e., $\mathbf{w}_j^* = \mathbf{v}_1(\mathbf{H}_j^\dagger\mathbf{H}_j)$ will be equal to the normalized channel vector, $\tilde{\mathbf{h}}_j = \mathbf{h}_j/\|\mathbf{h}_j\|$. By using the optimum beamforming vector, $\mathbf{w}_j^* = \tilde{\mathbf{h}}_j$, we can harvest $\|\mathbf{h}_j\|^2$ amount of energy at the frame $j$. It is well known that the PDF of $\|\mathbf{h}_j\|^2$ is given both by the chi-squared distribution with $2M$ degrees of freedom, and Gamma distribution with shape and scale parameters of $M$ and

1 respectively ,i.e., $\|\mathbf{h}_j\|^2 \sim \Gamma(M,1)$. Therefore, we have

$$f(x) = \frac{1}{\Gamma(M)} x^{M-1} e^{-x}. \tag{6.22}$$

The PDF in (6.22) can also be derived from (6.16) and (6.17) by substituting $K = 1$. By substituting the PDF in (6.22) to the optimum solution given in (6.10) and (6.11), we obtain the optimum harvested energy using $N$ frames for a point-to-point MISO network with Rayleigh faded channels as

$$R_{N-1}(P) = P \sum_{j=0}^{N-1} c_j \tag{6.23}$$

where, $c_0 = M$ and

$$c_j = \frac{1}{\Gamma(M)} \left[ \Gamma\left( M+1, \sum_{i=0}^{j-1} c_i \right) - \Gamma\left( M, \sum_{i=0}^{j-1} c_i \right) \sum_{i=0}^{j-1} c_i \right], j > 0 \tag{6.24}$$

and $\Gamma(t,x)$ denotes the upper incomplete gamma function which can be given by $\Gamma(t,x) = \int_x^\infty u^{(t-1)} e^{-u} du$.

### 6.5.4 Point-to-point SISO Network with Rayleigh Fading

In this section, we analyse the opportunistic wireless transfer problem for a point-to-point SISO network with Rayleigh faded channels. In this case, the channel matrix at the frame $j$, $\mathbf{H}_j$ reduces to a scalar $h_j$. As there is only one transmitting antenna, there is no beamforming vector. Therefore, we can harvest $|h_j|^2$ amount of energy at the frame $j$. It is well known that the PDF of $|h_j|^2$ is given both by the exponential distribution, i.e. $f(x) = e^{-x}$. By substituting the PDF to the optimum solution given in (6.10) and (6.11), we obtain the optimum harvested energy using $N$ frames for a point-to-point

MISO network with Rayleigh faded channels as

$$R_{N-1}(P) = P \sum_{j=0}^{N-1} c_j \tag{6.25}$$

where $c_0 = 1$ and $c_j = e^{-\sum_{i=0}^{j-1} c_i}$. The optimum transmit energy at frame $j$ is

$$\rho_j^* = \begin{cases} P - \sum_{i=j+1}^{N-1} \rho_i, & |h_j|^2 \geq \gamma_j, \\ 0, & \text{otherwise.} \end{cases} \tag{6.26}$$

where $\gamma_j$ is the threshold at frame $j$ given as

$$\gamma_j = \sum_{i=0}^{j-1} c_i. \tag{6.27}$$

#### 6.5.4.1 Genie-aided Energy Transfer for SISO Network with Rayleigh fading

For a performance comparison, we consider an energy transfer scheme with non-causal channel state information. This scheme is addressed as the genie-aided energy transfer scheme hereafter. If the energy transmitter knows all channel gains $h_j$s, $\forall j = 0, \cdots, N-1$, energy transmitter may transmit all $P$ energy at the frame with maximum channel gain. We denote that frame index as $j^*$ where $j^* = \arg\max_j \left(|h_{N-1}|^2, \cdots, |h_0|^2\right)$. Then, the expected harvested energy using $N$ frames can be given as

$$\begin{aligned} \tilde{E}_G &= P\mathbb{E}_{h_{j^*}}\left[|h_{j^*}|^2\right] = P\int_0^\infty x f_{|h_{j^*}|^2}(x)dx \\ &= P\int_0^\infty xNPe^{-x}(1-e^{-x})^{N-1} = P\sum_{n=1}^{N}\frac{1}{n}. \end{aligned} \tag{6.28}$$

#### 6.5.4.2 Asymptotic Analysis

In this section, we analyse the asymptotic behaviour of the optimum harvested energy for both opportunistic and genie-aided energy transfer schemes for SISO network with

Rayleigh fading, when the number of frames becomes infinitely large, i.e., $N \to \infty$. Theorem 2 gives the maximum expected total harvested energy convergence with $N$.

**Theorem 2.** *Without channel estimation energy ($e_t = 0$), the optimum expected total harvested energy converges with $N \to \infty$ as*

*For the opportunistic energy transfer:*

$$\lim_{N\to\infty} R_{N-1}(P) = P\ln(N) \tag{6.29}$$

*For genie-aided energy transfer:*

$$\lim_{N\to\infty} R_{N-1}(P) = P\gamma + P\ln(N) \tag{6.30}$$

*where $\gamma$ is the Euler-Mascheroni constant ($\gamma = 0.5772...$)[89].*

*Proof.* Define a sequence $U_N$ as $U_N \triangleq \sum_{j=0}^{N} c_j - \ln(N)$. The term $U_{N+1} - U_N$ can be give by

$$U_{N+1} - U_N = c_{N+1} - \ln(N+1) + \ln(N). \tag{6.31}$$

By using the mean value theorem, we have $\ln(N+1)-\ln(N) = \frac{1}{N+\theta}$, where, $0 < \theta < 1$. Therefore, (6.31) can be written as

$$U_{N+1} - U_N = c_{N+1} - \frac{1}{N+\theta}. \tag{6.32}$$

The term $c_{N+1} = e^{-\sum_{j=0}^{N} c_j}$ can also be given in a recursive formula as $c_{N+1} = c_N e^{-c_N}$. As $c_0 = 1$ and $0 < e^{-x} \leq 1$ for $x \geq 0$, by using this recursive structure of $c_N$, it can be shown that $c_N$ is a decreasing function which converges to zero, i.e., $\lim_{N\to\infty} c_N = 0$. Therefore, $\lim_{N\to\infty} U_{N+1} - U_N = c_{N+1} - \frac{1}{N+\theta} = 0$. In other words, the function $U_N$ converges. Furthermore, by computing $U_N$ for large $N$, we can show that the function $U_N$ converges to zero for large $N$. Therefore, for opportunistic energy transfer, the expected harvested energy for large $N$ converges as in (6.29).

For the genie aided method, the maximum expected total harvested energy is given as $\tilde{E}_G = P\sum_{n=1}^{N} 1/n$. The definition of Euler-Mascheroni constant is given as $\gamma = \sum_{n=1}^{N} 1/n - \ln(N)$ with $N \to \infty$ [89], [90]. Hence, $R_{N-1}(P)$ for genie aided method converges as (6.30). This completes the proof. □

By comparing (6.29) and (6.30), we can see that the cost of not being able to foresee the future is $\gamma$ for large $N$.

## 6.6 Numerical and Simulation results

This section provides numerical results to verify the analysis and to discuss the performance. We focus on the special cases of the problem given in 6.5. Recall that the energy conversion efficiency $\eta = 1$, and energy associated with noise is negligible. Further, we have normalized energy ($P = 1$) in this section.

### 6.6.1 Point-to-point MIMO Network with Rayleigh fading

In this case, we generate $N$ channel matrices, $\mathbf{H}_j$ with elements $h \sim \mathcal{CN}(0, 1)$ and obtain the maximum eigenvalue of each matrix $\lambda_1\left(\mathbf{H}_j^{\dagger}\mathbf{H}_j\right)$. We then sequentially compare the maximum eigenvalue $\lambda_1\left(\mathbf{H}_j^{\dagger}\mathbf{H}_j\right)$ with the threshold obtained by using (6.15) and Section 6.5.1, and obtain the optimum energy transfer $\rho^*$ in (6.12). Then we calculate the total harvested energy in all $N$ frames. For the genie-aided energy transfer scheme, we choose the frame $j^*$ with the largest value for $\lambda_1\left(\mathbf{H}_j^{\dagger}\mathbf{H}_j\right)$ among the $N$ frames, and transmit all the energy available at that frame.We average the harvested energy from each scheme by using $10^6$ set of channel realizations.

Figure 6.2 shows the variation of the expected harvested energy with the number of frames for opportunistic energy transfer and Genie-aided energy transfer when the number of receiving antennas is fixed at $K = 3$ and the number of transmitting antennas $M = 3$ and 6. For both $M = 3$ and $M = 6$ cases, the analytical results for opportunistic energy transfer scheme obtained using Theorem 1 and section 6.5.1 match closely with the simulation results which verifies our analysis. The genie-aided scheme

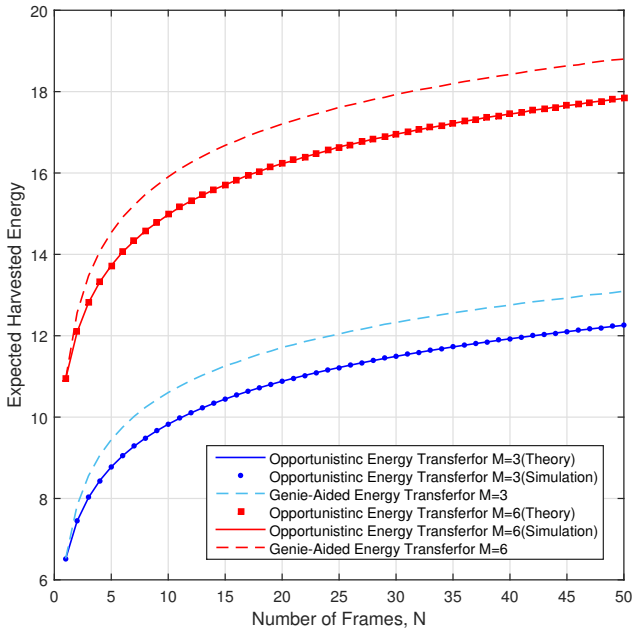


Figure 6.2: The variation of expected harvested energy with the number of frames for MIMO Network with Rayleigh fading.

outperforms the opportunistic energy transfer scheme. Further, we note that when the number of transmitting antennas is increased to $M = 6$, the expected harvested energy is higher compared to $M = 3$ case. This is because with higher degree of freedom, the beamforming vector can be finely tuned in order to obtain the maximum energy possible.

### 6.6.2 Point-to-point MIMO Network with Rician Fading

In this case, we generate $N$ channel matrices, $\mathbf{H}_j$ as given in (6.18) and obtain the maximum eigenvalue of each matrix $\lambda_1\left(\mathbf{H}_j^{\dagger}\mathbf{H}_j\right)$. We then sequentially compare the maximum eigenvalue $\lambda_1\left(\mathbf{H}_j^{\dagger}\mathbf{H}_j\right)$ with the threshold obtained by using (6.15) and Section 6.5.2. and obtain the optimum energy transfer $\rho^*$ in (6.12). Then we calculate the total harvested energy in all $N$ frames. For the genie-aided energy transfer scheme, we choose the frame $j^*$ with the largest value for $\lambda_1\left(\mathbf{H}_j^{\dagger}\mathbf{H}_j\right)$ among the $N$ frames, and transmit all the energy available at that frame. We average the harvested energy from

each scheme by using $10^6$ set of channel realizations.

Figure 6.3 shows the variation of the expected harvested energy with the number of frames for opportunistic energy transfer and Genie-aided energy transfer when for a network with $M = 2$ transmitting antennas and $K = 2$ receiving antennas for Rician factor $K_R = 1$ and 3. For both $K_R = 1$ and $K_R = 3$ cases, the analytical results for opportunistic energy transfer scheme obtained using Theorem 1 and section 6.5.2 match closely with the simulation results which verifies our analysis. The genie-aided scheme outperforms the opportunistic energy transfer scheme. Further, we note that $K_R = 3$ case slightly outperforms the $K_R = 1$ case when the number of frames $N$ is low, and then for higher number of frames, the $K_R = 1$ case outperforms $K_R = 3$ case. This is because the channel matrices are normalized to have unit energy. Which means for $K_R = 1$ case, the mean energy of each channel is low compared to the $K_R = 3$ case, and the variance of $K_R = 1$ case is higher compared to the $K_R = 3$ case. Therefore, the pdf of maximum eigenvalue for $K_R$ is widely spread compared to the $K_R = 3$ case. As the opportunistic energy transfer scheme benefits from the randomness of the channels, the effect of high line-of-sight components is overshadowed by the spread of the distribution of non-line-of-sight component.

### 6.6.3 Point-to-point MISO Network with Rayleigh Fading

In this case, we generate $N$ channel vectors, $\mathbf{h}_j$ with elements $h \sim \mathcal{CN}(0, 1)$ and obtain $\|\mathbf{h}_j\|^2$ for each frame. We then sequentially compare the $\|\mathbf{h}_j\|^2$ with the threshold obtained by using (6.15) and Section 6.5.3, and obtain the optimum energy transfer $\rho^*$ in (6.12). Then we calculate the total harvested energy in all $N$ frames. For the genie-aided energy transfer scheme, we choose the frame $j^*$ with the largest value for $\|\mathbf{h}_j\|^2$ among the $N$ frames, and transmit all the energy available at that frame. We average the harvested energy from each scheme by using $10^6$ set of channel realizations.

Figure 6.4 shows the variation of the expected harvested energy with the number of frames for opportunistic energy transfer and Genie-aided energy transfer when the number of transmitting antennas $M = 3$ and 6. For both $M = 3$ and $M = 6$ cases, the

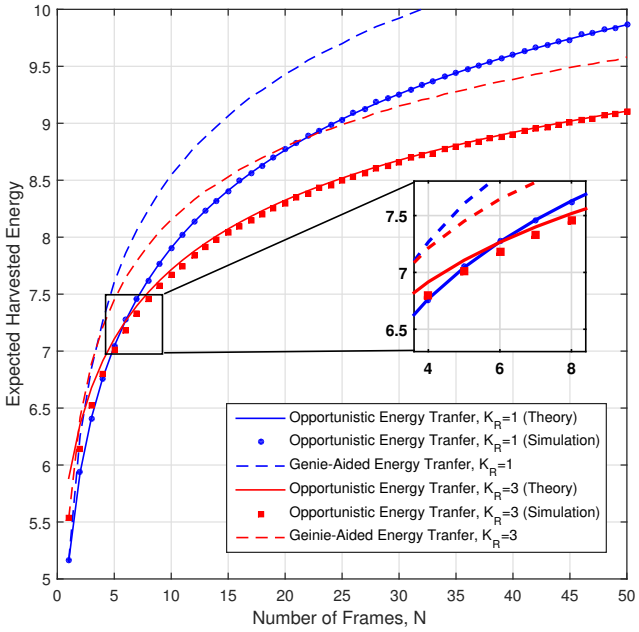


Figure 6.3: The variation of expected harvested energy with the number of frames for MIMO network with Rician fading.

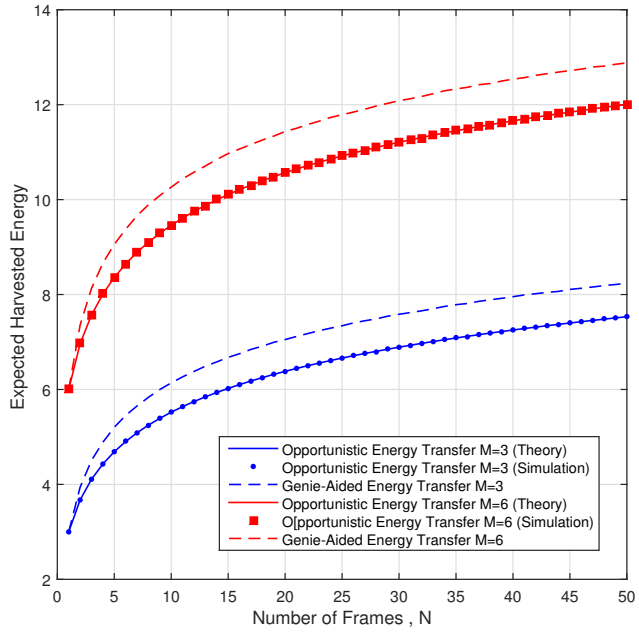


Figure 6.4: The variation of expected harvested energy with the number of frames for MISO network with Rayleigh fading.

analytical results for opportunistic energy transfer scheme obtained using Theorem 1 and section 6.5.3 match closely with the simulation results which verifies our analysis. The genie-aided scheme outperforms the opportunistic energy transfer scheme. Further, we note that when the number of transmitting antennas is increased to $M = 6$, the expected harvested energy is higher compared to $M = 3$ case. This is because with higher degree of freedom, the beamforming vector can be finely tuned in order to obtain the maximum energy possible.

### 6.6.4 Point-to-point SISO Network with Rayleigh Fading

In this case, we sequentially compare $|h_j|^2$ with $\gamma_j$ in (6.27) and obtain optimum energy transfer $\rho_j^*$ in (6.26). Then, we calculate the total harvested energy in all $N$ frames. For the genie-aided energy transfer scheme, we choose the frame $j^*$ with maximum $|h_j|^2$ among the $N$ frames, and transmit all the energy available at that frame. For equal energy transfer, we transfer $P/N$ amount of energy in each frame. For the random energy transfer, we transfer all the energy available in a randomly selected frame $j \in \{0, N-1\}$. We calculate the average total harvested energy by using $10^6$ set of channel realizations.

Figure 6.5 shows the variation of the expected harvested energy with the number of frames under four schemes. The analytical results for opportunistic and genie-aided energy transfer schemes in (6.25) and (6.28) match closely with the simulation results which verifies our analysis. The genie-aided scheme outperforms all other schemes, and optimum energy transfer scheme outperforms equal and random energy transfer schemes which have harvested energy as one. Compared to equal and random energy transfer schemes, the gain of expected harvested energy is approximately 4 times and 3.5 times for genie-aided energy transfer scheme and optimum EH scheme, respectively, at $N = 30$.

Figure 6.6 shows the variation of tern $R_{N-1}(P) - \ln(N)$ with the number of frames $N$. When $N$ increases, the simulated values approach to $\gamma$ and 0 for the genie-aided and the optimum energy transfer schemes, respectively. This verifies Theorem 2.

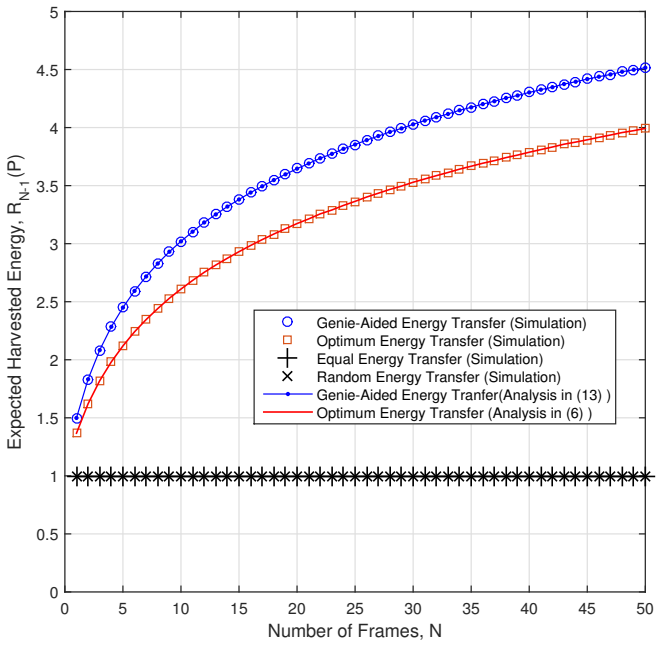


Figure 6.5: Expected harvested energy with number of frames for four energy transfer schemes when $e_t = 0$.

Figure 6.7 shows the variation of the outage probability of expected harvested energy with the transmit energy when the harvested energy threshold ($E_{Th}$) is 10dBm. We calculate the outage probability as $\mathbb{P}\left(\tilde{E}_T < E_{Th}\right)$. The Outage probabilities of genie-aided scheme improve as order $N$, i.e., order 1,2, and 3 for $N = 1, 2,$ and 3, respectively, because genie-aided scheme makes the decision based on $N$ independent statistics which helps for the diversity gain. Outage probabilities of optimum energy transfer scheme improve as order one irrespective of $N$, because its transmission is based on current frame only. However, it helps to provide an array gain, i.e., outage probability of approximately 0.1 is achieved with $P = 20,\ 18,$ and 16dBm for N=1,2, and 3, respectively. Outage probabilities of all other cases improve also as order one, but without any array gain.

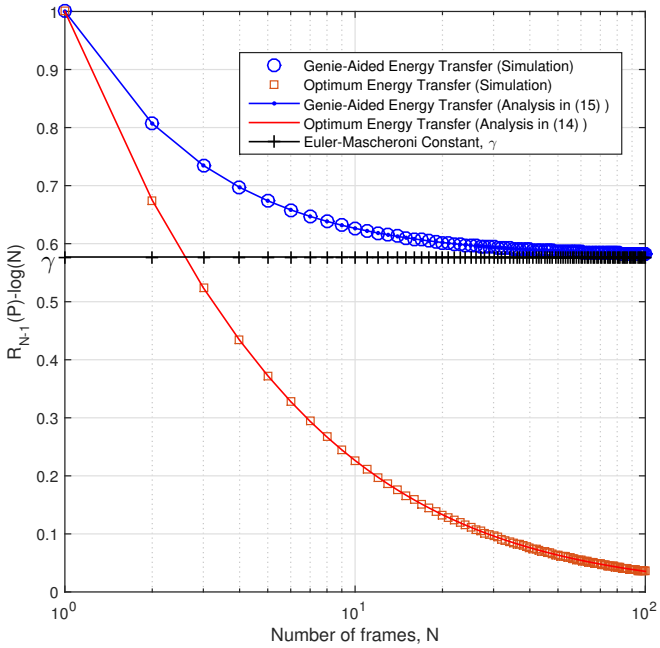


Figure 6.6: Asymptotic behaviour of expected harvested energy with opportunistic and genie-aided schemes when $e_t = 0$.

## 6.7 Conclusions

This chapter considers a point-to-point multi-antenna network with an energy constrained power transmitter and an energy receiver which has strict deadline on time. We derive the optimum energy transfer scheme for a general channel model in which we jointly optimize for the beamforming vector and the energy levels to be transmitted at each frame. We show that the optimum policy reduces to an all-or-nothing threshold policy. We derive the opportunistic energy beamforming scheme for special cases of multi-antenna systems and channel models. We also derive the maximum expected total harvested energy using the genie-aided scheme for performance comparison. For SISO Rayleigh channels, by analysing the asymptotic behaviour of two schemes, we show that the advantage of non-causality can be given by the Eular-Mascheroni constant.

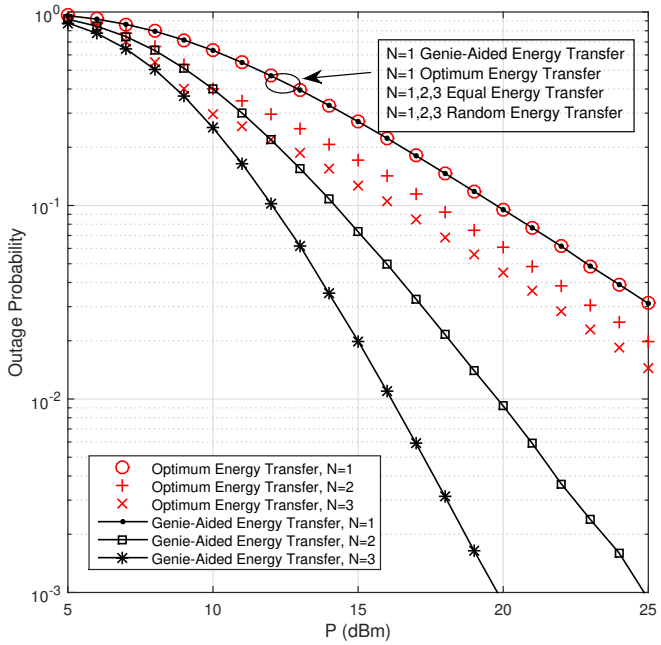


Figure 6.7: Outage Probability of expected harvested energy with transmit power $P$ for the energy threshold 10dBm and $e_t = 0$.

# Chapter 7

# Opportunistic Energy Transfer in Point-to-Point Networks with Channel Estimation Energy

*In previous chapters, we focused on the opportunistic energy transfer problem for a point-to-point network by neglecting the energy associated with channel estimation. However, this may not be the case in reality due to low efficiency of wireless energy transfer. Furthermore, such channel estimations are performed in each frame until the power transfer occurs. This may require significant energy for the channel estimation. Therefore, in this chapter, we investigate a similar problem by considering the energy associated with channel estimation at the beginning of each frame. We solve the optimization problem, and find the optimum threshold of each frame, optimum beamforming vector to be used, and the maximum expected total harvested energy of the network.*

## 7.1 Introduction

Wireless energy transfer enables energy constrained wireless nodes to prolong their life span without resorting to exhaustive battery replacements. However, wireless energy transfer undergoes severe propagation losses with the transmission distance [19]. To

improve the energy harvesting capability, advance signal processing techniques such as energy beamforming can be used. For this purpose, it is crucial to learn the channel state information such that the energy transfer scheme can be optimized to enhance the harvested energy levels. Conventionally, a training sequence is required to perform channel estimation (CE) before transferring energy [91]. However, such channel estimation is also energy consuming. Thus, it is important to consider the cost of energy associated in the channel estimation phase when designing energy efficient energy transfer schemes. This is the focus of this chapter.

In [92], a point-to-point energy transfer system is considered in order to obtain a received power-based channel estimation scheme. In the proposed scheme, the receiver measures the received power of the RF signal, that is sent by the transmitter with various beamforming weights. Then, the transmitter calculates the channel gains based on the received power measurements reported by the receiver. This allows simple circuitry compared to the symbol-based schemes.

In Chapter 6, We focus on point-to-point networks with an energy transmitter equipped with a limited energy resource and an energy receiver with a strict deadline to achieve energy harvesting. We assumed the energy associated with channel estimation in negligible. However, this may not be the case in practise. Especially, as channel estimation in carried out in every frame until all the energy is transferred to the user. Therefore, in this chapter, we reformulate the problem to consider the energy consumed in channel estimation.

The rest of this chapter is organized as follows, Section 7.2 provides the system model for the point-to-point network. Section 7.3 formulates the optimization problem by considering the energy utilized for channel estimation is significant. We prove that the optimum energy transfer policy reduces to an all-or-nothing threshold policy and then obtain the optimum policy in Section 7.4. We apply the general opportunistic energy transfer to SISO Rayleigh channels in Section 7.5. Section 7.6 gives the numerical results for SISO Rayleigh channels followed by the concluding remark in Section 7.7.

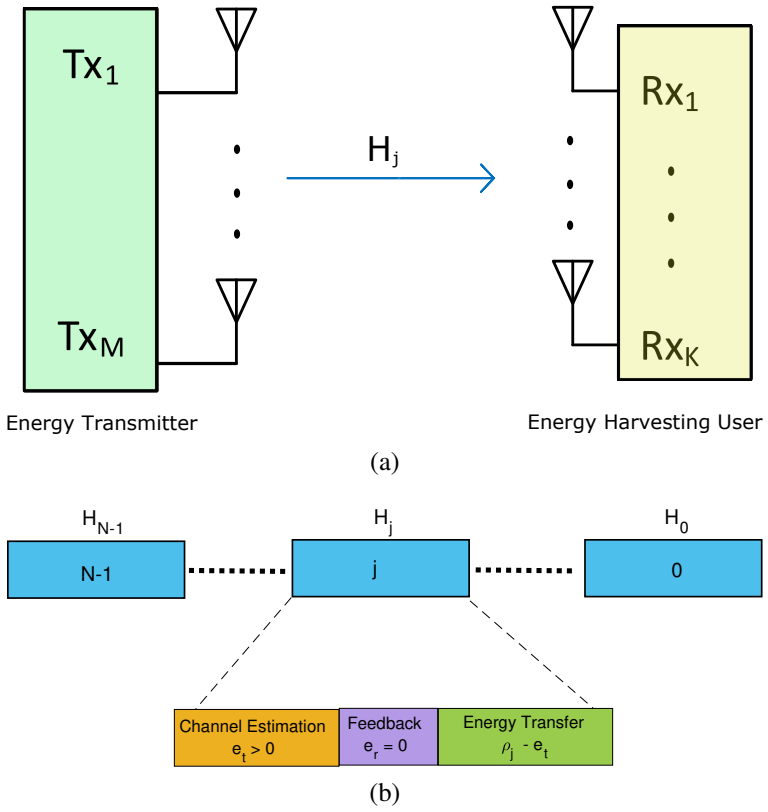


Figure 7.1: (a) A point-to-point SISO wireless network for EH; and (b) Frame structure for the energy transfer protocol.

## 7.2 System Model

This section describes the network model and the corresponding analytical model for a point-to-point SISO wireless network used for EH.

### 7.2.1 Network Model

We consider a point-to-point wireless network as shown in Figure 7.1a. The network consists of a power transmitter with $M$ co-located antennas, and an energy harvesting user with $K$ co-located antennas. The power transmitter has a fixed energy source with a maximum available energy level $P$ which can be used up to $N$ time frames. This means that power transmitter can transmit all $P$ energy to the EH user by using maximum $N$ frames. Then, the EH user can harvest energy within those time frames which are

indexed from $j = N-1$ to $j = 0$ in Figure 7.1b. It is important to note that the indexing of the frames is in the descending order, so that the frame index reveals the number of frames remaining for the future. We denote the block fading channels at the $j$th frame between $m$th transmit antenna $\text{Tx}_m$ and $k$th receiving antenna $\text{Rx}_k$ by $h_j^{m,k}$. We denote the channel matrix at the $j$th frame by $\mathbf{H}_j \in \mathbb{C}^{M \times K}$ which has $h_j^{m,k}$ at $(m, k)$th position.

Since we consider an opportunistic wireless energy transfer, the energy transmitter should know the channel matrix $\mathbf{H}_j$ before energy transfer to the EH user. We assume that perfect channel estimation is carried out at EH user. Since the EH user does not have any energy source, at the beginning of each frame, the energy transmitter transmits $e_t$ amount of energy towards EH user for the channel estimation. We denote the total energy transmitted by Tx in frame $j$ as $\rho_j$, which includes both energy transmitted for channel estimation and harvesting. Using that received signal, the EH user estimates the channel matrix $\mathbf{H}_j$, and calculates the transmit energy required for energy transfer within the same frame, $\rho_j - e_t$ and the normalized beamforming vector which can be used to focus the energy beam towards the EH user for maximum harvested energy. Then, the EH user informs this information to Tx during the feedback phase. We assume that the energy associated in the feedback phase is negligible, i.e., $e_r = 0$, and the EH user is sufficiently charged to perform the feedback. Then, the energy transmitter transmits, $\rho_j$ amount of energy using the beamforming vector provided by the EH user.

### 7.2.2 Analytical Model

Since the energy level for each set of $N$ frames at Tx is limited to $P$, the available energy at Tx at the beginning of frame $j$ which depends on all the transmit energy of previous frames, can be given as $P_{j,(available)} = P - \sum_{i=j+1}^{N-1} \rho_i$. Then, the energy transmitted at the frame $j$, $\rho_j$ also depends on the energy transmitted at the previous frames. Although, this $\rho_j$ may be a function of all previous channel gains, i.e., $\rho_j(\mathbf{H}_{N-1}, \cdots, \mathbf{H}_{j-1})$, we use $\rho_j$ for the sake of simplicity. We denote the state of energy availability at frame $j$ as $s_j$, where $s_j = 1$ if there is energy available at the frame $j$, i.e., $P - \sum_{i=j+1}^{N-1} s_i \rho_i > 0$,

and $s_j = 0$ if the energy source has run out. Therefore, $s_j$ can be given as

$$s_j = U\left(P - \sum_{i=j+1}^{N-1} s_i \rho_i\right) \tag{7.1}$$

where $U(\cdot)$ denotes the unit step function. The importance of $s_j$ lies in the case of $\rho_j < e_t$ which means that the leftover energy at frame $j$ is not sufficient for the channel estimation. In such situations, the state $s_j$ sets to zero in order to ensure non-negativity of the harvested energy.

The harvested energy at the frame $j$ can be given as

$$E_j = \eta_j s_j \left(\rho_j - e_t\right) \mathbf{w}_j^{\dagger} \mathbf{H}_j^{\dagger} \mathbf{H}_j \mathbf{w}_j + \sigma_{n_j}^2 \tag{7.2}$$

where, $\eta_j$ is the energy conversion efficiency, and $\sigma_{n_j}^2$ is the energy associated with received noise. Without loss of generality, we assume perfect energy conversion efficiency, i.e., $\eta_j = 1$, and the energy associated with noise is negligible, i.e., $\sigma_{n_j}^2 = 0$. Then, the expected total harvested energy for $N$ frames can be given as

$$\tilde{E}_T = \sum_{j=0}^{N-1} \mathbb{E}_{\mathbf{H}_j}\Big[s_j \left(\rho_j - e_t\right) \mathbf{w}_j^{\dagger} \mathbf{H}_j^{\dagger} \mathbf{H}_j \mathbf{w}_j\Big], \tag{7.3}$$

where $\mathbb{E}_{\mathbf{H}_j}(.)$ is the expectation operation with respect to $\mathbf{H}_j$. We can achieve maximum harvested energy within $N$ frames by maximizing $\tilde{E}_T$. This can be done by optimizing the energy transfer at each frame, $\rho_j$ based on the past and present channel knowledge only, i.e., $\mathbf{H}_i$ $i \in [N-1, j]$. However, knowledge of the future channels, i.e., $\mathbf{h}_i$ $i \in [j-1, 0]$, are unknown. This procedure may be called as *opportunistic* energy transfer which is discussed in detail in the next section.

## 7.3 Opportunistic Energy Transfer

In this section, we maximize the expected total harvested energy over $N$ time frames with the transmit energy budget $P$. In particular, we optimize the amount of energy to be transmitted in each frame, i.e., $\rho_j$, $\forall j \in [0, N-1]$. In general, the corresponding optimization problem can be given as

$$\max_{\rho_j, s_j} \quad \tilde{E}_T == \sum_{j=0}^{N-1} \mathbb{E}_{\mathbf{H}_j}\left[s_j\left(\rho_j - e_t\right)\mathbf{w}_j^{\dagger}\mathbf{H}_j^{\dagger}\mathbf{H}_j\mathbf{w}_j\right] \tag{7.4a}$$

$$\text{s. t.} \quad \sum_{j=0}^{N-1} s_j\rho_j \leq P, \tag{7.4b}$$

$$\rho_j \geq e_t \;\; \forall j = \{j; j \in [0, N-1], s_j \neq 0\}, \tag{7.4c}$$

where (7.4b) is for total transmit energy constraint, and (7.4c) is to ensure that the available energy is adequate for channel estimation when $s_j \neq 0$. We note that $\rho_j$s are sequential. Thus, the optimization problem in (7.4) needs to be reformulated to obtain a recursive formula.

## 7.4 Optimum Solution

In this section, we consider the problem in (7.4) and reformulate the problem such that it can be solved recursively. We denote the optimum value of the objective function in (7.4) as $R_{N-1}(P)$. Hence, the optimization problem can be reformulated as

$$\begin{aligned} R_{N-1}(P) = \max_{\rho_{N-1},\, \mathbf{w}_{N-1}\in\mathbb{C}^M} \mathbb{E}\Big[& s_{N-1}\left(\rho_{N-1} - e_t\right)\mathbf{w}_{N-1}^{\dagger}\mathbf{H}_{N-1}^{\dagger}\mathbf{H}_{N-1}\mathbf{w}_{N-1} \\ & + R_{N-2}(P - \rho_{N-1})\Big] \\ \text{s. t.} \quad & s_{N-1}e_t \leq \rho_{N-1} \leq P \\ & R_{N-1}(P) \geq 0. \end{aligned} \tag{7.5}$$

It is worth noting that the problem in (7.5) has the recursive structure and the number of decision variables has reduced to two, which are the energy transmitted and the beamforming vector used at the frame $N-1$, i.e., $\rho_{N-1}$ and $\mathbf{w}_{N-1}$. Since the beamforming vector, $\mathbf{w}_{N-1}$ represents the proportions of the transmit energy to be distributed over the transmit antennas, $\mathbf{w}_{N-1}$ is independent form the total transmit energy of all antennas at the frame $N-1$, $\rho_{N-1}$ and the beamforming vectors used and the total transmit energy at the other frames. Thus, we can solve for the optimum beamforming vector, $\mathbf{w}_{N-1}^{*}$ independent form $\rho_j,\ \forall j \in [0, N-1]$ and $\mathbf{w}_j,\ \forall j \in [0, N-2]$. In order to solve for the optimum beamforming vector we consider the problem

$$\begin{aligned} &\max_{\mathbf{w}_j \in \mathbb{C}^M} \mathbb{E}\left[\mathbf{w}_j^{\dagger}\mathbf{H}_j^{\dagger}\mathbf{H}_j\mathbf{w}_j\right] \\ &\text{s. t.} \quad \|\mathbf{w}_j\|^2 = 1. \end{aligned} \tag{7.6}$$

We note that the harvested energy is non-negative. Thus we can simply omit the expectation function, $\mathbb{E}(.)$ without changing the objective function. Therefore, the problem can be reduced to

$$\begin{aligned} &\max_{\mathbf{w}_j \in \mathbb{C}^M} \mathbf{w}_j^{\dagger}\mathbf{H}_j^{\dagger}\mathbf{H}_j\mathbf{w}_j \\ &\text{s. t.} \quad \|\mathbf{w}_j\|^2 = 1. \end{aligned} \tag{7.7}$$

This is a well studied problem for which the optimum beamforming vector is given by $\mathbf{w}_j^{*} = \mathbf{v}_1(\mathbf{H}_j^{\dagger}\mathbf{H}_j)$ and the optimum harvested energy is given by $\lambda_1(\mathbf{H}_j^{\dagger}\mathbf{H}_j)$, where $\lambda_1(\mathbf{A})$ and $\mathbf{v}_1(\mathbf{A})$ denotes the principle eigenvalue and the corresponding eigen-vector of a matrix $\mathbf{A}$, respectively [22], [84], [85]. Hence, the problem in (7.5) can be given as

$$\begin{aligned} R_{N-1}(P) = \max_{\rho_{N-1}} \ &\mathbb{E}\left[s_{N-1}\left(\rho_{N-1} - e_t\right)\lambda_1(\mathbf{H}_{N-1}^{\dagger}\mathbf{H}_{N-1}) + R_{N-2}(P-\rho_{N-1})\right] \\ \text{s. t.} \quad &s_{N-1}e_t \leq \rho_{N-1} \leq P \\ &R_{N-1}(P) \geq 0. \end{aligned} \tag{7.8}$$

We solve the problem using Theorems 3 and 4. In Theorem 3, we prove that the optimum policy for opportunistic energy transfer reduces to an all-or-nothing threshold policy. By using Theorem 3, we give the optimum policy and the optimum harvested energy in Theorem 4.

**Theorem 3.** *When the channel estimation energy is significant the optimum policy for opportunistic energy transfer is given by an all-or-nothing threshold policy.*

*Proof.* We consider the scenario where the expected energy harvested by using $j$ frames with $\rho_j$ level of transmit energy can be given as

$$\tilde{E}_j(\rho_j) = s_j(\rho_j - e_t)C \tag{7.9}$$

where $C$ is a positive constant. We now consider a set of $j+1$ frames with $P$ energy level. In such case, the optimization problem in (7.8) can be given as

$$R_{j+1}(P) = \max_{\rho_{j+1}} \ \mathbb{E}\left[s_{j+1}\left(\rho_{j+1} - e_t\right)\lambda_1(\mathbf{H}_{j+1}^{\dagger}\mathbf{H}_{j+1}) + s_j(P - \rho_{j+1} - e_t)C\right] \tag{7.10a}$$

$$\text{s. t.} \quad s_{j+1}e_t \leq \rho_{j+1} \tag{7.10b}$$

$$\rho_{j+1} \leq P \tag{7.10c}$$

$$R_{j+1}(P) \geq 0. \tag{7.10d}$$

There are three feasible regions for this problem: i) constraint (7.10b) is active; ii) constraint (7.10c) is active; or iii) none of the constraints are active. Next we consider the problem for each case.

*Case I*: When constraint (7.10b) is active

In this case we have, $s_{j+1}e_t = \rho_{j+1}$ which means there will be no energy harvesting in frame $j+1$. When $s_{j+1} = 1$, this may only occur for a subset of $\mathbf{H}_{j+1}$ in which the channel is considerably poor. For this subset of channel matrices we have

$$\lambda_1\left(\mathbf{H}_{j+1}^{\dagger}\mathbf{H}_{j+1}\right) \leq T_1 \tag{7.11}$$

where $T_1$ denotes a certain threshold used to consider whether the channel is poor. In this case, (7.10a) can be given as $R_{j+1}(P) = \int_0^{T_1} m(x)f(x)dx$ where $f(x)$ is the probability density of $\lambda_1(\mathbf{H}_{j+1}^{\dagger}\mathbf{H}_{j+1})$ and $m(x)$ is given by

$$m(x) = (P - 2e_t)\, C \tag{7.12}$$

.

*Case II*: When constraint (7.10c) is active

In this case we have, $\rho_{j+1} = P$ which means all the available energy will be transmitted in frame $j+1$. Therefore, energy available for the rest of $j$ frames is zero, i.e., $s_j = 0$. This may only occur for a subset of $\mathbf{H}_{j+1}$ in which the channel is considerably good. For this subset of channel matrices we have

$$\lambda_1 \left(\mathbf{H}_{j+1}^{\dagger}\mathbf{H}_{j+1}\right) \geq T_2 \tag{7.13}$$

where $T_2$ denotes a certain threshold used to consider whether the channel is good. In this case, (7.10a) can be given as $R_{j+1}(P) = \int_0^{T_1} l(x)f(x)dx$ where $l(x)$ is given by

$$l(x) = (P - e_t)\, x. \tag{7.14}$$

*Case III*: When none of the constraints are active

In this case, energy transfer occurs in both frame $j+1$ and in rest of the $j$ frames. Therefore $s_{j+1} = s_j = 1$ and the objective function in (7.10) reduces to

$$R_{j+1}(P) = \max_{\rho_{j+1}(x)} \int_{T_1}^{T_2} \Big[ (\rho_{j+1}(x) - e_t)\,(x - C) + (P - \rho_{j+1}(x) - e_t)C \Big] f(x)dx \tag{7.15}$$

Here, we denote $\rho_{j+1}(x) = \rho_{j+1}$ in order to represent the dependence of the transmit

energy $\rho_{j+1}$ on the channel instance, $x$. Now we consider the function $g(x)$ as,

$$g(x) = (\rho_{j+1}(x) - e_t)(x - C) + (P - \rho_{j+1}(x) - e_t)C \tag{7.16}$$

for the set $T_1 \leq x \leq T_2$. Then from (7.15) we have $R_{j+1}(P) = \max_{\rho_{j+1}(x)} \int_{T_1}^{T_2} g(x)f(x)dx$. Now we consider two sub-cases: a) when $g(x) > l(x)$; and b) when $g(x) > m(x)$.

*Case III-a*: When $g(x) > l(x)$

In this sub-case, for the given instance of $x$, the energy harvested by transmitting energy in both frame $j+1$ and other $j$ frames is greater than energy harvested using transmitting all available energy at frame $j+1$. By using (7.14) and (7.16), we have

$$x < \frac{P - 2\rho_{j+1}(x)}{P - \rho_{j+1}(x)}C \tag{7.17}$$

where the denominator, $P - \rho_{j+1}(x) \neq 0$ in $T_1 < x < T_2$ region as both frames should transmit energy.

*Case III-b*: When $g(x) > m(x)$

In this sub-case, for the given instance of $x$, the energy harvested by transmitting energy in both frame $j+1$ and other $j$ frames is greater than energy harvested using transmitting all available energy in the last $j$ frames. By using (7.12) and (7.16), we have

$$x > 2C \tag{7.18}$$

because, $\rho_{j+1}(x) \neq e_t$ in $T_1 < x < T_2$ region as both frames should transmit energy.

For the subset of instances of $x$ where both sub-cases are true, the energy harvested by transmitting energy in both frames will be higher than the energy harvested by transmitting all energy in $j+1$ frame or the rest for $j$ frames. In this case, the subset of of $x$ should satisfy both (7.17) and (7.18). Since, $e_t < \rho_{j+1}(x) < P$ in the region $T_1 < x < T_2$, these two conditions are contradicting. Therefore, the subset of channels in which the energy harvested by transmitting energy in both frames is greater than

transmitting all the energy in either frame $j+1$ or the rest of the $j$ frames, is empty. Furthermore, we have $T_1 = T_2$. In other words, the optimum policy for opportunistic energy transfer reduces to an all-or-nothing threshold policy regardless of the distribution of channels. This completes the proof. □

According to Theorem 3, the optimum policy is an all-or-nothing threshold policy which is similar to the problem discussed in Chapter 6. Hence, the user may only be required to send feedback once. This is because for frames that do not exceed the threshold the user may remain idle in the feedback phase and only transmit feedback for the frame that exceeds the threshold. Channel estimation on the other hand must be performed at every frame. Therefore, the total energy spent on channel estimation, $e_t$ may be considerably large compared to the energy utilized for the feedback phase, $e_r$. Furthermore, for a point-to-point SISO network, only one bit is required to send as feedback to let the energy transmitter know to transmit energy or not. This is because the user is not required to inform the energy transmitter regarding the optimum beamforming vector to be used as there is only one antenna. This effect further justifies the assumption of negligible feedback energy, i.e., $e_r = 0$. We now use the Theorem 3 to obtain the optimum policy for opportunistic energy transfer.

**Theorem 4.** *With channel estimation energy ($e_t > 0$), the optimum expected total harvested energy using $N$ frames over block fading i.i.d. channels is*

$$R_{N-1}(P) = s_{N-1}(P - e_t)\Big[G_{N-1}(P) + \gamma_{N-1}(P)F\left(\gamma_{N-1}(P)\right)\Big] \tag{7.19}$$

*and the optimum threshold for frame $j$ is*

$$\gamma_j(P) = \frac{P - 2e_t}{P - e_t}\Big[G_{j-1}(P - e_t) + \gamma_{j-1}(P - e_t)F(\gamma_{j-1}(P - e_t))\Big] \tag{7.20}$$

*where,*

$$G_j(P) = \int_{\gamma_j(P)}^{\infty} xf(x)dx, \tag{7.21}$$

*with $f(x)$ and $F(x)$ are the probability density function and the cumulative distribution function of $\lambda_1\left(\mathbf{H}^\dagger\mathbf{H}\right)$, respectively.*

*Proof.* We use method of induction to prove Theorem 4.

Base Case: For one frame ($N = 1$), problem in (7.8) can be given as

$$\begin{aligned} R_0(P) = \max_{\rho_0(x)} & \int_0^\infty \left(\rho_0(x) - e_t\right) x f(x) dx \\ \text{s. t.} \quad & s_0 e_t \leq \rho_0(x) \leq P. \end{aligned} \tag{7.22}$$

It is obvious that the optimum transmit energy $\rho_0^*(x)$ is $P$, i.e., all the available energy is transmitted in the same frame regardless of the channel condition. Therefore, $R_0(P) = s_0(P - e_t)G_0(P)$ with threshold $\gamma_0(P) = 0$. It is worth noting that the energy harvested using 1 frame, $R_0(P)$ is in the form of (7.9).

Inductive hypothesis: Assume that the solution in (7.19) is true for $N = n$. Then, we have

$$R_{n-1}(P) = s_{n-1}(P - e_t)\Big[G_{n-1}(P) + \gamma_{n-1}(P)F\left(\gamma_{n-1}(P)\right)\Big] \tag{7.23}$$

where the optimum thresholds are given by (7.20). We note that (7.23) takes the form of (7.9) for a given $P$.

Inductive Step: Consider the case $N = n + 1$. The optimization problem in (7.8) can be given as

$$\begin{aligned} \max_{\rho_n} \quad & R_n(P) = \mathbb{E}\Big[s_n(\rho_n - e_t)\lambda_1\left(\mathbf{H}_n^\dagger\mathbf{H}_n\right) + R_{n-1}(P - \rho_n)\Big] \\ \text{s. t.} \quad & s_n e_t \leq \rho_n \leq P. \end{aligned} \tag{7.24}$$

Since (7.23) takes the form of (7.9), we can use Theorem 3 to show that the optimum policy reduces to an all-or-nothing threshold policy. Therefore, we have two cases: i) $\rho_n = e_t$ for $\lambda_1\left(\mathbf{H}_n^\dagger\mathbf{H}_n\right) < \gamma_n(P)$ which leads to $s_{n-1} = 1$; and ii) $\rho_n = P$ for $\lambda_1\left(\mathbf{H}_n^\dagger\mathbf{H}_n\right) > \gamma_n(P)$ which leads to $s_{n-1} = 0$, where $\gamma_n(P)$ is the threshold at frame

$n$. Thus, the objective function of (7.24) can be given as

$$\begin{aligned} R_n(P) = s_n \int_0^{\gamma_n(P)} (P - 2e_t) \Big[ & G_{n-1}(P - e_t) \\ & + \gamma_{n-1}(P - e_t) F\left(\gamma_{n-1}(P - e_t)\right) \Big] f(x) dx \\ & + s_n \int_{\gamma_n(P)}^{\infty} (P - e_t) x f(x) dx. \end{aligned} \tag{7.25}$$

By using Leibniz integral rule we have

$$\begin{aligned} \nabla_{\gamma_n(P)} R_n(P) = s_n (P - 2e_t) \Big[ & G_{n-1}(P - e_t) \\ & + \gamma_{n-1}(P - e_t) F\left(\gamma_{n-1}(P - e_t)\right) \Big] f(\gamma_n(P)) \\ & - s_n (P - e_t) \gamma_n(P) f(\gamma_n(P)). \end{aligned} \tag{7.26}$$

Assuming the function $R_n(P)$ to be a quasi-concave function, the Kuhn-Tucker-Lagrange (KTL) conditions [93] for the problem in (7.24) can be given as

$$(1 + \lambda) \nabla_{\gamma_n(P)} R_n(P) \leq 0 \tag{7.27a}$$

$$\gamma_n(P)(1 + \lambda) \nabla_{\gamma_n(P)} R_n(P) = 0 \tag{7.27b}$$

$$\lambda \gamma_n = 0 \tag{7.27c}$$

$$R_n(P) \geq 0, \;\; \gamma_n(P) \geq 0, \;\; \lambda \geq 0. \tag{7.27d}$$

By solving this system of equations for $\gamma_n(P)$ and $R_n(P)$, we have (7.19) and (7.20) for $N - 1 = n$. Based on the rule of induction, Theorem 4 is true for all $N > 0$. This completes the proof. □

This means that the optimum transmit energy at each frame is given by a threshold policy. Specifically, at the time frame $j$, if the eigenvalue $\lambda_1(\mathbf{H}_j^{\dagger}\mathbf{H}_j)$ is greater than the expected harvested energy from the remaining frames by using available energy after channel estimation at frame $j$, all the available energy $\rho_j^* = P$ will be transmitted at the

$j$th frame using the optimum beamforming vector, $\mathbf{v}_1(\mathbf{H}_j^\dagger \mathbf{H}_j)$.

If we are able to foresee all the channels matrices, it is obvious that by choosing the frame $j^*$ that yields the largest $\lambda_1(\mathbf{H}_j^\dagger \mathbf{H}_j)$, i.e. $j^* = \arg\max_j \lambda_1(\mathbf{H}_j^\dagger \mathbf{H}_j)$, we can maximize the expected harvested energy. Unfortunately, we do not have the luxury of seeing into the future. Therefore, we will use this method (addressed as genie aided method hereafter) as an upper bound of the proposed algorithm.

## 7.5 For SISO Rayleigh Channels

For SISO Networks with Rayleigh distributed channels, the Theorem 4 reduces to

$$R_{N-1}(P) = s_{N-1}(P - e_t)\left[\gamma_{N-1}(P) + e^{-\gamma_{N-1}(P)}\right] \tag{7.28}$$

where the optimum thresholds are

$$\gamma_j(P) = \begin{cases} \frac{P-2e_t}{P-e_t}\left[\gamma_{j-1}(P - e_t) + e^{-\gamma_{j-1}(P-e_t)}\right], & P > 2e_t \\ 0, \text{ otherwise.} \end{cases} \tag{7.29}$$

Now we analyze the behaviour of $R_{N-1}(P)$. The function in (7.28) has the form of $f : \mathbb{R}_+ \to \mathbb{R}_+$ with $f(x) = a\,(1 - e^{-x}) + b\,(1 + x)\,e^{-x}$ where $a, b \in \mathbb{R}$. Then, we have $\nabla f(x) = (a - bx)\,e^{-x}$. As $e^{-x} > 0$ for $x \in \mathbb{R}_+$, we have the following three cases. i) the function $f(x)$ is strictly increasing when $bx < a$ because $\nabla f(x) > 0$; ii) the unique stationary point of $f(x)$ is obtained when $bx = a$; and iii) the function $f(x)$ is strictly decreasing when $bx > a$ because $\nabla f(x) < 0$. This proves that the function $f(x)$ has a unique maximum. Furthermore, we note that strictly increasing/ decreasing functions are quasi-concave. Therefore, the function $f(x)$ is quasi-concave. This means $R_n(P)$ is quasi-concave. Thus, the quasi-concavity assumption for $R_{N-1}(P)$ holds for SISO Rayleigh distributed channels.

## 7.6 Numerical and Simulation Results

This section provides numerical results to verify the analysis and to discuss the performance for SISO Rayleigh distributed channels, i.e., $h_j \sim \mathcal{CN}(0,1)$. Recall that the energy conversion efficiency $\eta = 1$, and energy associated with noise is negligible. Further, we have normalized energy ($P = 1$) unless otherwise specified.

In frame $N-1$, we compare $|h_{N-1}|^2$ with $\gamma_{N-1}(P)$ in (7.29) and obtain the optimum energy transfer $\rho^*_{N-1}$ in (7.29). If $\rho^*_{N-1} = e_t$, we update the available energy at next frame $(N-2)$ as $P_{(N-2,available)} = 1 - e_t$. This procedure is repeated for all frames $N$. For the genie aided energy transfer scheme, we calculate energy available for harvesting at frame $j$ as $P_{j,(available)} = 1 - (N-j-1)e_t$ and choose the frame $j^*$ with maximum $(P_{j,(available)} - e_t)|h_j|^2$ among the $N$ frames, and transmit available energy $P_{j^*,(available)}$ at this frame. For the equal energy transfer, we transfer $P/N - e_t$ amount of energy in each frame. For the random energy transfer, we transfer all the energy available, $P - e_t$ in a randomly selected frame $j \in \{0, N-1\}$. We calculate the average total harvested energy by using $10^5$ set of channel realizations. Figure 7.2 shows the variation of the thresholds, $\gamma_j(P)$ for each frame with $N = 10$ and $e_t = 0,\ 0.01P,\ 0.05P$ and $0.10P$. For a given frame number, the threshold reduces when $e_t$ increases because the energy available for the future frame reduces significantly with large $e_t$. Therefore, harvesting at the current frame which may have a worse channel gain may result in large amount of harvested energy than harvesting in the future frame which may have a better channel gain but with low available energy. Furthermore, the threshold $\gamma_0(P) = 0$ for all cases of $e_t$ because all available energy must be harvested at the last frame regardless of the channel. The threshold $\gamma_1(P) = 0$ for frame 1 with $e_t = 0.10P$ demonstrates the effect of $R_n(P) \geq 0$ constraint in (7.24). As the available energy $P_{1,(available)} = 2e_t$, all available energy must be transmitted at frame 1 regardless of the channel quality. Hence the threshold $\gamma_1(P)$ is zero.

Figure 7.3 shows the variation of expected harvested energy with the number of frames $N$ for four schemes when $e_t = 0.10P$. When $N = 1$, the expected harvested

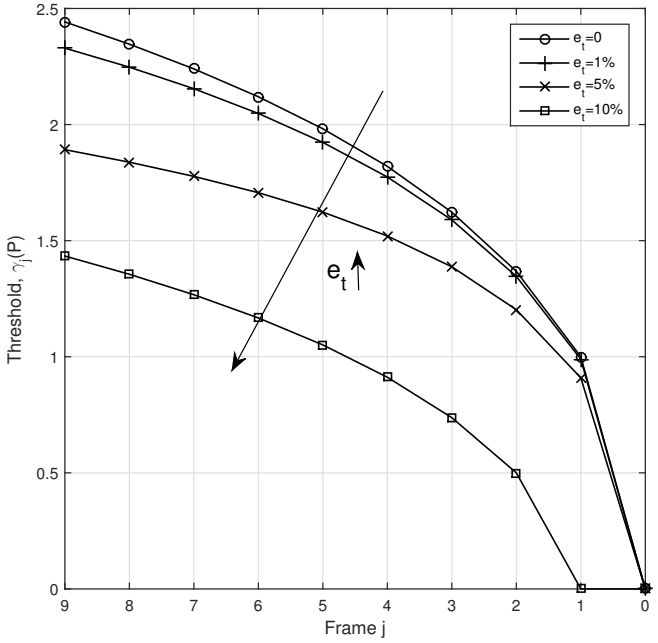


Figure 7.2: Threshold of frame $j$, $\gamma_j(P)$, with frame index $j$ for different $e_t$ values when $N = 10$.

energy from all four schemes is $0.9$. As there is only one frame, all the energy available, $1 - e_t = 0.9$, is transmitted in all four schemes. The harvested energy converges from 1 to 1.67 and from 1 to 1.50 for genie-aided and optimum energy transfer schemes, respectively, because no energy is available even for channel estimation when $N > 10$ at $e_t = 0.10P$. The harvested energy with the equal energy transfer scheme drops to zero because the energy utilized for energy transfer decreases as all the frames are used. When $N = 10$, all the energy is utilized for channel estimation leaving no energy for energy transfer. Thus, the expected harvested energy for $N = 10$, $E_9(P)$ is zero for equal energy transfer scheme. The expected harvested energy with random energy transfer scheme remains constant at $0.9$ because only one frame is utilized for energy transfer. Thus, the random energy transfer scheme outperforms the equal energy transfer scheme.

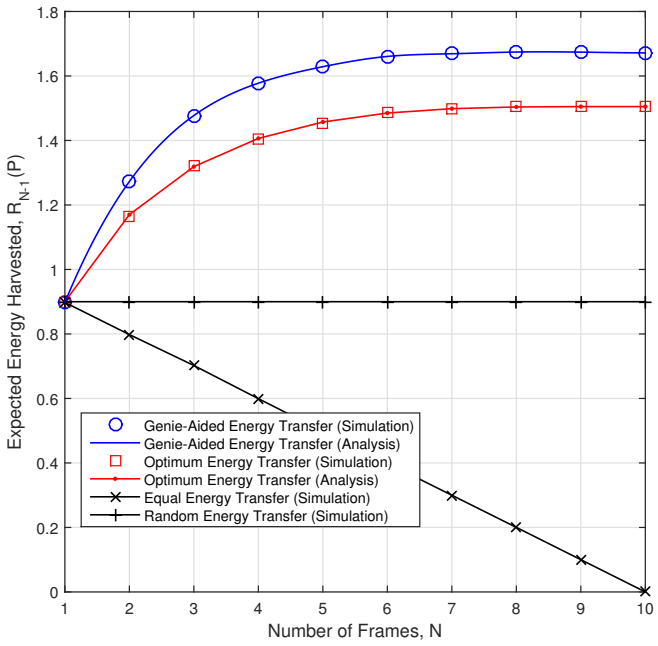


Figure 7.3: Expected harvested energy with number of frames for four energy transfer schemes when $e_t = 0.10P$

## 7.7 Conclusion

This chapter considers a point-to-point network with an energy constrained power transmitter and an energy receiver which has strict deadline on time. We obtain an opportunistic optimum energy transfer scheme together with optimum beamforming scheme to maximize the expected total harvested energy when the energy associated with channel estimation at each frame is significant. We show that the optimum policy is a threshold policy. We compare the performance using genie-aided energy transfer, equal energy transfer and random energy transfer schemes. We observe that the thresholds for each frame reduces with large channel estimation energy.

# References


[1] IEEE, "IEEE 5G and beyond technology roadmap white paper," *IEEE White paper*, p. 1, 2017.

[2] I. Cisco, "Cisco visual networking index: Forecast and methodology, 2011–2016," *CISCO White paper*, pp. 2011–2016, 2012.

[3] Q. Zhao and B. Sadler, "A survey of dynamic spectrum access," *Signal Processing Magazine, IEEE*, vol. 24, no. 3, pp. 79–89, May 2007.

[4] E. Hossain, M. Rasti, H. Tabassum, and A. Abdelnasser, "Evolution toward 5G multi-tier cellular wireless networks: An interference management perspective," *Wireless Communications, IEEE*, vol. 21, no. 3, pp. 118–127, June 2014.

[5] C.-X. Wang, F. Haider, X. Gao, X.-H. You, Y. Yang, D. Yuan, H. Aggoune, H. Haas, S. Fletcher, and E. Hepsaydir, "Cellular architecture and key technologies for 5g wireless communication networks," *Communications Magazine, IEEE*, vol. 52, no. 2, pp. 122–130, February 2014.

[6] Z. Ding, C. Zhong, D. W. K. Ng, M. Peng, H. A. Suraweera, R. Schober, and H. V. Poor, "Application of smart antenna technologies in simultaneous wireless information and power transfer," *CoRR*, vol. abs/1412.1712, 2014. [Online]. Available: http://arxiv.org/abs/1412.1712

[7] W. C. Brown, "Experiments involving a microwave beam to power and position a helicopter," *Aerospace and Electronic Systems, IEEE Transactions on*, vol. AES-5, no. 5, pp. 692–702, Sept 1969.

[8] M. Dong, K. Ota, L. T. Yang, S. Chang, H. Zhu, and Z. Zhou, "Mobile agent-based energy-aware and user-centric data collection in wireless sensor networks," *Computer Networks*, vol. 74, Part B, pp. 58 – 70, 2014, special Issue on Mobile Computing for Content/Service-Oriented Networking Architecture. [Online]. Available: http://www.sciencedirect.com/science/article/pii/S1389128614003156

[9] O. Diallo, J. Rodrigues, M. Sene, and J. Lloret, "Distributed database management techniques for wireless sensor networks," *Parallel and Distributed Systems, IEEE Transactions on*, vol. 26, no. 2, pp. 604–620, Feb 2015.

[10] R. Vullers, R. Schaijk, H. Visser, J. Penders, and C. Hoof, "Energy harvesting for autonomous wireless sensor networks," *Solid-State Circuits Magazine, IEEE*, vol. 2, no. 2, pp. 29–38, Spring 2010.

[11] A. Davis and H. Chang, "Underwater wireless sensor networks," in *Oceans, 2012*, Oct 2012, pp. 1–5.

[12] J. Zhu, L. Hattaway, and S. Altamimi, "Ambient energy harvesting and self-sustainability for transportation infrastructure monitoring wireless sensor networks," in *Sensors Applications Symposium (SAS), 2013 IEEE*, Feb 2013, pp. 93–97.

[13] M. Popa, O. Prostean, and A. Popa, "A classification of solutions for the energy limitation in wireless sensor networks," in *Computational Cybernetics (ICCC), 2013 IEEE 9th International Conference on*, July 2013, pp. 293–297.

[14] H. Unterassinger, M. Dielacher, M. Flatscher, S. Gruber, G. Kowalczyk, J. Prainsack, T. Herndl, J. Schweighofer, and W. Pribyl, "A power management unit for ultra-low power wireless sensor networks," in *AFRICON, 2011*, Sept 2011, pp. 1–6.

[15] W. Seah and J. Olds, "Data delivery scheme for wireless sensor network powered by RF energy harvesting," in *Wireless Communications and Networking Conference (WCNC), 2013 IEEE*, April 2013, pp. 1498–1503.

[16] H. Ostaffe, "Practical applications of RF energy harvesting," *PowerCast Corporation*, 2009.

[17] H. Ju and R. Zhang, "Throughput maximization in wireless powered communication networks," *Wireless Communications, IEEE Transactions on*, vol. 13, no. 1, pp. 418–428, January 2014.

[18] K. Huang and V. Lau, "Enabling wireless power transfer in cellular networks: Architecture, modeling and deployment," *Wireless Communications, IEEE Transactions on*, vol. 13, no. 2, pp. 902–912, February 2014.

[19] X. Lu, P. Wang, D. Niyato, D. I. Kim, and Z. Han, "Wireless networks with rf energy harvesting: A contemporary survey," *Communications Surveys Tutorials, IEEE*, vol. 17, no. 2, pp. 757–789, Secondquarter 2015.

[20] G. Y. Li, Z. Xu, C. Xiong, C. Yang, S. Zhang, Y. Chen, and S. Xu, "Energy-efficient wireless communications: tutorial, survey, and open issues," *IEEE Trans. Comput.*, vol. 18, no. 6, pp. 28–35, December 2011.

[21] Z. Wang, L. Duan, and R. Zhang, "Adaptively directional wireless power transfer for large-scale sensor networks," *IEEE J. Select. Areas Commun.*, vol. 34, no. 5, pp. 1785–1800, May 2016.

[22] R. Zhang and C. K. Ho, "MIMO broadcasting for simultaneous wireless information and power transfer," *IEEE Trans. Wireless Commun.*, vol. 12, no. 5, pp. 1989–2001, May 2013.

[23] S. Bi, C. K. Ho, and R. Zhang, "Recent advances in joint wireless energy and information transfer," in *IEEE Infor. Theory Workshop*, Nov 2014, pp. 341–345.

[24] J. Xu and R. Zhang, "Energy beamforming with one-bit feedback," in *Proc. IEEE Int. Conf. Acoustics, Speech, and Signal Processing (ICASSP)*, May 2014, pp. 3513–3517.

[25] Q. Shi, W. Xu, T.-H. Chang, Y. Wang, and E. Song, "Joint beamforming and power splitting for MISO interference channel with SWIPT: An SOCP relaxation and decentralized algorithm," *IEEE Trans. Signal Processing*, vol. 62, no. 23, pp. 6194–6208, Dec 2014.

[26] M. Khandaker and K.-K. Wong, "SWIPT in MISO multicasting systems," *IEEE Commun. Lett.*, vol. 3, no. 3, pp. 277–280, June 2014.

[27] W. Wu and B. Wang, "Robust downlink beamforming design for multiuser MISO communication system with SWIPT," in *Proc. IEEE Int. Conf. Commun. (ICC)*, June 2015, pp. 4751–4756.

[28] Z. Zhu, Z. Wang, X. Gui, and X. Gao, "Robust downlink beamforming and power splitting design in multiuser MISO SWIPT system," in *Proc. IEEE Int. Conf. Commun. (ICC)*, October 2014, pp. 271–275.

[29] E. Ackerman, "Wireless power takes charge," *IEEE Spectrum*, vol. 53, no. 1, pp. 13–14, January 2016.

[30] R. Horn and C. Johnson, *Matrix Analysis*, ser. Matrix Analysis. Cambridge University Press, 2012. [Online]. Available: https://books.google.com.au/books?id=5I5AYeeh0JUC

[31] N. El Karoui, "Tracy-widom limit for the largest eigenvalue of a large class of complex sample covariance matrices," *Ann. Probab.*, vol. 35, no. 2, pp. 663–714, 03 2007. [Online]. Available: http://dx.doi.org/10.1214/009117906000000917

[32] A. Onatski, "The Tracy-Widom limit for the largest eigenvalues of singular complex Wishart matrices," *Ann. Appl. Probab.*, vol. 18, no. 2, pp. 470–490, 2008.

[33] Z. Bao, G. Pan, and W. Zhou, "Universality for the largest eigenvalue of sample covariance matrices with general population," *Ann. Statist.*, vol. 43, no. 1, pp. 382–421, 2015.

[34] P. Bleher and A. Its, *Random matrix models and their applications*. Cambridge university press, 2001, vol. 40.

[35] C. Tracy and H. Widom, "Level-spacing distributions and the Airy kernel," *Communications in Mathematical Physics*, vol. 159, no. 1, pp. 151–174, 1994.

[36] A. Bejan, *Largest eigenvalues and sample covariance matrices*. M.Sc. dissertation, Univ. Warwick, Coventry, U.K., 2005.

[37] S. Geman, "A limit theorem for the norm of random matrices," *Ann. Probab.*, vol. 8, no. 2, pp. 252–261, 04 1980. [Online]. Available: http://dx.doi.org/10.1214/aop/1176994775

[38] J. Baik, G. Ben Arous, and S. Peche, "Phase transition of the largest eigenvalue for nonnull complex sample covariance matrices," *Ann. Probab.*, vol. 33, no. 5, pp. 1643–1697, 09 2005.

[39] N. E. Karoui, "On the largest eigenvalue of Wishart matrices with identity covariance when n, p and p/n tend to infinity," *arXiv preprint math/0309355*, 2003.

[40] M. Xia and S. Aissa, "On the efficiency of far-field wireless power transfer," *IEEE Trans. Signal Processing*, vol. 63, no. 11, pp. 2835–2847, June 2015.

[41] J. Nocedal and S. J. Wright, *Numerical optimization*, ser. Springer series in operations research and financial engineering. New York : Springer, c2006., 2006.

[42] N. Sidiropoulos, T. Davidson, and Z.-Q. Luo, "Transmit beamforming for physical-layer multicasting," *IEEE Trans. Signal Processing*, vol. 54, no. 6, pp. 2239–2251, June 2006.

[43] W.-K. Ma, T. Davidson, K. M. Wong, Z.-Q. Luo, and P.-C. Ching, "Quasi-maximum-likelihood multiuser detection using semi-definite relaxation with application to synchronous CDMA," *IEEE Trans. Signal Processing*, vol. 50, no. 4, pp. 912–922, April 2002.

[44] S. Corroy and R. Mathar, "Semidefinite relaxation and randomization for dynamic cell association in heterogeneous networks," in *Proc. IEEE Global Telecommn. Conf. (GLOBECOM)*, Dec 2012, pp. 2373–2378.

[45] G. Wang, Y. Li, and R. Wang, "New semidefinite relaxation method for acoustic energy-based source localization," *IEEE Sensor Journal*, vol. 13, no. 5, pp. 1514–1521, May 2013.

[46] D. I. Kim, D. Niyato, and D. Hwang, "Wireless energy harvesting communications: Beamforming and stochastic optimization," in *Int. Conference on Information and Communication Technology Convergence (ICTC)*, Oct 2014, pp. 760–762.

[47] M. Gregori and M. Payaro, "Energy-efficient transmission for wireless energy harvesting nodes," *IEEE Trans. Wireless Commun.*, vol. 12, no. 3, pp. 1244–1254, March 2013.

[48] L. Berbakov, J. Matamoros, and C. Anton-Haro, "Greedy transmission strategies for collaborative beamforming with energy harvesting sensors," in *Int. ITG Workshop on Smart Antennas (WSA)*, March 2013, pp. 1–6.

[49] Q. Sun, G. Zhu, C. Shen, X. Li, and Z. Zhong, "Joint beamforming design and time allocation for wireless powered communication networks," *IEEE Commun. Lett.*, vol. 18, no. 10, pp. 1783–1786, Oct 2014.

[50] G. Yang, C. K. Ho, and Y. L. Guan, "Dynamic resource allocation for multiple-antenna wireless power transfer," *IEEE Trans. Signal Processing*, vol. 62, no. 14, pp. 3565–3577, July 2014.

[51] Y. Zeng and R. Zhang, "Optimized training for net energy maximization in multi-antenna wireless energy transfer over frequency-selective channel," *IEEE Trans. Commun.*, vol. 63, no. 6, pp. 2360–2373, June 2015.

[52] G. Yang, C. K. Ho, R. Zhang, and Y. L. Guan, "Throughput optimization for massive MIMO systems powered by wireless energy transfer," *IEEE J. Select. Areas Commun.*, vol. 33, no. 8, pp. 1640–1650, Aug 2015.

[53] L. Liu, R. Zhang, and K.-C. Chua, "Secrecy wireless information and power transfer with MISO beamforming," *IEEE Trans. Signal Processing*, vol. 62, no. 7, pp. 1850–1863, April 2014.

[54] T.-Q. Wu and H.-C. Yang, "On the performance of overlaid wireless sensor transmission with RF energy harvesting," *IEEE J. Select. Areas Commun.*, vol. 33, no. 8, pp. 1693–1705, Aug 2015.

[55] M. Naderi, P. Nintanavongsa, and K. Chowdhury, "RF-MAC: a medium access control protocol for re-chargeable sensor networks powered by wireless energy harvesting," *IEEE Trans. Wireless Commun.*, vol. 13, no. 7, pp. 3926–3937, July 2014.

[56] H. Visser and R. Vullers, "RF energy harvesting and transport for wireless sensor network applications: Principles and requirements," *Proceedings of the IEEE*, vol. 101, no. 6, pp. 1410–1423, June 2013.

[57] H. Tabassum, E. Hossain, M. Jahangir Hossain, and D. I. Kim, "On the spectral efficiency of multiuser scheduling in RF-powered uplink cellular networks," *IEEE Trans. Wireless Commun.*, vol. 14, no. 7, pp. 3586–3600, July 2015.

[58] Y. L. Che, L. Duan, and R. Zhang, "Spatial throughput maximization of wireless powered communication networks," *IEEE J. Select. Areas Commun.*, vol. 33, no. 8, pp. 1534–1548, Aug 2015.

[59] S. Park, H. Kim, and D. Hong, "Cognitive radio networks with energy harvesting," *IEEE Trans. Wireless Commun.*, vol. 12, no. 3, pp. 1386–1397, March 2013.

[60] A. Nasir, X. Zhou, S. Durrani, and R. Kennedy, "Relaying protocols for wireless energy harvesting and information processing," *IEEE Trans. Wireless Commun.*, vol. 12, no. 7, pp. 3622–3636, July 2013.

[61] S. Atapattu, H. Jiang, J. Evans, and C. Tellambura, "Time-switching energy harvesting in relay networks," in *2015 IEEE International Conference on Communications (ICC)*, June 2015, pp. 5416–5421.

[62] S. Atapattu and J. Evans, "Optimal power-splitting ratio for wireless energy harvesting in relay networks," in *2015 IEEE 82nd Vehicular Technology Conference (VTC2015-Fall)*, Sept 2015, pp. 1–6.

[63] B. Du, Y. Jiang, X. Xu, and X. Dai, "Transmit beamforming for MIMO multicast channels," in *Proc. IEEE Int. Conf. Commun. (ICC)*, June 2012, pp. 3800–3805.

[64] M. Grant, S. Boyd, and Y. Ye, "CVX users guide," 2009.

[65] I. Krikidis, S. Timotheou, S. Nikolaou, G. Zheng, D. W. K. Ng, and R. Schober, "Simultaneous wireless information and power transfer in modern communication systems," *IEEE Commun. Mag.*, vol. 52, no. 11, pp. 104–110, Nov. 2014.

[66] J. Habibi, A. Ghrayeb, and A. G. Aghdam, "Energy-efficient cooperative routing in wireless sensor networks: A mixed-integer optimization framework and explicit solution," *IEEE Trans. Commun.*, vol. 61, no. 8, pp. 3424–3437, Aug. 2013.

[67] X. Qi, K. Wang, A. Huang, L. Shu, and Y. Liu, "A harvesting-rate oriented self-adaptive algorithm in energy-harvesting wireless body area networks," in *Industrial Informatics (INDIN), 2015 IEEE 13th International Conference on*, July 2015, pp. 966–971.

[68] X. Qi, K. Wang, D. Yue, L. Shu, Y. Liu, and H. Zhao, "Adaptive tdma-based mac protocol in energy harvesting wireless body area network for mobile health," in *Industrial Electronics Society, IECON 2015 - 41st Annual Conference of the IEEE*, Nov 2015, pp. 004 175–004 180.

[69] J. Elias, "Optimal design of energy-efficient and cost-effective wireless body area networks," *Ad Hoc Networks*, vol. 13, Part B, pp. 560 – 574, 2014.

[70] L. Liu, R. Zhang, and K.-C. Chua, "Multi-antenna wireless powered communication with energy beamforming," *IEEE Trans. Commun.*, vol. 62, no. 12, pp. 4349–4361, Dec 2014.

[71] W. Huang, H. Chen, Y. Li, and B. Vucetic, "On the performance of multi-antenna wireless-powered communications with energy beamforming," *IEEE Trans. Veh. Technol.*, vol. 65, no. 3, pp. 1801–1808, Mar 2016.

[72] P. Tseng, "Further results on approximating nonconvex quadratic optimization by semidefinite programming relaxation," *SIAM J. on Optimization*, vol. 14, no. 1, pp. 268–283, Jan. 2003.

[73] S. Zhang, "Quadratic maximization and semidefinite relaxation," *Mathematical Programming*, vol. 87, no. 3, pp. 453–465, 2000.

[74] R. M. Corless, G. H. Gonnet, D. E. G. Hare, D. J. Jeffrey, and D. E. Knuth, "On the LambertW function," *Advances in Computational Mathematics*, vol. 5, pp. 329–359, 1996.

[75] C. Xu, "Completely positive matrices," *Linear algebra and its applications*, vol. 379, pp. 319–327, 2004.

[76] A. Berman and N. Shaked-Monderer, *Completely Positive Matrices*. World Scientific Publishing Company, 2003.

[77] L. Xie, Y. Shi, Y. T. Hou, and A. Lou, "Wireless power transfer and applications to sensor networks," *IEEE Wireless Commun.*, vol. 20, no. 4, pp. 140–145, Aug. 2013.

[78] H. Wang, W. Wang, and Z. Zhang, "Opportunistic wireless information and energy transfer for sustainable cooperative relaying," in *Proc. IEEE Int. Conf. Commun. (ICC)*, June 2015, pp. 160–165.

[79] C. Zhai, H. Chen, X. Wang, and J. Liu, "Opportunistic spectrum sharing with wireless energy transfer in stochastic networks," *IEEE Trans. Commun.*, vol. PP, no. 99, Aug. 2017.

[80] O. Ozel, K. Tutuncuoglu, J. Yang, S. Ulukus, and A. Yener, "Transmission with energy harvesting nodes in fading wireless channels: Optimal policies," *IEEE J. Select. Areas Commun.*, vol. 29, no. 8, pp. 1732–1743, Sept. 2011.

[81] C. K. Ho and R. Zhang, "Optimal energy allocation for wireless communications with energy harvesting constraints," *IEEE Trans. Signal Processing*, vol. 60, no. 9, pp. 4808–4818, Sept. 2012.

[82] A. Baknina and S. Ulukus, "Single-user channel with data and energy arrivals: Online policies," in *IEEE Int. Symposium on Inform. Theory*, June 2017, pp. 824–828.

[83] J. Gmez-Vilardeb, "Competitive design of energy harvesting communications in wireless fading channels," *IEEE/ACM Trans. Netw.*, vol. 25, no. 6, pp. 3863–3872, Dec 2017.

[84] A. Thudugalage, S. Atapattu, and J. Evans, "Beamforming for total energy maximization in MISO networks," in *2016 Australian Communications Theory Workshop (AusCTW)*, Jan 2016, pp. 112–117.

[85] S. Bi, C. K. Ho, and R. Zhang, "Recent advances in joint wireless energy and information transfer," in *IEEE Infor. Theory Workshop*, Nov 2014, pp. 341–345.

[86] P. A. Dighe, R. K. Mallik, and S. S. Jamuar, "Analysis of transmit-receive diversity in rayleigh fading," *IEEE Trans. Commun.*, vol. 51, no. 4, pp. 694–703, April 2003.

[87] M. Kang and M. S. Alouini, "Largest eigenvalue of complex wishart matrices and performance analysis of MIMO MRC systems," *IEEE J. Select. Areas Commun.*, vol. 21, no. 3, pp. 418–426, April 2003.

[88] I. S. Gradshteyn and I. M. Ryzhik, *Table of integrals, series, and products*, 7th ed. Elsevier Science, 2007.

[89] C. Mortici, "Fast convergences towards Euler-Mascheroni constant," *Computational & Applied Mathematics*, vol. 29, pp. 479 – 491, 2010.

[90] J. Lagarias, "Eulers constant: Eulers work and modern developments," *Bulletin of the American Mathematical Society*, vol. 50, no. 4, pp. 527–628, 2013.

[91] J. Li, P. Chen, and H. Zhang, "Throughput optimization for wireless energy transfer in massive MIMO systems: A superimposed pilot aided approach," in *2015 IEEE 26th Annual International Symposium on Personal, Indoor, and Mobile Radio Communications (PIMRC)*, Aug 2015, pp. 547–552.

[92] K. W. Choi, D. I. Kim, and M. Y. Chung, "Received power-based channel estimation for energy beamforming in multiple-antenna RF energy transfer system," *IEEE Trans. Signal Processing*, vol. 65, no. 6, pp. 1461–1476, March 2017.

[93] K. J. Arrow and A. C. Enthoven, "Quasi-concave programming," *Econometrica*, vol. 29, no. 4, pp. 779–800, 1961.

# List of Publications

Summarized below is the list of publications related to the research conducted during the course of completing my Ph.D. candidature.

- **A. Thudugalage**, S. Atapattu, and J. Evans, Beamforming for total energy maximization in MISO networks, in *2016 Australian Communications Theory Workshop (AusCTW)*, Melbourne, Australia, Jan 2016, pp. 112-117.
- **A. Thudugalage**, S. Atapattu, and J. Evans, Beamformer design for wireless energy transfer with fairness, in *Proc. IEEE Int. Conf. Commun. (ICC)*, Kuala Lumpur, Malaysia, May 2016.
- **A. Thudugalage** , S. Atapattu, and J. Evans, "Beamforming for Wireless Powered MU-MISO Networks with Throughput Fairness" submitted to *IEEE Transactions on Vehicular Technology*.
- **A. Thudugalage** , S. Atapattu, and J. Evans, "'Opportunistic Wireless Energy Transfer in Point-to-Point Links" submitted to *IEEE Wireless Commun. and Networking Conf.*, Morocco, April 2019.
- **A. Thudugalage** , S. Atapattu, and J. Evans, "Opportunistic Wireless Energy Transfer with Beamforming in point-to-point Networks" in preparation for *IEEE Transactions on Green Communications and Networking*.